

NATIONAL ACADEMY OF SCIENCES OF UKRAINE
INSTITUTE OF SEMICONDUCTOR PHYSICS

A.E. Belyaev, E.F. Venger, I.B. Ermolovich,
R.V. Konakova, P.M. Lytvyn, V.V. Milenin,
I.V. Prokopenko, G.S. Svechnikov,
E.A. Soloviev, L.L. Fedorenko

**EFFECT OF MICROWAVE
AND LASER RADIATIONS
ON THE PARAMETERS
OF SEMICONDUCTOR STRUCTURES**

Київ “Інтас” 2002

ВПЛИВ НВЧ І ЛАЗЕРНОГО ВИПРОМІНЮВАНЬ НА ПАРАМЕТРИ НАПІВПРОВІДНИКОВИХ СТРУКТУР.

Беляєв О.Є., докт. фіз.-мат. наук, проф.;

Венгер Є.Ф., член-кор. НАН України,

докт. фіз.-мат. наук, проф.;

Єрмолович І.Б., докт. фіз.-мат. наук;

Конакова Р.В., докт. техн. наук, проф.;

Литвин П.М., канд. фіз.-мат. наук;

Мілецін В.В., канд. фіз.-мат. наук;

Прокопенко І.В., докт. фіз.-мат. наук;

Свєчніков Г.С., канд. фіз.-мат. наук;

Соловйов Є.О., канд. техн. наук;

Федоренко Л.Л., канд. фіз.-мат. наук

У монографії систематизовані та узагальнені результати дослідження модифікації властивостей широкого класу технічно важливих напівпровідників (GaAs, GaP, InP, InSb, Cd_xHg_{1-x}Te, SiC) і контактних структур на їх основі при дії на них потужних НВЧ випромінювань і наносекундних лазерних імпульсів. Розглянуті фізичні моделі виникнення, анігіляції та відпалу точкових дефектів і домішково-дефектних комплексів в опромінених матеріалах. Проаналізовані особливості стимульованих опроміненням процесів масопереносу, хімічних реакцій, утворення нових фаз у контактних структурах різної природи та встановлений їхній зв'язок із параметрами поверхнево-бар'єрних структур. Значне місце приділене релаксації пружних напруженень, зумовленій впливом НВЧ опромінювання, залежно від вихідного домішково-дефектного стану матеріалів, морфології їхньої поверхні та умов опромінювання. Автори суттєво спираються на власний досвід у цій галузі та акцентують увагу на використанні НВЧ і лазерних обробок для поліпшення структурної досконалості напівпровідникових матеріалів і створення на їх основі омічних і бар'єрних контактів із поліпшеними параметрами.

Монографія призначена для науковців і фахівців у галузі напівпровідникової електроніки. Вона може стати в пригоді також викладачам, аспірантам і студентам старших курсів, яким доводиться мати справу з вищевказаними проблемами.

For a wide range of semiconductors (GaAs, GaP, InP, InSb, Cd_xHg_{1-x}Te, SiC), as well as contact structures based on them, that are of importance in engineering, the monograph gives, in a systematized and generalized form, the results of investigation of their properties modification under action of high-power microwave radiations and nanosecond laser pulses. The physical models for production, annihilation and annealing of point defects and impurity-defect complexes in irradiated materials are considered. An analysis is

made of the features of radiation-stimulated mass transport, chemical reactions, formation of new phases in various contact structures, and they are related to the parameters of surface-barrier structures. Much space is given to the elastic stress relaxation due to microwave radiation, depending on the initial impurity-defect condition of materials, their surface morphology and irradiation mode. The authors substantially lean on their own experience in this area. They pay special attention to the use of microwave and laser processing of semiconductor materials for improvement of their structural perfection and development, on their basis, of ohmic and barrier contacts having improved parameters.

The monograph is intended for researchers and specialists engaged in semiconductor electronics. It may be of use also to lecturers, post-graduates and undergraduates dealing with the above problems.

В монографии систематизированы и обобщены результаты исследования модификации свойств широкого класса технически важных полупроводников (GaAs, GaP, InP, InSb, Cd_xHg_{1-x}Te, SiC) и контактных структур на их основе при воздействии на них мощных СВЧ излучений и наносекундных лазерных импульсов. Рассмотрены физические модели возникновения, аннигиляции и отжига точечных дефектов и примесно-дефектных комплексов в облученных материалах. Проанализированы особенности стимулированных облучением процессов массопереноса, химических реакций, образования новых фаз в контактных структурах разной природы и установлена их связь с параметрами поверхностно-барьерных структур. Значительное место уделено релаксации упругих напряжений, обусловленной действием СВЧ облучения, в зависимости от исходного примесно-дефектного состояния материалов, морфологии их поверхности и условий облучения. Авторы существенно опираются на собственный опыт в этой области и акцентируют внимание на использовании СВЧ и лазерных обработок для повышения структурного совершенства полупроводниковых материалов и создания на их основе омических и барьерных контактов с улучшенными параметрами.

Монография предназначена для научных работников и специалистов в области полупроводниковой электроники. Она может пригодиться также преподавателям, аспирантам и студентам старших курсов, которым приходится иметь дело с указанными вопросами.

ISBN 966-02-2541-5

© текст

Беляев О.Є., Венгер Є.Ф.,
Єрмолович І.Б., Конакова Р.В.,
Литвин П.М., Міленін В.В.,
Прокопенко І.В., Свєчніков Г.С.,
Соловйов Є.О., Федоренко Л.Л.
2002

CONTENTS

PRINCIPAL ACRONYMS AND SYMBOLS	8
INTRODUCTION	12
Part 1. INVESTIGATION OF BOUNDARIES BETWEEN PHASES IN HETEROGENEOUS STRUCTURES AND THEIR MODIFICATION UNDER MICROWAVE RADIATION 16	
INTRODUCTION	16
1.1. EXPERIMENTAL TECHNIQUES.....	18
1.2. EFFECT OF HIGH-POWER ELECTROMAGNETIC RADIATION ON THE DEFECT STRUCTURE OF SEMICONDUCTOR MATERIALS.....	20
1.2.1. III-V semiconductor compounds.....	20
1.2.2. $\text{Cd}_x\text{Hg}_{1-x}\text{Te}$ semiconductor solid solutions.....	31
1.3. INTERACTIONS BETWEEN PHASES IN Me–GaAs (InP) CONTACTS STIMULATED BY MICROWAVE IRRADIATION.....	36
1.3.1. Effect of magnetron irradiation on the physico- chemical processes in Me–GaAs (InP) contacts	36
1.3.2. Structural-chemical processes in Me–GaAs contacts stimulated by gyrotron irradiation	44
1.3.3. Effect of microwave treatment on the electrophysical parameters of surface-barrier structures	50

1.4. EFFECT OF MICROWAVE RADIATION ON THE PARAMETERS OF RESONANT TUNNELING DIODES	61
1.4.1. GaAs tunneling diode with two δlayers in SCR	61
1.4.2. Two-barrier resonant tunneling diode.....	66
1.5. THE FEATURES OF STRUCTURAL CHANGES IN GaAs SINGLE CRYSTALS UNDER MICROWAVE IRRADIATION.....	67
1.6. EFFECT OF MICROWAVE IRRADIATION ON THE PROCESSES OF INTRINSIC STRESS RELAXATION IN GaAs EPITAXIAL STRUCTURES	82
1.7. EFFECT OF MICROWAVE RADIATION ON THE GaAs MESFET CHARACTERISTICS.....	89
1.8. EFFECT OF MICROWAVE RADIATION ON THE PARAMETERS OF DISCRETE DEVICES AND INTEGRATED CIRCUITS.....	94
Part 2. LASER METHODS FOR DIAGNOSTICS AND MODIFICATION OF SEMICONDUCTOR COMPOUNDS (GaAs, InSb, SiC), AS WELL AS FORMATION AND DIAGNOSTICS OF STABLE OHMIC CONTACTS.....	101
INTRODUCTION	101
2.1. MODEL FOR DEFECT PRODUCTION IN III-V SEMICONDUCTOR COMPOUNDS BY NANOSECOND LASER PULSES	104
2.2. TECHNIQUES AND EQUIPMENT	108
2.2.1. A plant for laser pulse sputtering	108
2.2.2. A plant for laser modification of semiconductors	109
2.3. LASER MODIFICATION OF GaAs AND InSb	111
2.4. LASER DIAGNOSTICS OF NONEQUILIBRIUM CHARGE CARRIERS IN SEMICONDUCTORS	121
2.4.1. A contactless technique for determination of bipolar diffusion coefficient for nonequilibrium charge carriers.....	121

2.4.2. A complex technique for diagnostics of electron-hole plasma	123
2.4.3. Photoconductivity of InSb under picosecond excitation	130
2.5. DEVELOPMENT OF STABLE OHMIC CONTACTS TO <i>n</i>-α-SiC AND <i>p</i>-GaAs USING LASER TECHNOLOGY.....	138
 2.5.1. Contacts to <i>n</i>-α-SiC.....	138
 2.5.2. Contacts to <i>p</i>-GaAs	144
2.6. LASER-THERMAL DIAGNOSTICS OF METAL– SEMICONDUCTOR CONTACT STRUCTURES	149
CONCLUSION.....	162
REFERENCES	163

PRINCIPAL ACRONYMS AND SYMBOLS

A	- acceptor
AES	- Auger electron spectroscopy
D	- donor
G-(ir)radiation	- gyrotron (ir)radiation
IC	- integrated circuit
LI	- laser irradiation
LM	- laser modification
MBE	- molecular-beam epitaxy
MCE	- magnetoconcentration effect
MESFET	- metallized semiconductor field-effect transistor
M-(ir)radiation	- magnetron (ir)radiation
NCC	- non-equilibrium charge carriers
PC	- photoconductivity
PL	- photoluminescence
PR	- plasma resonance
QFR	- quasi-forbidden reflection
RTD	- resonant tunneling diode
SB	- Schottky barrier
SCR	- space-charge region
TBRTD	- two-barrier resonant tunneling diode
TIQFR	- total intensity of quasi-forbidden reflections
USP	- ultrashort pulses
XPS	- x-ray photoelectron spectroscopy
XRD	- x-ray diffraction
<i>A</i> [*]	- Richardson constant
<i>B</i>	- magnetic induction
<i>C</i>	- capacitance
<i>c</i>	- concentration in atomic %
<i>D</i>	- diffusion coefficient

d	- thickness
d_0	- crystal lattice constant
d_f	- film thickness
d_δ	spacing between two δ -layers
d'	- depth measured from the sample surface
E	- energy; electric field
E_a	- activation energy
E_b	- electron binding energy
E_F	- Fermi energy
E_g	- semiconductor energy gap
E_j	- electric field in the p - n junction
E_p	- pulse energy
E_t	- energy position of recombination center; impurity energy level
E_{th}	- electric degradation threshold
F	- force
f	- magnetron (gyrotron) frequency
H	- magnetic field
$H_{1/2}$	- PL band half-width
h ($= 2\pi\hbar$)	- Planck's constant
I	- radiation intensity; current
I_c	- cutoff current
I_{ch}	- channel current
I_d	- drain current
I_{ex}	- excess current
I_i	- flow of diffusing ions of the i -th type
I_{PL}	- intensity of photoluminescence
I_R	- reverse current
I_{th}	- threshold value of radiation intensity
K	- light absorption coefficient
k	- Boltzmann constant
L	- NCC bipolar diffusion length

L_D	- Debye shielding length
L_p	- hole diffusion length
l	- mean free path
l_j	- width of p - n junction
N_A	- acceptor concentration
N_D	- donor concentration
N_d	- dislocation density
N_i	- concentration of ions of i -th type
N_p	- number of laser pulses
N_t	- concentration of recombination centers; impurity concentration
N_v	- vacancy concentration
N_δ	- impurity concentration in the δ -layers
n	- electron concentration; ideality factor
n_i	- intrinsic charge carrier concentration
n_s	- surface electron concentration
P	- power
p	- hole concentration
Q^*	- heat of vacancy migration
q_0	- elementary charge
R_c	- contact resistance
R_H	- Hall constant
r	- bulk recombination rate
r, θ, z	- cylindrical coordinates
r_{AD}	- distance between D and A
S	- transconductance
S_b	- laser beam cross section
S_c	- contact area
S_r	- surface recombination velocity
S_s	- sample surface area
T	- temperature
t	- time

$t^{\text{G(M)}}$	- duration of gyrotron (magnetron) irradiation
t_p	- pulse duration
V	- voltage
V_c	- cutoff voltage
V_R	- reverse voltage
W	- irradiance
W_B	- potential barrier height
W_{th}	- thermal degradation threshold
w	- width of space-charge region
Δ	- depth of electromagnetic field penetration
ε	- electron energy
ε_0	- semiconductor permittivity
η	- quantum efficiency of photoionization
λ	-wavelength
μ	-charge carrier mobility
μ_0	-semiconductor permeability
$\nu = E/\hbar$	- frequency
ρ	- resistivity
σ	- conductance
σ_{hkl}	- specific surface energy
τ_p	- hole lifetime
φ	- potential
φ_B	- Schottky barrier height
ω	- angular frequency

INTRODUCTION

The scientific and technological progress in solid-state electronics and related areas derives, to a great extent, from use of high technologies. Among them are the so-called "beam" technologies, namely, laser and microwave ones [1-8]. Their feature is a wide range of applications involving both military and non-military ones. To illustrate, the above technologies have been used when developing the means for functional damage (the "Star Wars" and Strategic Defense Initiative programs) [9-11]. As to their non-military applications, they involve, among others, controlled synthesis of new materials [12-16], novel gettering techniques [17,18] and formation of ohmic and barrier contacts [19-23]. Besides, the above technologies are used in fundamental investigations of interaction between focused beams and nonuniform media [24,25] (in particular, studies of diffusion and mass transport [26,27]). Simulation of laser and microwave actions on discrete semiconductor devices and integrated circuits [28,29] is intensely used to predict reliability of the developed element base.

Microwave and laser treatments are used for rapid annealing of semiconductor layers after ion implantation [30-33]. Many authors have studied various effects of such treatments on the properties of GaAlAs/GaAs/GaAlAs/GaAl thin-film multilayer structures [34], electrical parameters of threadlike Si crystals, Ge–Si solid solutions, GaAs and GaAsP, strength of

GaAs [35] and Si [36] crystals, photoelectric properties of nonuniform CdS single crystals and nonequilibrium effects in CdS photodetectors [37,38], possibilities for control over the defect structure of Si and Ge single crystals [39].

Numerous practical aspects of using microwave and laser radiations in technology of semiconductor materials and devices are protected by many patents issued in different countries. To illustrate, let us note only those dealing with processing of semiconductor materials and devices [40-44], silicon ingot slicing [46], doping of semiconductor materials and formation of low-resistance contacts [19]. One can see that they cover practically all stages of manufacturing of semiconductor materials, structures and devices.

Application of microwave and laser processing becomes particularly efficient when producing devices of submicron sizes. These techniques make it possible to get rid of a number of technological flaws inherent in traditional thermal processing. In this case one can exert control over the micro-device characteristics and correct them using electromagnetic radiation. In recent years such experiments have been performed for tunnel diodes [47,48] and planar-epitaxial multiplying diodes 2A604 [49-52]. These experiments demonstrated that negative differential resistance might appear in the above devices. This was concluded from the form of the forward branch of I - V curves of tunnel diodes (at voltages below the peak values) and multiplying diodes. The above effect is of importance for understanding of interaction between microwave radiation and such complex semiconductor objects.

The physical effects occurring in thin semiconductor films and at semiconductor surfaces exposed to laser radiation have been discussed as early as 30–35 years ago by Vavilov and Galkin [53,54] and Fairfield, Schwuttke, Harper

and Cohen [55,56]. In that time many research centers all over the world have enjoyed the "laser" boom. As a result, the efforts of numerous investigators have been focused on laser physics and its applications in solid state physics. The pioneer works on laser pulse annealing of ion-implanted semiconductor layers have been made by Khaibullin (Physico-Technical Institute of the Kazan Division of the Academy of Sciences of the USSR) and Smirnov et al. (Institute of Semiconductor Physics of the Siberian Division of the Academy of Sciences of the USSR) [57-61]. Various practical aspects have been considered by Hess, Olson, Gibbons and other researchers who were at the outset of application of laser techniques in electronic industry [62-64]. Similar investigations have been also made at the Institute of Semiconductors of the Academy of Sciences of the Ukrainian SSR (now Institute of Semiconductor Physics of the National Academy of Sciences of Ukraine) by Litovchenko, Glinchuk, Lysenko, Malyutenko et al. [65-67], Institute of Physics of the Academy of Sciences of the Ukrainian SSR by Brodin et al. [68,69] and Institute of Applied Problems of Mechanics and Mathematics by Tovstyuk, Kiyak et al. [70-72]. It is practically impossible to name all the research teams that have contributed to understanding of physical foundations of laser technologies and their application for manufacturing of semiconductor materials and devices.

However, despite the fact that the technologies using electromagnetic radiation seem rather simple and our knowledge of the corresponding processes is extensive, a number of problems, both fundamental and technological, still remain unsolved. They involve, in particular:

- micrometallurgical processes at semiconductor surfaces and interfaces enhanced by electromagnetic radiation;

- defect production in semiconductor near-surface layers and at interfaces;
- processes of stress generation and relaxation induced by microwave and laser radiations;
- structural phase transitions occurring in the nano- and sub-nanosecond ranges of irradiation duration.

Some aspects of approaches to solution for these problems are given in this book. The authors made an attempt to generalize the existing material in the area leaning upon their own results, as well as those known from literature. They do not lay claim to an exhaustive presentation of all the problems touched upon in this book because new works dealing with interaction between microwave radiation and various semiconductor objects still continue to appear every day.

* * *

The authors are grateful to all those researchers from the Institute of Semiconductor Physics of the National Academy of Sciences of Ukraine (Kiev), Institute of Physics of the National Academy of Sciences of Ukraine (Kiev), E.O. Paton Institute of Electric Welding of the National Academy of Sciences of Ukraine (Kiev), Physico-Technical Institute of the National Academy of Sciences of Ukraine (Kharkov) and Institute of Technical Physics of the Hungarian Academy of Sciences (Budapest) who took part in experimental investigations and whose results are presented in this book.

Part 1. INVESTIGATION OF BOUNDARIES BETWEEN PHASES IN HETEROGENEOUS STRUCTURES AND THEIR MODIFICATION UNDER MICROWAVE RADIATION

INTRODUCTION

Requirements for the semiconductor element base involve its high tolerance to various beam actions, in particular, to high-power microwave irradiation. So far most of theoretical and experimental studies have been aimed at elucidation of the role of static (or rather low-frequency) actions in degradation processes that occur in semiconductor materials and devices during their operation. The problem of interaction between high-power microwave electromagnetic fields and semiconductor materials and devices that would combine approaches of both physics and materials science has not been studied up to the present. There are practically no data relating electro-physical properties of the above objects to the features of their microstructure and chemical composition.

At the same time it is known that exposure of device structures and finished products (both discrete and integrated) to microwave irradiation results, in a number of cases, to their degradation and even failure [1–4]. Of all the components of any circuit, semiconductor elements are most sensitive to high-power microwave radiation [2]. Depending on the absorbed power, frequency, temporal parameters of action and object tolerance, one can observe different stages of device degradation, namely, (i) short-duration failures - at low levels

of action; (ii) irreversible changes of parameters and characteristics with relative retention of efficiency – at moderate levels of action; (iii) complete failures (accompanied by thermal effects and electric breakdown) leading to loss of efficiency – at high levels of action. The power (frequency) of radiation that leads to device degradation ranges between several μW and several hundreds W (50 MHz and ≥ 10 GHz).

On the other hand, some authors have indicated at a possibility for microwave treatment application to modify defect structure in semiconductors [5–8]. To illustrate, it was shown in [5] that microwave radiation of frequency $f = 2.5$ GHz could be used for post-implantation annealing of silicon, and such treatment proved to be more efficient than thermal annealing. The authors of [6] stressed that high-power microwave radiation is promising for rapid contactless annealing of GaAs. They reasoned that no abrupt temperature gradients and diffusion stresses appeared in this case.

A considerable modification of dislocation structure due to microwave annealing ($f = 37$ GHz, power $P = 0.1$ kW) has been found in [7] for silicon wafers. The kinetics of residual stress relaxation was found to substantially differ from that in the case of traditional thermal annealing in the air or vacuum. It was characterized by complicated oscillations with pronounced non-thermal sections. In [8] microwave relaxometry has been applied to demonstrate that microwave irradiation of n -Si results in changing parameters of impurity aggregations and growth of charge carrier lifetime.

The above results served as a reason for performing some experimental studies whose objective was to determine effect of microwave radiation beams on structural-chemical and electrophysical characteristics of both semiconductor materials and device structures. The results obtained are given in what follows.

1.1. EXPERIMENTAL TECHNIQUES

The investigations were concerned with different subjects. First of all, we dealt with single-crystalline wafers of gallium arsenide, indium phosphide and gallium phosphide, with free electron concentration n from about 10^{16} up to $2 \times 10^{17} \text{ cm}^{-3}$. They were prepared for production of device structures using standard technological procedures. Besides, we studied $n\text{-Cd}_x\text{Hg}_{1-x}\text{Te}$ ($x = 0.21\text{--}0.24$) wafers that have been cut out of ingots and put through mechanical treatment and etching.

The second class of subjects used by us involved metal–semiconductor structures of III–V type. They were prepared in a vacuum (pressure of 10^{-4} Pa) using thermal or electron-beam evaporation of metals onto chemically cleansed surfaces of GaAs, GaP and InP. The metals used for contact formation enabled us to obtain either chemically inert or chemically active metal–semiconductor interfaces [9]. In the latter case it was possible, by proper choice of heteropairs, provide domination of either diffusion processes at interfaces or chemical reactions between the contact pair components.

Contact structures with antidiffusion barriers based on metal nitrides and borides belonged to the third class of subjects that we investigated. They were fabricated using magnetron sputtering [10]. And still another group of subjects was made by $\text{Al}_x\text{Ga}_{1-x}\text{As}$ –GaAs resonant tunneling homo- and heterostructures that were formed using molecular-beam epitaxy (MBE) [11].

The samples (wafers) studied were exposed to directional irradiation from cm and mm wavelength ranges under free-space conditions. The output signal power P for magnetron irradiation (M-irradiation) was 5 kW at a frequency $f = 2.45 \text{ GHz}$. That for gyrotron irradiation (G-irradiation) was 50 kW at $f = 84 \text{ GHz}$. To

perform comprehensive studies of the features of interaction between microwave radiation and subjects of investigation, we applied a complex of techniques that enabled us to obtain information on electrophysical parameters of samples, their defect structure and chemical composition.

The spectra of local states due to structural defects were found from analysis of photoluminescence (PL) curves taken at a temperature $T = 77$ K in the 0.6–2.0 eV spectral range. The samples were illuminated with light ($h\nu > 2$ eV) from a high-power incandescent lamp ПЖ-100.

Measurements of Hall effect and dark conductivity gave us data on electron concentration n and mobility μ in the samples studied. The lifetime τ_p of minority charge carriers (holes), as well as concentration N_t and energy position E_t of recombination centers, were determined from temperature dependence of photoconductivity (PC) [12]. An analysis of steady-state $I-V$ curves [13] enabled us to determine the following characteristics: from forward branches – the contact barrier height $\varphi_B = \frac{kT}{q_0} \ln \frac{A^* T^2 S_c}{I_c}$ (here I_c is the cutoff current, A^* is Richardson constant, k is Boltzmann constant, q_0 is the elementary charge, S_c is the contact area) and ideality factor $n = \frac{q_0}{kT} \frac{\partial V}{\partial(\ln I)}$; from backward branches – effective lifetime of minority charge carriers $\tau_p = \frac{q_0 n_i w S_c}{2 I_R}$ (here I_R is the reverse current, w is the space-charge region (SCR) width, n_i is the intrinsic charge carrier concentration).

The concentration depth profiles of the heterostructure components were determined using Auger electron spectroscopy (AES) [14] combined with layer-by-layer etching by Ar^+ ions (energy of 1 keV). The Auger spectra were taken in the

differential mode. The primary electron energy was 3 keV. The component concentrations in the transition layer were calculated using the elemental sensitivity coefficients [14].

The information concerning phase composition of the subjects studied was obtained using x-ray photoelectron spectroscopy (XPS) [14]. Mg $K\alpha$ emission ($h\nu = 1253.6$ eV) served as source of excitation.

1.2. EFFECT OF HIGH-POWER ELECTROMAGNETIC RADIATION ON THE DEFECT STRUCTURE OF SEMICONDUCTOR MATERIALS

1.2.1. III-V semiconductor compounds

Shown in Figs.1.1–1.5 are the PL spectra of some III–V semiconductor compounds, as well as band intensity I_{PL} , half-width $H_{1/2}$ and peak position $h\nu_m$ as function of time t of exposure to magnetron and gyrotron treatments. The treatment modes are given in figure captions [15].

One can see that there are two overlapping bands in the PL spectra of initial GaAs crystals. Their peak positions $h\nu_m^1$ and $h\nu_m^2$, as well as ratio between intensities, depend on the dopant type and sample surface orientation.

GaAs:Sn (111). In these crystals the spread of $h\nu_m^{1,2}$ values for the observed PL bands is bigger than those in other samples. It was possible to separate the samples studied into three groups, namely, those with $h\nu_m^1 = 1.150, 1.200$ and 1.186 eV. The $h\nu_m^2$ values for the second band demonstrated smaller spread; they were $h\nu_m^2 = 0.993\text{--}1.010$ eV. The intensity of band 1 was by a factor of 2–5 bigger than that of band 2. The half-width of band 2 was, as a rule, less than that of band 1 (100–150 and 200–230 meV, respectively).

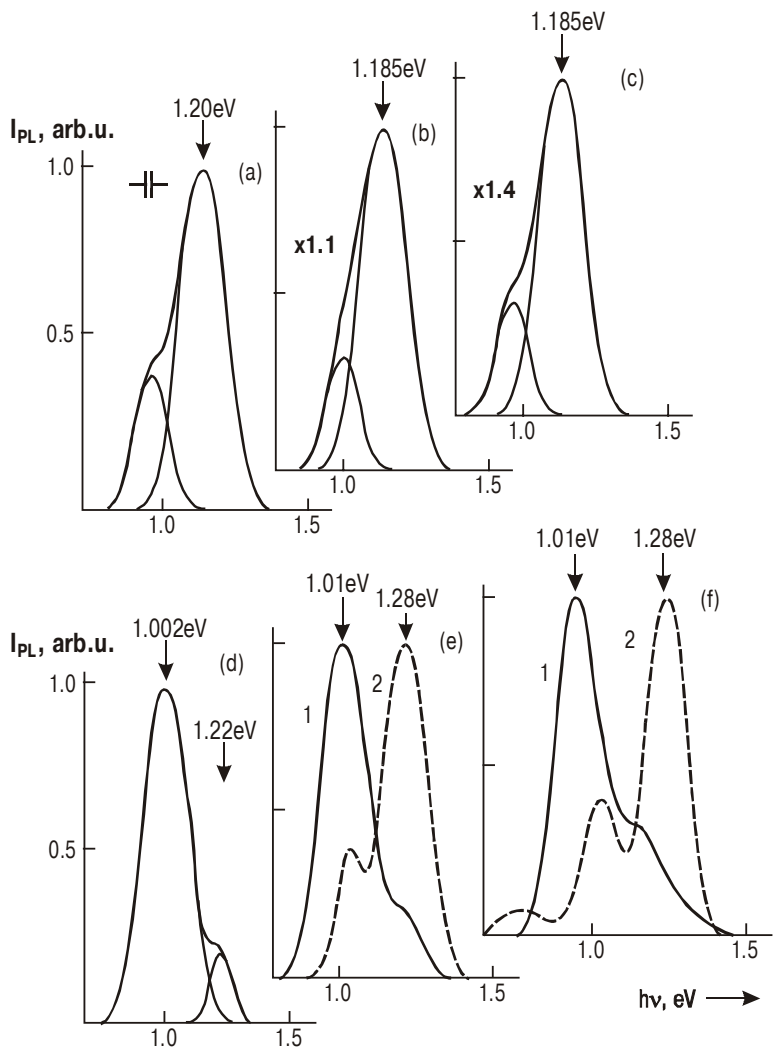


Fig.1.1. PL spectra taken at $T = 77$ K for GaAs:Sn (111) (a–c) and GaAs:Sn (100) (d–f) samples before (a, d) and after magnetron (exposure time $t^M = 10$ s (b), 60 s (c)) and gyrotron (exposure time $t^G = 1$ s (e1), 10 s (e2), 4 s (f1), 40 s (f2)) irradiation [15].

The band 1 parameters are more affected by microwave irradiation. In the case of M-irradiation even at exposure time $t^M < 2$ s the $h\nu_m^{1,2}$ values become the same for the samples from all groups: $h\nu_m^1 = 1.185$ eV, $h\nu_m^2 = 1.010$ eV. These are just the values that are observed for the initial samples from the third group. The $h\nu_m^{1,2}$ values change unevenly; for the samples belonging to the first group both band intensity and half-width change just in this way.

For the crystals from the first and second groups the intensity of band 1 grows slightly with t^M , and this band becomes narrower, while the parameters of band 2 remain practically the same. For the crystals belonging to the second group at $t^M = 10$ and 20 s $h\nu_m^2 = 1.280$ eV, and the intensity of band 2 becomes higher than that of band 1. M-irradiation does not affect the parameters of both bands in crystals from the third group.

G-irradiation of the crystals belonging to the first group strongly decreases the intensity of band 1, while slightly affecting that of band 2. The case of the mode with time of exposure $t^G = 40$ s is an exception: the intensity of band 1 drops even more abruptly, but that of band 2 increases and becomes higher than the intensity of band 1. In crystals from the third group the PL peak positions do not shift (just as in the case of M-irradiation), but intensities of both bands grow (that of band 2 grows somewhat stronger). As a rule, M- and G-irradiations of the crystals from all groups lead to a decrease of the half-widths of both bands. When the $h\nu_m$ values change abruptly, then the half-widths of both PL bands also change abruptly at the same values of $t^{M,G}$.

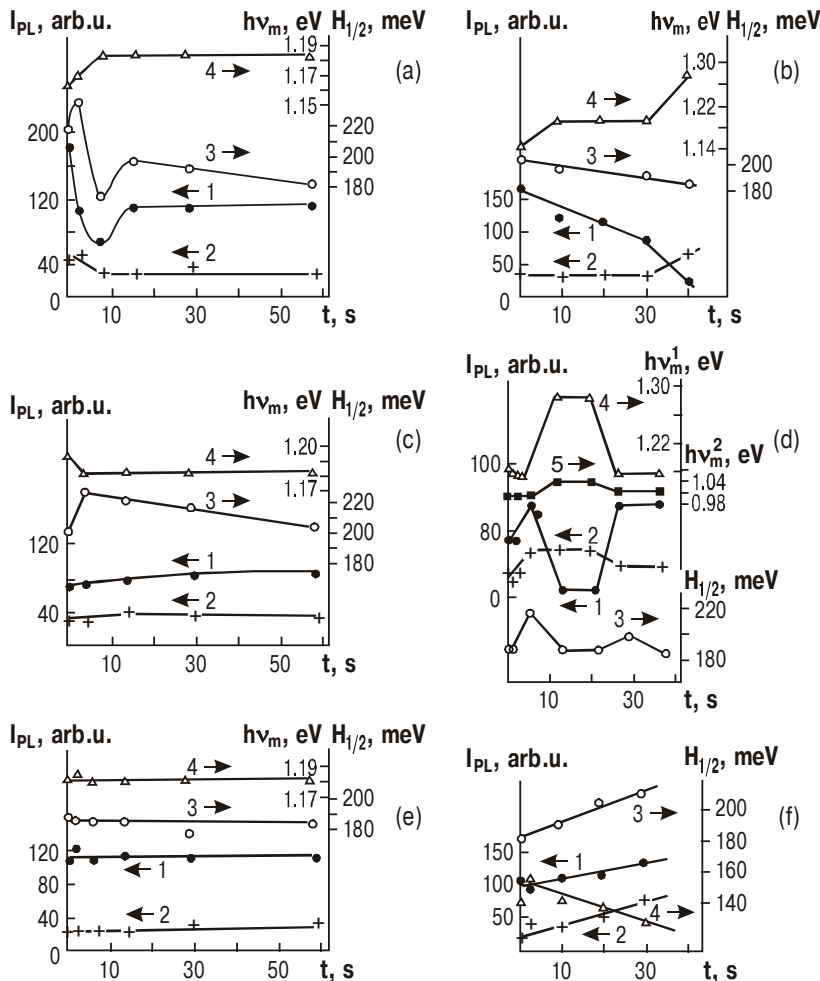


Fig.1.2. Band intensity I_{PL} (curves 1, 2), half-width $H_{1/2}$ (curve 3) and peak position $\hbar\nu_m$ (curves 4, 5) as function of exposure time t for bands 1 (curves 1, 3, 4) and 2 (curves 2, 5) taken at $T = 77$ K for GaAs:Sn(111) samples from groups 1 (a, b), 2 (c, d) and 3 (e, f). a, c, e – magnetron irradiation, b, d, f – gyrotron irradiation [15].

GaAs:Sn (100). At this orientation of the GaAs:Sn crystal surface two overlapping PL bands are also observed. In this case, however, the band 2 with $h\nu_m^2 = 0.996 \pm 1.002$ eV is more intense. For the band 1 $h\nu_m^1 = 1.220 \pm 1.240$ eV for different samples in the initial state (see Fig.1.3). At $t^M = 2$ s the intensity of band 2 drops abruptly, and the peak positions become $h\nu_m^1 = 1.240$ eV and $h\nu_m^2 = 1.010$ eV. For times of exposure t^M lying in the 2–30 s range $h\nu_m^{1,2}$ retain their values; the intensity of band 1 decreases, while that of band 2 grows. At $t^M = 60$ s the $h\nu_m^1$ value becomes equal to 1.280 eV, as that for the GaAs:Sn (111) samples.

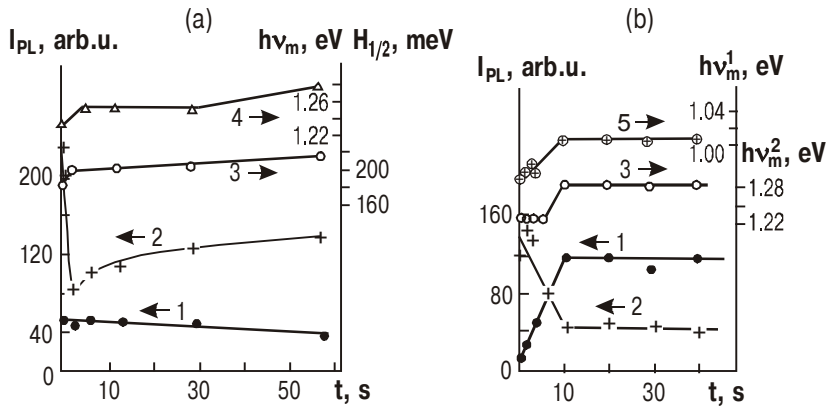


Fig.1.3. Band intensity I_{PL} (curves 1, 2), half-width $H_{1/2}$ (curve 3) and peak position $h\nu_m$ (curves 4, 5) as function of exposure time t for bands 1 (curves 1, 3, 4) and 2 (curves 2, 5) taken at $T = 77$ K for GaAs:Sn (100) samples. a – magnetron irradiation, b – gyrotron irradiation [15].

At $t^G = 1$ s the intensity of band 1 (2) grows (decreases); the $h\nu_m^1$ value does not change and is 1.240 eV, while $h\nu_m^2$ value becomes 1.010 eV. At $t^G = 10$ s the $h\nu_m^1$ value becomes 1.280 eV and remains the same for t^G up to 40 s. In this case the intensity of band 1 is higher than that of band 2, and such relationship between them retains up to the maximal value (40 s) of the time of exposure t^G used – Fig.1.3b.

GaAs:Te (111). The M-radiation practically does not affect both the half-width and $h\nu_m$ value for the PL band 1.200 eV, while its intensity grows with time of exposure t^M (Fig.1.4b). G-radiation does not influence the band form too, while its intensity changes non-monotonically: it grows at t^G up to 10s and then decreases down to the initial value (at $t^G = 40$ s) – Fig.1.4c.

InP (100). Three PL bands are observed in the PL spectrum of the initial crystals: that with $h\nu_m^1 = 1.410$ eV, a band at 1.150 eV with structural features and a band at 0.820 eV. The most intense is the band at 1.410 eV - see Fig.1.5. Both M- and G-radiations do not change the peak positions for the observed bands, but that at 1.150 eV becomes devoid of its structure. The intensity of band 1.410 eV slightly drops at small times of exposure t^M and then becomes to grow. The intensities of the rest of bands grow too but much more slightly than that of the band 1.410 eV – see Fig.1.5b, c.

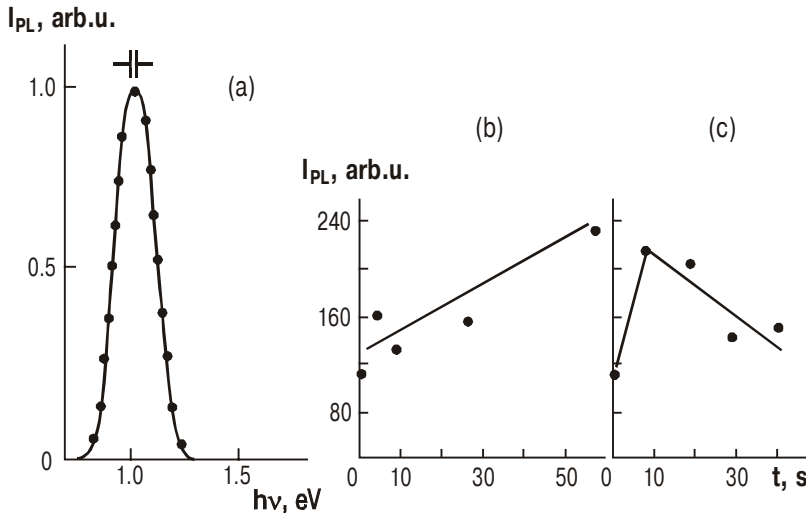


Fig.1.4. a - PL spectra taken at $T = 77$ K for GaAs:Te (111) samples before (full curve) and after (dots) gyrotron irradiation (exposure time $t^G = 40$ s); b (c) – band intensity I_{PL} as function of exposure time for magnetron (gyrotron) irradiation [15].

The above results evidence that the initial impurity-defect state of the GaAs near-surface layers is determined by the type of dopant and crystallographic orientation of the wafer face, as well as by unintentional impurities that can “contaminate” the crystal surfaces during their treatment (for instance, from the etchant). In addition, one should take into account that intrinsic stresses (that appear in the GaAs wafers during single crystal slicing and further chemical-mechanical treatment) can also affect the defect composition of the near-surface layers through their enrichment or depletion with vacancies.

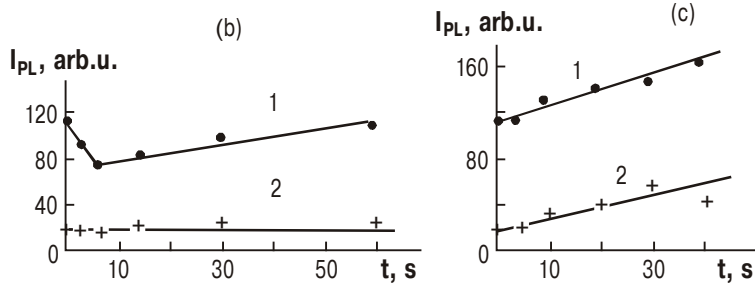
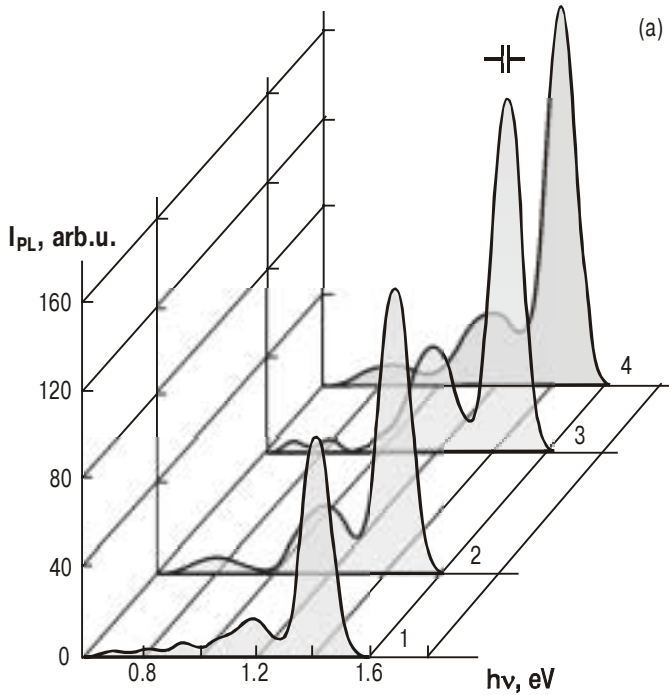


Fig.1.5. a - PL spectra taken at $T = 77$ K for InP (100) samples before (1) and after gyrotron irradiation (exposure time $t^G = 10$ s (2), 30 s (3), 40 s (4)); b (c) – band intensity I_{PL} as function of exposure time for bands 1.41 eV (curves 1) and 1.15 eV (curves 2). b – magnetron irradiation, c – gyrotron irradiation [15].

It is known from literature that the centers responsible for the band 1 in GaAs:Sn with $h\nu_m^1 = 1.150\text{--}1.220$ eV are the donor-acceptor (D–A) complexes ($V_{\text{Ga}} + \text{Sn}_{\text{Ga}}$), while those responsible for the band 2 are the individual acceptors Cu_{Ga} (see, e.g., [16]). Our experimental results, in particular the fact that the band 2 is rather narrow as compared to the band 1, are not in contradiction with the above suggestions. A spread of the $h\nu_m^{1,2}$ values that has been observed by many authors, as well as by us for different initial samples, could result from both different distances r_{AD} between donor (D) and acceptor (A) in the above complexes and a possibility of nonequivalent D and/or A positions in the crystal lattice. The latter factor may stem from the presence of other defects, intrinsic stresses, dislocations, etc. in the nearest neighborhood of D and A. All this determines the so-called nonuniform broadening of the PL bands.

The ratio between the intensities of bands 1 and 2 in the GaAs:Sn wafers that have been cut of the same single-crystalline ingot and exposed to the same chemical-mechanical treatment but have different orientation of crystallographic planes may vary from sample to sample. This may be related to high V_{Ga} concentration in the near-surface layers of the GaAs (111) face as compared to the case of the (100) face. It is known that the energy properties of III–V crystals are anisotropic. This means that the surface energy values for principal crystallographic planes are different [17]: $\sigma_{100} > \sigma_{110} > \sigma_{111}$, where σ_{hkl} is the specific surface energy. So one could assume that concentration of intrinsic defects (vacancies) is higher at the crystal face with smaller surface energy.

Both abrupt change of the peak position for band 1 in GaAs:Sn (111) and change of the band half-width occur at

very short times of exposure t^M . This fact indicates that even such short-term microwave actions lead to lattice ordering and make the r_{AD} values in complexes equal for different samples. The centers responsible for $h\nu_m^1 = 1.185$ eV were found to be the most stable D-A complexes. It will be recalled that just the same value of $h\nu_m^1$ was observed in the PL spectra for the samples belonging to the third group. Their PL properties did not change during M-irradiation up to the highest exposures ($t^M = 60$ s). It seems likely that the GaAs:Sn (111) crystals from the third group were the most perfect (uniform) among all the crystals we studied.

The effect of M-irradiation on the band 1 in GaAs:Sn (111) crystals is characterized by some selectivity. This fact indicates that when lattice becomes more ordered during microwave irradiation in the modes used, then the channel of radiationless recombination is not affected. Otherwise the intensities of both bands would change in similar ways ($\sum_i R_i = 1$ under the same conditions of PL excitation before

and after microwave action; here R_i is the fraction of the recombining charge carriers flow through the i -th channel of radiation(less) recombination [18]). Just such similar behavior of both bands has been observed for the GaAs:Sn (111) crystals from the third group under G-irradiation. This fact indicates that G-irradiation reduces the contribution from the radiationless recombination channel to the total recombination flow.

Some small growth of the band 1 intensity with time of exposure t^M for the GaAs:Sn (111) crystals from the first and second groups seems to result from the fact that M-radiation either enhances V_{Ga} concentration growth in the near-surface layers of the above crystals or favors more intense formation of complexes by V_{Ga} and Sn_{Ga} that are present there. (The lat-

ter process is realized through lattice ordering by removing other defects that could prevent the complex formation.) The first of the above ways should be favored because, if the second way would realize, then one could observe transformation of a PL band related to V_{Ga} into the 1.185 eV band, and this has not been experimentally found. The experiments also evidence that the band 2 is related to the unintentional individual Cu_{Ga} impurities. In the case of GaAs:Sn (111) M-radiation practically does not affect this band.

In the GaAs:Sn (100) crystals the PL band with $h\nu_m^1 = 1.240$ eV was observed. The centers responsible for this band are acceptors Sn_{As} [16]. At $t^M = 60$ s and $t^G \geq 10$ s the V_{Ga} concentration increases, and the $(\text{Cu}_{\text{Ga}} + V_{\text{Ga}})$ complexes responsible for the 1.280 eV band are formed [16]. That complex formation occurs at the above irradiation modes is confirmed by the fact that the intensity changes for both bands are proportional (Fig.1.3).

In the GaAs:Te (111) crystals the centers $(V_{\text{Ga}} + \text{Te}_{\text{Ga}})$ responsible for the only band with $h\nu_m = 1.200$ eV [18] are stable. Neither M- nor G-radiation changes the form of this band. And the band intensity change with $t^{M,G}$ seems to result from the effect of irradiation on the radiationless recombination centers.

No unambiguous interpretation of the band 1.410 eV in InP exists in literature. Some authors relate it to the Si unintentional impurity that is encountered most often, while the others relate it to the V_p (vacancies of phosphorus) or band-to-band recombination of the nonequilibrium charge carriers (NCC). The asymmetric band in the 1.060–1.150 eV range that often has a phonon structure is related to the $(\text{Fe}_{\text{In}} + V_p)$ complexes [16]. The fact that the 1.410 eV band is relatively narrow (as compared to the 1.150 eV band) enables one to

prefer the model of individual acceptors (V_p) for centers responsible for that band. An increase in the intensities of both bands after M- and G-irradiations indicates at a possible growth of the concentration of phosphorus vacancies V_p (responsible for the 1.410 eV band) that are among the centers responsible for the second band. The individual acceptors V_p have larger capture cross-section for nonequilibrium holes as compared to the case of D-A complexes [18]. Therefore growth of the V_p concentration has to make a strong effect on the intensity of the 1.410 eV band. This is just what has been observed experimentally.

Thus we have shown that microwave irradiation of GaAs and InP crystals affects their defect structure and modification of centers responsible for radiative recombination. The features of this influence depend on the dopant type and wafer face orientation. We have demonstrated an important role of vacancies in transformation of local centers in the near-surface regions of differently oriented GaAs wafers. The origin of centers responsible for PL in GaAs has been made clear. The facts that PL bands become narrower and PL peak positions are the same under M- and G-irradiations seem to be due to local heating of the nonuniformity regions.

The structure of GaP local centers practically did not change under microwave irradiations of cm and mm wavelength ranges that have been used in the cases of GaAs and InP [19].

1.2.2. $\text{Cd}_x\text{Hg}_{1-x}\text{Te}$ semiconductor solid solutions

Generally both the initial impurity-defect composition and morphology of semiconductor material influence the character of changes in its electrophysical parameters due to microwave irradiation. Indeed such influence has been confirmed by the

results of our studies of the narrow-gap semiconductors based on $\text{Cd}_x\text{Hg}_{1-x}\text{Te}$ solid solutions [19].

To illustrate, presence in the initial sample (#1 - see Table 1) of nonuniformities capable of leading to anomalies on the Hall constant vs temperature curve $R_H(T)$ (see Fig.1.6) manifests itself after microwave treatment through conduction type conversion and abrupt change in the minority charge carrier lifetime τ_p (Fig.1.7). For the rather uniform samples (#2, 3), however, the character of changes is qualitatively different. Microwave treatment of such samples leads to a substantial rise of τ_p . In this case the Hall constant R_H grows slightly in the impurity conduction region, and mobility μ somewhat decreases. The results obtained from the temperature dependence of τ_p evidence that the concentration of the active recombination centers whose energies are in the upper half of the gap decreases.

Table 1.1. Effect of microwave irradiation ($f = 2.45$ GHz, $W = 5$ kW/cm 2 , $t^M = 5$ s) on the electrophysical parameters (free electron concentration n and mobility μ , impurity ionization energy E_t and concentration N_t) of $\text{Cd}_x\text{Hg}_{1-x}\text{Te}$ at $T = 77$ K [19].

Sample #	Composition (x)	Type of treatment	n , cm $^{-3}$	μ , cm $^2/\text{V}\cdot\text{s}$	τ_p , μs	E_t , eV	N_t cm $^{-3}$
1	0.24	I*	6.9×10^{15}	2×10^4	0.61		
		MI	2.54×10^{16}	6×10^3	0.246		
2	0.21	I	5.12×10^{14}	2×10^5	1.4	0.1	1.1×10^{14}
		MI	4.9×10^{14}	1.5×10^5	2.4	0.1	3.6×10^{13}
3	0.22	I	4.82×10^{14}	1.4×10^5	2.1	0.7	6.25×10^{13}
		MI	4.6×10^{14}	9.6×10^4	3.0	0.7	2.5×10^{13}

* I – initial sample; MI – that after microwave irradiation.

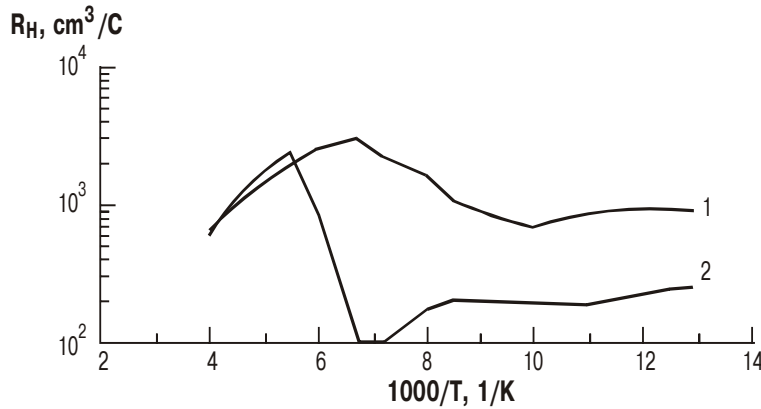


Fig.1.6. Hall coefficient R_H vs inverse temperature curves for sample 1 ($\text{Cd}_{0.24}\text{Hg}_{0.76}\text{Te}$) before (1) and after microwave irradiation for 5 s (2) [19].

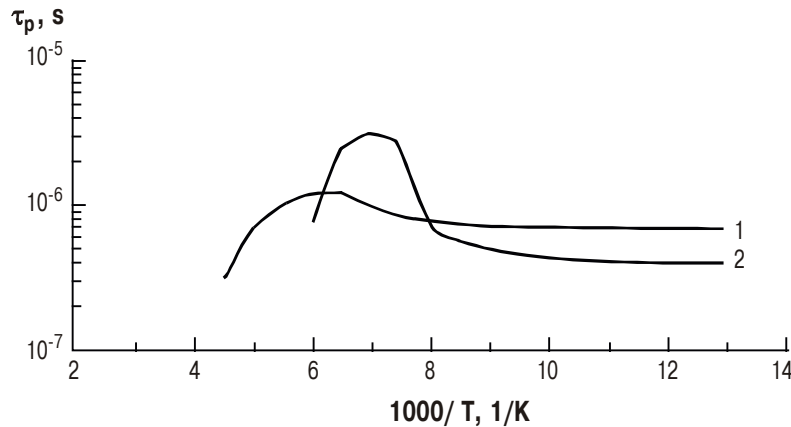


Fig.1.7. Minority charge carrier lifetime τ_p vs inverse temperature curves for sample 2 ($\text{Cd}_{0.21}\text{Hg}_{0.79}\text{Te}$) before (1) and after microwave irradiation for 5 s (2) [19].

Investigations of the effect of plastic deformation on the properties of samples from this group were performed both before and after microwave treatment. They have revealed an effect of improved tolerance of the electrophysical parameters of the irradiated samples for plastic deformation. We realized plastic deformation of the samples by indentation with a Wickers prism. The indenter load was 10 g; the indentation density was $N_{ind} = 10^4 \text{ cm}^{-2}$. One can conclude from Fig.1.8 that after microwave treatment the temperature dependencies of τ_p taken for the samples exposed to indentation were the same as those before microwave treatment [20].

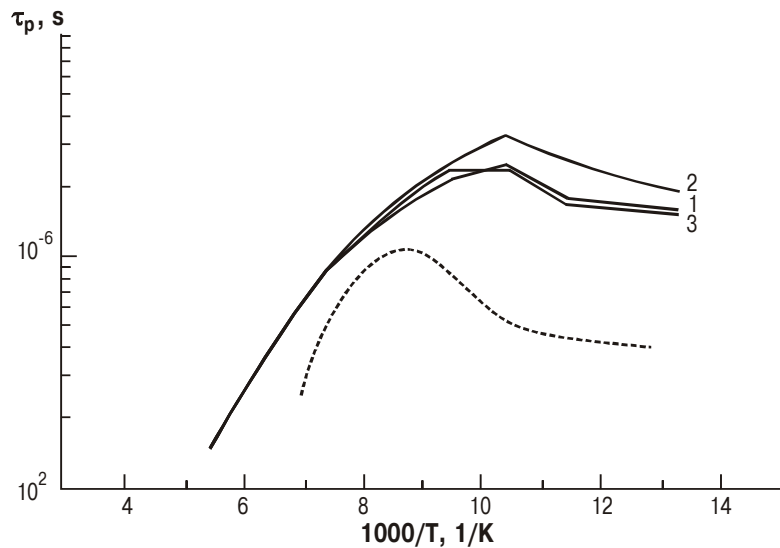


Fig.1.8. Minority charge carrier lifetime τ_p vs inverse temperature curves for $\text{Cd}_{0.2}\text{Hg}_{0.8}\text{Te}$ samples before (1) and after microwave treatment (2); 3 – 18 h after microwave treatment and indentation. Dotted line corresponds to the case of indentation load of 10 g and indentation density of 10^4 cm^{-2} [20].

No R_H changes in the impurity conduction region have been observed, and the ionization energy of the active recombination centers remained the same, contrary to the case of the samples that were not exposed to microwave treatment.

If one assumes that the main energy dissipation mechanism in the irradiated samples is heating, then the observed features of the changes in material parameters could result from the enhanced migration of the active recombination point defects and impurities to the energy-stable drains, such as low-angle boundaries, dislocations, etc. One should not also exclude decay of the metastable defects that are "frozen" at room temperature and diffusion of their components to the thermally stable extended defects. Such enhanced gettering manifests itself through some τ_p growth. The dislocations that are introduced under indentation penetrate through the whole sample thickness rather quickly (the τ_p values measured for both indented and non-indented sample surfaces are the same). However, formation of their atmospheres occurs under conditions when the number of defects that are forming the impurity dislocation atmospheres is substantially below that in the samples that were not exposed to microwave treatment. As a result, the dislocations that are introduced under indentation cannot form the impurity atmospheres that could qualitatively modify the recombination characteristics of a sample.

Thus microwave treatment of semiconductor materials essentially influences the structure-sensitive characteristics for not only wide-gap semiconductors but narrow-gap ones as well. A degree of this influence depends on the nature and past history of semiconductor material, as well as irradiation modes. Microwave treatment can result in improvement of the material parameters (homogenization, defect gettering) and

their degradation as well. To give the ultimate answer concerning mechanisms for structural relaxation in semiconductors exposed to microwave treatments, further investigations are needed.

1.3. INTERACTIONS BETWEEN PHASES

IN Me–GaAs (InP) CONTACTS STIMULATED BY MICROWAVE IRRADIATION

The structural-chemical processes that occur at boundaries between phases in contacts results in changes of the electro-physical characteristics of contacts and affect their operating stability at abrupt changes of the operating modes [21,22]. Therefore the required structure of boundaries between phases, as well as possibility for its realization over large areas, should be provided during device manufacturing.

In what follows the principal physico-chemical processes are considered that affect the characteristics of the transition layers in contact exposed to microwave treatment, as well as dependence of these processes on the nature of deposited material and deposition modes.

1.3.1. Effect of magnetron irradiation on the physico-chemical processes in Me–GaAs (InP) contacts

Shown in Figs.1.9, 1.10 are the Auger concentration depth profiles for the components of Al– n - n^+ -GaAs and Al– n - n^+ -InP contacts taken both before and after microwave treatments. These profiles represent the character of the structural-chemical transformations that occur at boundaries between phases in the structures studied.

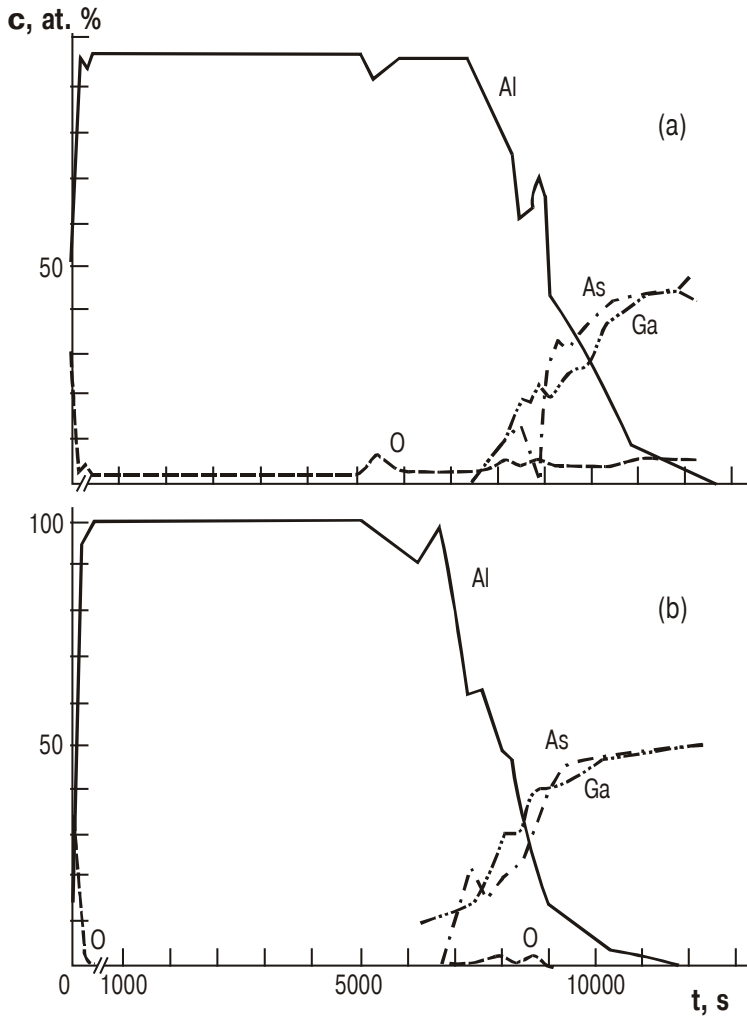
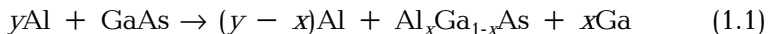


Fig.1.9. Auger concentration depth profiles for the components of $\text{Al}-n-n^+$ -GaAs heteropair before (a) and after (b) magnetron irradiation (irradiance of 100 W/cm^2 , exposure time $t^M = 1 \text{ min}$); t is duration of ion etching [20].

The profiles taken for the Al- n - n^+ -GaAs contacts are monotone, contrary to those measured for the Al- n - n^+ -InP contacts. Taking into account the character of non-monotony for the concentration depth profiles of Al, Ga and As in the Al- n - n^+ -GaAs contacts, one can assume that at the Al-GaAs interface exposed to microwave treatment the following substitution reaction seems most likely to occur:



even though rather high (> 725 K) temperature is needed for its intense proceeding. Besides, microwave treatment results in formation of an oxide layer on the Al surface (see Fig.1.9) [20].

Contrary to the above, one can conclude from Fig.1.10 that in the case of the Al- n - n^+ -InP contact no chemical reactions stimulated by microwave irradiation occur, and the transition layer width somewhat decreases. Thus the effect of microwave irradiation on the studied heteropairs Al- n - n^+ -GaAs and Al- n - n^+ -InP is realized through different mechanisms for interactions between phases. In the Al- n - n^+ -GaAs contact exchange reactions seem to be predominant, while in the Al- n - n^+ -InP heterostructure interdiffusion of the contact pair components occurs. Such character of processes and corresponding formation of the end products should lead to distinctions in the effect of microwave irradiation on the parameters of Al- n - n^+ -GaAs and Al- n - n^+ -InP Schottky barriers (SBs).

Now let us consider what mechanism for interaction between phases is realized in the Au-Cr-GaAs contacts with chemically active boundaries between phases. In [23] thermochemical calculations have been made for the Cr- n - n^+ -GaAs system, and it was shown that Cr-As compounds of different stoichiometric ratios could be formed.

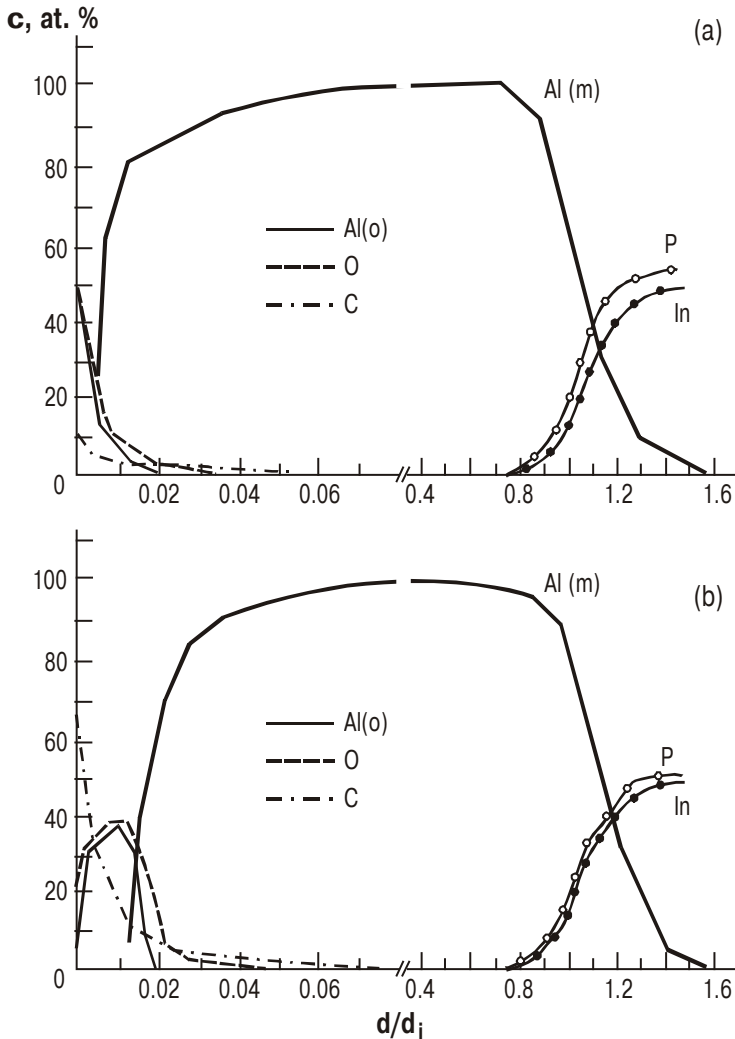


Fig.1.10. Auger concentration depth profiles for the components of $\text{Al}-n^+ \text{-InP}$ contact before (a) and after (b) microwave irradiation (d_i is the initial metal layer thickness).

A possibility for formation of compounds by Cr and Ga has not been considered. The results of study of the Cr, Ga and As concentration depth profiles in the Au–Cr–GaAs contacts exposed to microwave treatment (see Fig.1.11) indicate at high probability of formation of compounds involving chromium, as well as release of metallic gallium, even though such exchange interaction is not very intense [24]. One should also note that concentration of chromium atoms in the semiconductor near-surface layers is increased as a result of microwave irradiation.

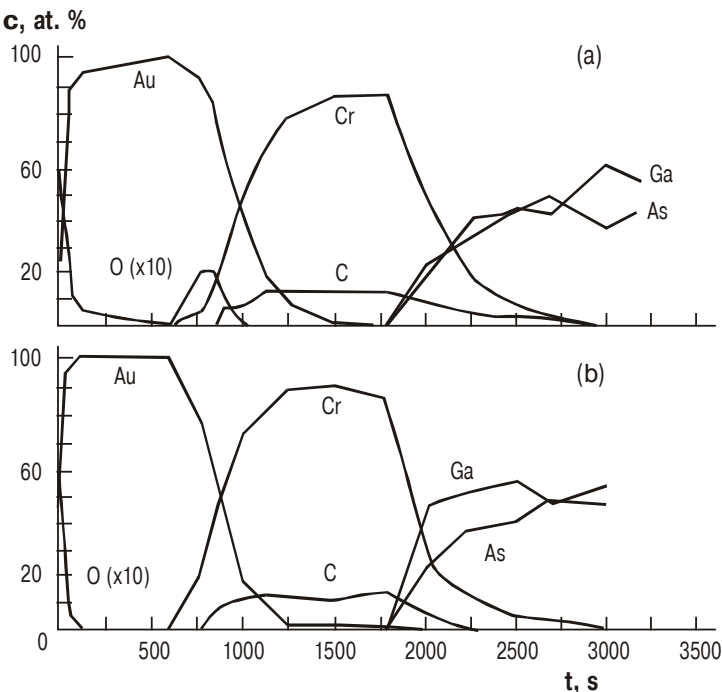


Fig.1.11. Auger concentration depth profiles for the components of $\text{Au}-\text{Cr}-n-n^+-\text{GaAs}$ contact and unintentional O and C impurities before (a) and after (b) microwave treatment [24].

Titanium is close to chromium in its chemical activity. The pronounced chemical reactions between Ti and GaAs are observed at thermal annealing at a temperature of about 500 °C. Specificity of these interactions under microwave treatment is demonstrated by Fig.1.12. Along the concentration depth profiles of the Au-Ti- n - n^+ -GaAs contact components, the changes in binding energies E_b of core electrons (Ga 3d, As 3d, O 2s and Ti 2p) are also presented there. These data enable one to judge how the phase composition changes across the transition region width [25].

From the above data it follows that chemical compositions of the transition layers after microwave irradiation remain the same as those for the initial structures. The most pronounced features of the transition layer induced by microwave irradiations are (i) Ga 3d-electron binding energy shift towards higher values (as compared with its value for GaAs) and (ii) more clear structure of the Ti concentration depth profile. In addition, the main distinction in the component distributions for irradiated and non-irradiated structures is penetration of gold atoms to the Ti- n - n^+ -GaAs interface. These results enable us to assume that change of the chemical composition in the transition region occurs mainly through intensification of the oxidation processes (as in [26]). Judging from the character of binding energy change for Ga 3d-electrons, their catalyst is AuGa alloy that takes part in oxygen atoms activation.

Thus the chemical processes occurring between barrier-forming metal and semiconductor can be substantially changed when atoms of another type are present in the metallization composition. The role of microwave treatment in this case lies mainly in the enhancement of diffusion penetration of the above atoms to the boundaries between phases.

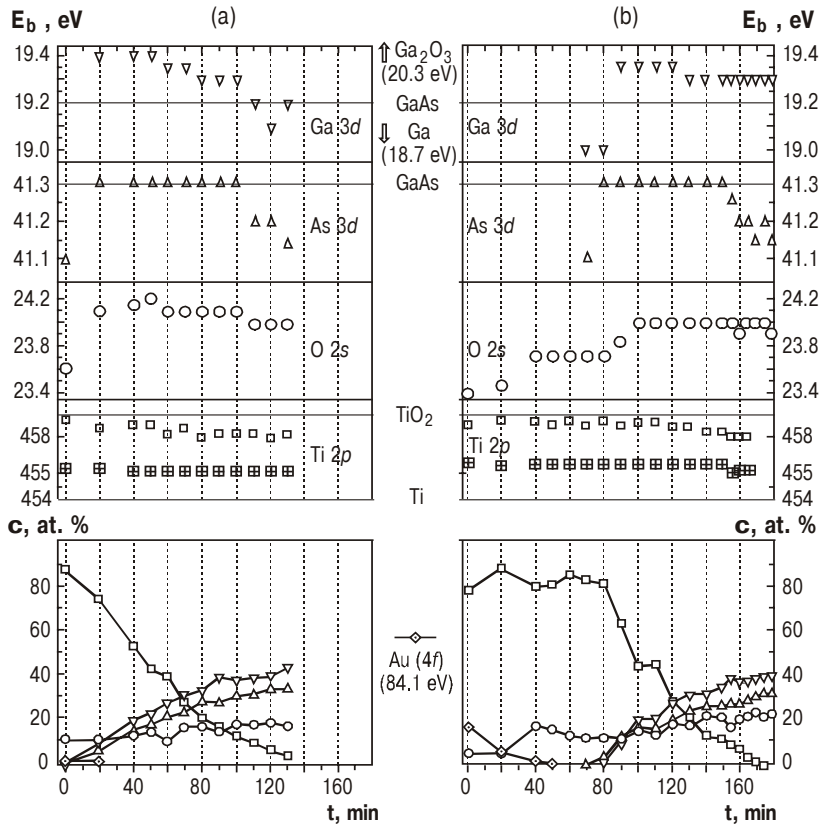


Fig.1.12. Auger concentration depth profiles (bottom) and electron binding energies E_b for the components of $\text{Au}-\text{Ti}-n-n^+-\text{GaAs}$ contact and unintentional O impurity before (a) and after (b) microwave treatment; t is duration of ion etching [25].

In conclusion let us dwell on some features of the processes enhanced by microwave radiation that occur in contacts formed by amorphous alloys and GaAs. Tungsten silicide can serve as example of such alloy. The metallization using $\text{W}_x\text{Si}_{1-x}$

attracts attention because it provides contact tolerance to high temperatures.

Shown in Fig.1.13 are the results of layer-by-layer Auger analysis of the $W_xSi_{1-x}-n-n^+$ -GaAs contact made before and after microwave treatment.

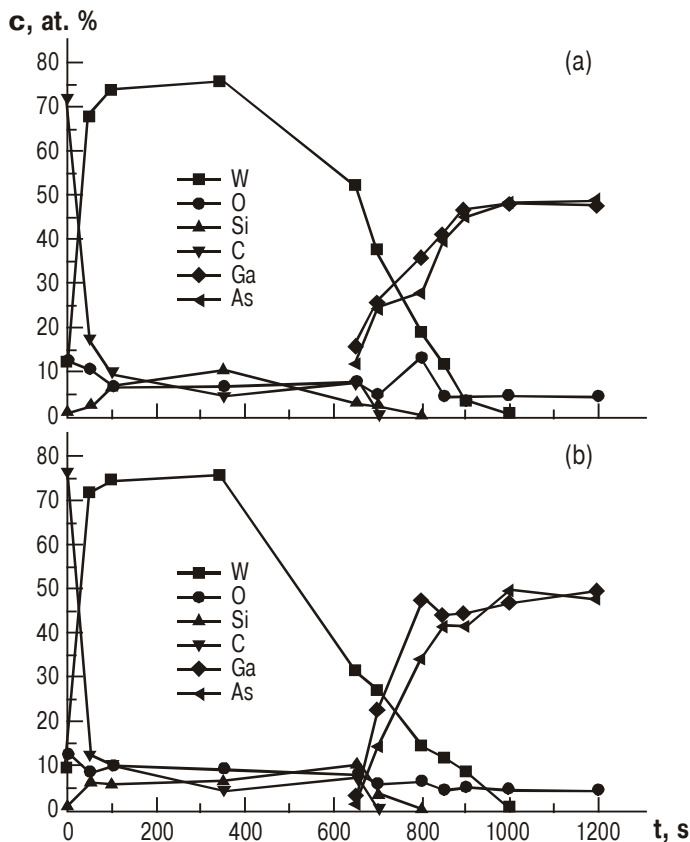


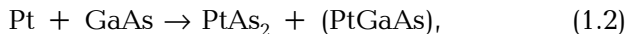
Fig.1.13. Auger concentration depth profiles for the components of $W_xSi_{1-x}-n-n^+$ -GaAs contact and unintentional O impurity before (a) and after (b) microwave treatment.

The results obtained enable one to conclude that microwave irradiation practically does not change distribution of the above contact pair components. It seems that no reactions occur between W_xSi_{1-x} and GaAs. In other words, the considered structure is stable in the metallurgical sense. Some small redistribution of the components due to microwave treatment should be related to structural changes in the metallization layer, as well as relaxation of intrinsic stresses (they can reach such values in a film that are enough for its cracking).

1.3.2. Structural-chemical processes in Me–GaAs contacts stimulated by gyrotron irradiation

Let us discuss the structural-chemical modification of the Me–GaAs interfaces (Me stands for metal) at increased G-irradiation power. Shown in Figs.1.14, 1.15 are the results of our investigations of the effect of microwave irradiation on the contacts of two types (one- and two-layer metallization) but involving the same barrier-forming metal [20,27]. One can see that microwave action leads to changes in chemical compositions of the contact transition layers. These changes are different for contacts of different types.

For contacts with one-component metallization microwave treatment enhances diffusion intermixing of phases. As a result, the gallium content in metal layer grows abruptly (up to 20%) [27]. In the multilayer Au–Pt–Cr–Pt– n – n^+ –GaAs structure the metallurgical processes resulting from microwave irradiation are more pronounced. They may be represented by the following equation:



where (PtGaAs) is an alloy.

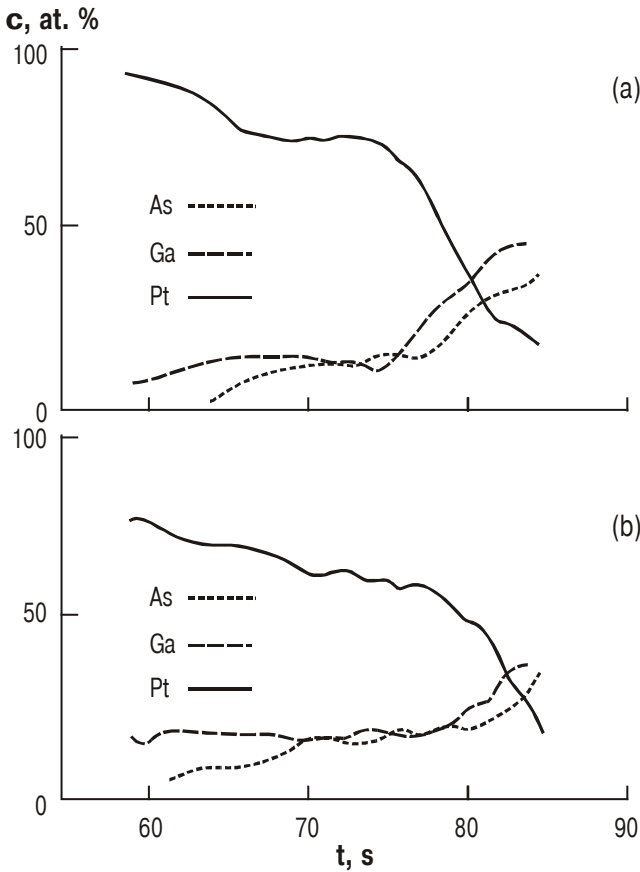


Fig.1.14. Auger concentration depth profiles for the components of $\text{Pt}-n-n^+-\text{GaAs}$ contact before (a) and after (b) gyrotron treatment [27].

Many authors have comprehensively studied chemical processes and kinetics of reactions at the $\text{Pt}-n-n^+-\text{GaAs}$ interface. (The appropriate works are reviewed in [28].) Different modes of thermal annealing have been used as active actions

on the Pt– n – n^+ –GaAs contact. It seems to be of interest to compare how two different external actions (thermal annealing and microwave irradiation) affect the contact characteristics.

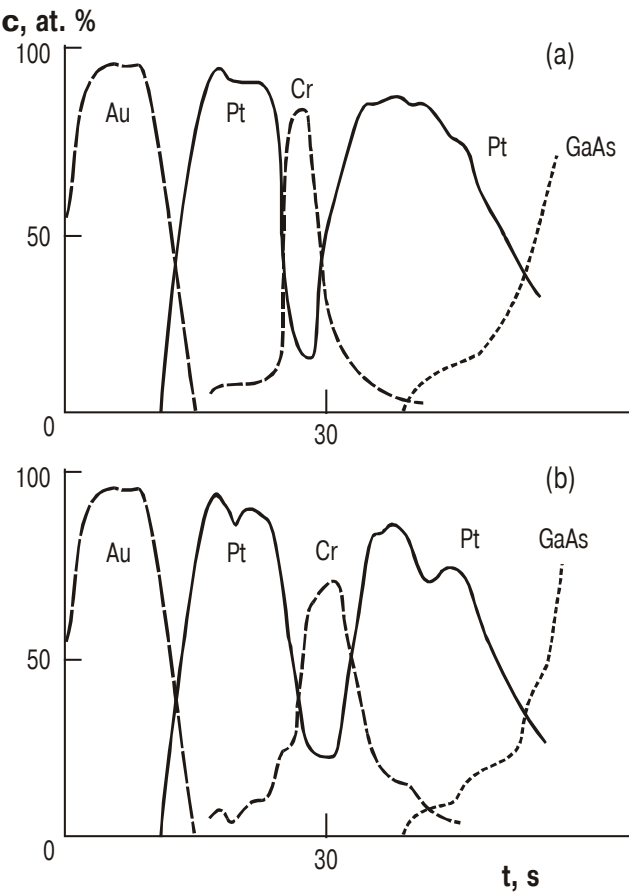


Fig.1.15. Auger concentration depth profiles for the components of Au–Pt–Cr–Pt– n – n^+ –GaAs contact before (a) and after (b) gyrotron treatment [20].

1. It follows from the studies of temperature dependence of the reaction kinetics in the Pt- $n-n^+$ -GaAs structure that the activation energy of the reaction between platinum and gallium arsenide is rather high (~ 2.3 eV) [23]. This is about 1.5–2 times bigger than the values that are usually characteristic of atom diffusion along the grain boundaries. In other words, for chemical interaction between Pt and GaAs to occur, rather high temperatures are needed that exceed, by a factor of 1.5–2, those realized in the above experiments (150–200 °C).

2. As in the case of thermal annealing at rather moderate (about 400 °C) temperatures and thick (≥ 200 nm) Pt films, the reaction does not reach its final stage.

3. Contrary to the case of thermal annealing, no predominant Ga migration from GaAs and its uniform distribution over the Pt film thickness occur.

4. Microwave treatment does not lead to formation of a layered contact structure with clearly separated regions that involve products of Pt reaction with Ga and As (as it takes place at thermal annealing).

All the above facts evidence that microwave “annealing” is not adequate to thermal one. This conclusion has been also confirmed by the results of studies performed for the W- $n-n^+$ -GaAs structure (see Fig.1.16). One should note that distribution of its components is qualitatively similar to that in the case of the Pt- $n-n^+$ -GaAs structure discussed above, although the thermal characteristics that describe chemical activity toward GaAs are essentially different for W and Pt. Nevertheless, non-monotonic behavior of the contact pair components distribution indicates that intense chemical processes occur at boundaries between phases in the irradiated W- $n-n^+$ -GaAs contacts. It was shown in [29,30] that in-

terface in this contact is tolerant to high-temperature actions. Chemical reactions between W and GaAs (leading to production of the W_2As_3 phase) are observed only at annealing temperatures over 700 °C.

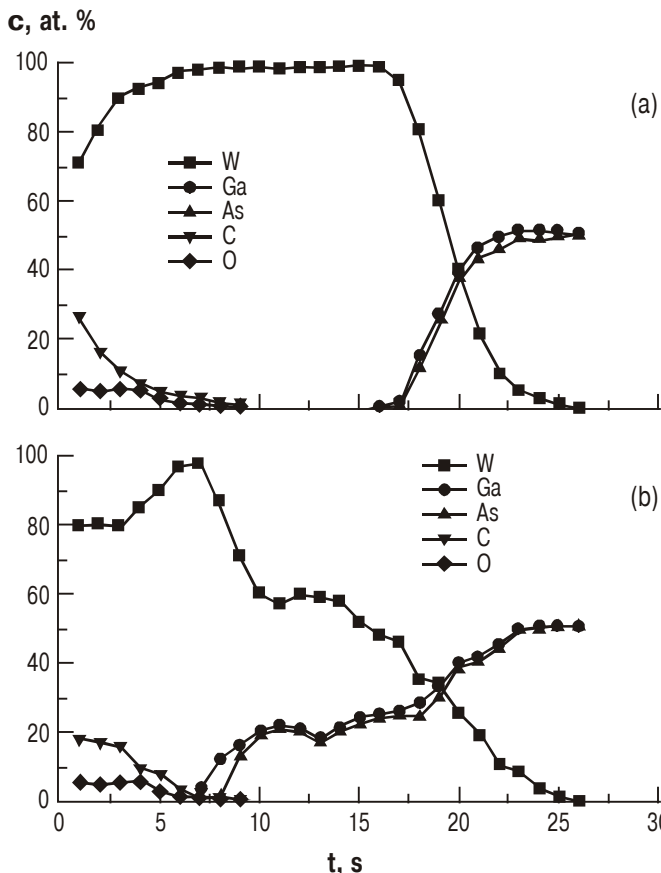


Fig.1.16. Auger concentration depth profiles for the components of $W-n^+-GaAs$ contact and unintentional O and C impurities before (a) and after (b) microwave treatment.

Degradation processes in W- n - n^+ -GaAs contacts at lower temperatures were related to intensification of mass transport between phases. But the concentration depth profiles obtained by us for the W- n - n^+ -GaAs contacts after microwave irradiation cannot be explained by the diffusion mechanism only, although the temperatures realized during our experiments have been much below those required for chemical reactions to occur. So the results obtained for the W- n - n^+ -GaAs structure evidence that, when analyzing the behavior of contacts exposed to high-power G-irradiation, one has also to take into account some non-thermal factors that affect the structural-chemical modification of the boundaries between phases.

Thus, depending on the irradiation mode, either kinetic mechanism for metal-semiconductor interface formation or chemical diffusion may occur. A discrete and localized (in time and space) character of heat release during irradiation determines the characteristics of atomic intermixing between phases. This process is determined by the balance between the thermal excitation energy for the local regions of the substrate, rate of interdiffusion at the interface and rate of heat removal to the substrate.

A radical difference between microwave "annealing" and thermal one is related to the peculiarities of temperature distribution in the heterocontacts. It seems that for microwave "annealing" an "internal" local overheating occurs at small deviations of the average temperature in the heterocontact from room one. Such overheating of local regions serves to intensify chemical reactions. Another factor that affects both structure and phase composition of the boundaries between phases is related to the action of the electric field of electromagnetic wave. This electric field may reach values over the breakdown one.

1.3.3. Effect of microwave treatment on the electrophysical parameters of surface-barrier structures

Microwave irradiation leads to structural-chemical modification of the boundaries between phases in metal–semiconductor systems, as well as changes in the characteristics of local centers in such systems. These processes are to be accompanied by changes in the electrophysical parameters of SB.

In [22] it was shown that ion diffusion in a crystal lattice could be enhanced by the crystal electron subsystem. Not only phonons take part in ion hopping from one position to another but electrons as well. A deficiency of energy required for a diffusing particle to execute hopping is supplied from the electron subsystem. In this case the diffusing particle changes its charge state. Thus, on the one hand, the height W_B of the potential barrier that the diffusing particle has to overcome is changed; on the other hand, the charged particle gets an additional portion of energy ε_v from the electron subsystem. This portion is equal to the energy of the local level resulting from the particle transfer from a lattice site to another state of equilibrium.

According to conservation of energy, it is electrons of high ($\varepsilon > kT$), and not medium, energies that actively influence hopping [31]. Therefore one can substantially intensify ion hopping (in other words, the diffusion coefficient) by increasing the number of high-energy electrons through excitation of the electron subsystem (in our case by using microwave irradiation).

Action of microwave radiation on a solid can lead to crystal lattice heating with Joule heat. This disturbs the oriented ion motion. The characteristic time of lattice heating is much greater than that of electron gas heating. One can practically exclude the crystal lattice heating by applying micro-

wave power in the pulse, and not continuous, mode. In this case the electron gas manages to heat up, and the crystal lattice does not. The characteristic time of the electron gas heating in GaAs is about 10^{-9} s, while it takes several minutes for atom transfer through the near-contact layers due to Joule heating.

From [31,32] it follows that the ion diffusion coefficient D is given by the following expression:

$$D = D_0 \exp[-(W_B - \varepsilon_V) / kT + a\hbar\nu(1 - T_0 / T) / 2kT_0]. \quad (1.3)$$

Here $D_0 = \nu d_0^2$ (ν is the atomic vibration frequency and d_0 is the crystal lattice constant); T is the temperature of electron gas (it differs from that of crystal lattice, T_0); a is a parameter that characterizes interaction between the diffusing atom (ion) and crystal lattice. The typical values to be used in further calculations could be chosen as follows: $D_0 \sim 10^{-20} \text{ cm}^2/\text{s}$; $\nu \sim (10^{13}-10^{15}) \text{ s}^{-1}$; $W_B \sim 2 \text{ eV}$; $\varepsilon_V \sim 0.5 \text{ eV}$; $a\hbar\nu \sim 5 \text{ kT}_0$; $T_0 \sim 300 \text{ K}$.

Strictly speaking, the concept of electron temperature can be introduced only for the optical phonons at low temperatures or for the electron-electron interaction (the latter is of no significance at energy values that are of interest for us). To obtain D in other cases, one should average the transition probability not over the Maxwell distribution with a temperature $T \neq T_0$ but over the distribution obtained from the exact solution of the kinetic equation. However, taking into account that our further considerations are approximate, we shall use the effective electron temperature (as it has been done in [33]).

If the electric vector E of the microwave field is normal to the static built-in electric field E_1 of the bulk charge, then one can neglect heating action of that static field and write down the effective electron temperature as

$$T = T_0 \left[1 + (q_0 E l)^2 / 3\delta(kT_0)^2 \right]. \quad (1.4)$$

Here l is the electron mean free path; δ is the fraction of energy loss at an inelastic collision. At $l = 10^{-6}$ cm, $\delta \sim 1/25-1/30$ and $E = 10^4$ V/cm the additional term $(q_0 E l)^2 / 3\delta(kT_0)^2$ is equal to unity. This means that the effective temperature increases two-fold and, as a result, the diffusion coefficient increases by a factor of 10^{10} . (Of course, this value is overestimated because the energy that electron has got from the electric field is spent not only for particle hopping.)

In [34] the change in the SCR width w under microwave irradiation has been calculated. The calculation was based on solving a set of equations that involved equations for flows I_i of diffusing ions (whose type was labeled by i), continuity of these flows and the Poisson's equation:

$$I_i = -EN_i + \frac{\partial N_i}{\partial x}, \quad (1.5)$$

$$\frac{\partial N_i}{\partial t} + \frac{\partial I_i}{\partial x} = 0, \quad (1.6)$$

$$\frac{\partial^2 \varphi}{\partial x^2} = 1 - N_D. \quad (1.7)$$

This set of equations is written down for dimensionless quantities. The units of measurement of the flows I_i are $D_i N_i / L_D$ where N_i is the concentration of ions of i -th type (measured in units N_D , i.e., the donor concentration). $L_D = (\epsilon_0 k T_0 / 4\pi q_0^2 N_D)^{1/2}$ is the Debye shielding length (it also serves as unit of measurement of dimensionless distance x) and ϵ_0 is the semiconductor permittivity. The potential φ is measured in kT/q , while the unit for measurement of the electric field E is $kT/L_D(d\varphi/dx)|_{x=0}$.

The unit for time measurement is D / L_D^2 (it was noted above

that the diffusion coefficient D depends on the microwave electric field).

Strict approach to solving the above set of equations is very complicated. So let us use a simplifying assumption that the diffusion front practically is not blurred. This enables us to determine a change $L_{1,2} = L_1 + L_2$ of the depletion layer width (here L_1 (L_2) is the change due to acceptor (donor) ion diffusion):

$$L_{1,2} = 2\pi E_1^{1/2} \left[2 + E_1^{1/2} \operatorname{erf}(E_1 t)^{1/2} \right] / \operatorname{erf}(E_1 t)^{1/2}, \quad (1.8)$$

where $\operatorname{erf}(x)$ is the error function. (If the depletion layer width decreases due to ion diffusion, then one should take the right-hand side of expression (1.8) with the "minus" sign.) It should be stressed that the solution (1.8) is approximate. It was obtained using the assumption that change in concentration due to diffusion and corresponding penetration of atoms into the depletion layer does not exceed the impurity concentration in that layer.

The experimental results presented in [34] corresponded to the case of microwave irradiation with angular frequency $\omega = 1$ GHz and irradiance of 100 W/cm 2 . The metallization layer thickness was less than skin depth, so one could assume that almost all the above power was absorbed in the contact structure and semiconductor. At the above irradiance value the microwave electric field is 10^4 V/cm. In this case the $L_{1,2}$ value is of the same order as the Debye shielding length L_D (or even may exceed it) if all microwave power is spent on changing $L_{1,2}$. At the above experimental conditions the transition region width changed substantially.

At microwave irradiation of higher (about 10^2 GHz) frequency the time needed to heat up the electron gas becomes comparable to the period of the microwave electromagnetic

field. In addition, the skin depth goes down with electromagnetic field frequency. This results in decreasing the irradiation power received by the contact.

After the microwave field is switched off, the diffusion coefficient abruptly drops. Therefore the spatial distribution of diffusing particles that has resulted from the action of both microwave irradiation and applied static electric field remains "frozen" for a long period.

Thus the microwave irradiation enhances diffusion of point defects and impurities in the near-contact layers through excitation of the electron subsystem in a semiconductor. This effect is to be more pronounced at application of pulsed microwave irradiation, since in this case some side effects (say, Joule heating of the crystal lattice) are excluded. The frequency of microwave radiation has to be of the order of inverse time of the electron gas heating, i.e., about 10^9 s⁻¹. So one should expect some distinctions between changes in the electrophysical parameters for contacts exposed to M- and G-irradiations.

Shown in Fig.1.17a are typical I - V curves of a surface-barrier diode [19]. One can see that after microwave irradiation for 2 s the range of exponential portion of the forward branch of I - V curve increased by an order of magnitude, the barrier height ϕ_B remained the same and the ideality factor n dropped. As to the backward branch of I - V curve, the reverse current I_R significantly decreased. This seems to result from the structural defect annihilation that increases the charge carrier effective lifetime. This conclusion is supported by the fact that the dopant concentration did not change under microwave irradiation — this follows from the reverse capacitance squared vs voltage curves ($1/C^2(V)$) presented in Fig.1.17b.

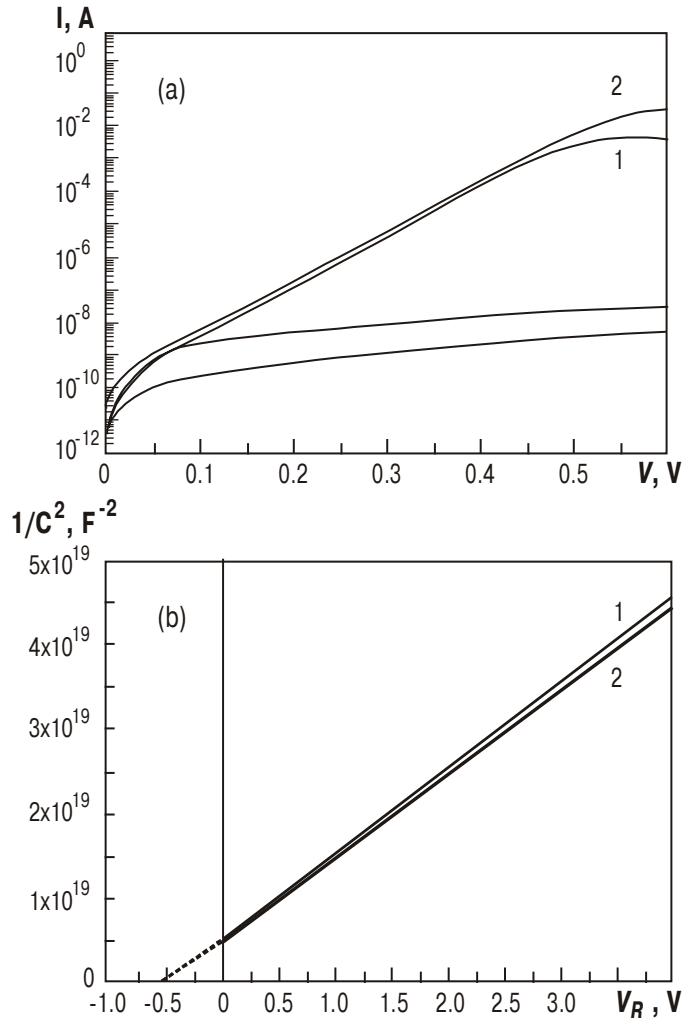


Fig.1.17. I - V curves (a) and function $1/C^2 = f(V_R)$ (b) for Schottky TiN- n^+ -GaAs contact before (1) and after (2) microwave treatment [19].

The results of our studies of the effect of microwave irradiation on SBs formed by different metals with some III–V compounds are summarized in Tables 1.2 and 1.3. An analysis of these results enables one to draw the following conclusions:

- a) Whatever the metallization type (the only exception being Pt– n - n^+ -GaAs structures), short-term M-irradiations improve the electrophysical parameters of the contacts involving GaAs;
- b) Microwave irradiation affects the barrier height φ_B slightly and the ideality factor n somewhat stronger; the corresponding changes are bigger for those structures where the initial n value is higher. The reverse current I_R changes most considerably under microwave irradiation. The semiconductors used by us had low donor concentrations that did not change under irradiation. So one can assume that in this case the reverse current decrease is related to weakening of the electron-hole pair generation in the depletion region. This means that microwave irradiation enhances partial annihilation of the initial structural defects in the near-contact layers and thus increases the charge carrier effective lifetime;
- c) Changes of the SB parameters under microwave irradiation are similar for structures based on GaP and GaAs. But for structures based on InP both parameters (the barrier height φ_B and ideality factor n) decreased after irradiation.

Table 1.2. Changes under magnetron irradiation (frequency $f = 2.45$ GHz, power $P = 5$ kW, duration $t^M = 1$ s) in the electrophysical parameters of Schottky diodes (barrier height ϕ_B , ideality factor n and hole diffusion length L_p) [20].

Contacts	Type of treatment	ϕ_B , eV	n	L_p , μm
Al–GaAs	I	0.55–0.58	1.68–2.20	1.6–1.9
	MI	0.57–0.58	1.30–1.40	2.0
Pt–GaAs	I	0.88–0.95	1.12–1.37	2.1–2.2
	MI	0.88–0.89	1.18–1.24	2.1–2.2
Au–Pt–GaAs	I	0.88–0.92	1.17–1.30	2.0–2.2
	MI	0.90–0.92	1.12–1.15	2.3–2.5
Cr–GaAs	I	0.73–0.75	1.17–1.24	6.5–7.0
	MI	0.76–0.77	1.08–1.09	7.2–7.4
Au–Cr–GaAs	I	0.70–0.76	1.12–1.17	0.9–1.1
	MI	0.75–	1.04–1.08	1.0–1.3
Mo–GaAs	I	0.68–0.69	1.16–1.23	2.3–2.8
	MI	0.68–0.69	1.09–1.14	2.5–2.7
W–GaAs	I	0.65–0.66	1.20–1.40	1.7–2.0
	MI	0.69–0.70	1.09–1.12	2.1–2.2
$\text{Mo}_x\text{Si}_{1-x}$ –GaAs	I	0.70–0.71	1.15–1.17	2.4–2.5
	MI	0.72	1.09–1.10	2.6–2.7
$\text{W}_x\text{Si}_{1-x}$ –GaAs	I	0.72–0.73	1.15–1.17	2.2–2.4
	MI	0.74	1.07–1.09	2.5
TiN–GaAs	I	0.75	1.24	1.6–1.75
	MI	0.76	1.02	1.8–1.82
Cr–InP	I	0.67–0.69	1.5–1.8	1.52–1.6
	MI	0.63–0.65	1.2–1.4	1.7–1.75
Al–InP	I	0.77–0.80	1.73–2.73	1.55–1.7
	MI	0.75	1.14–1.73	1.73–1.8
Au–GaP	I	1.52	1.75	0.65
	MI	1.70	1.10	0.78
Cr–GaP	I	1.63	1.72	0.53
	MI	1.85	1.30	0.87

Table 1.3. Effect of gyrotron irradiation on the Schottky barrier parameters (barrier height φ_B , ideality factor n and hole lifetime τ_p) [20].

Contacts	Parameters and their spreads									
	Before irradiation					After irradiation				
	$\bar{\varphi}_B$, eV	$\Delta\varphi$, eV	\bar{n}	Δn ,	$\tau_{p'}^{''}$ 10 ⁻¹⁰ s	$\bar{\varphi}_B$, eV	$\Delta\varphi$, eV	\bar{n}	Δn ,	$\tau_{p'}^{''}$ 10 ⁻¹⁰ s
Pt–GaAs	0.91	0.06	1.2	0.2	25.2	0.88	0.02	1.21	0.07	25.2
W–GaAs	0.65	0.01	1.3	0.2	28.9–40	0.69	0.01	1.26	0.06	36.1–40
Al–GaAs	0.56	0.03	1.9	0.4	19.4	0.59	-	2.5	0.35	20.7
Au–Pt–GaAs	0.92	0.07	1.2	0.13	23.4	0.86	0.08	1.5	0.2	25
Cr–Pt–GaAs	0.91	0.06	1.2	0.11	22.7	0.91	0.06	1.2	0.11	22.7
Au–Ti–GaAs	0.7	0.1	1.3	0.2	19.8	0.7	0.1	1.3	0.2	19.8
TiN–Ti–GaAs	0.72	0.09	1.3	0.14	19.8	0.73	0.08	1.3	0.14	22.4

Taking into account the results of investigations presented in sections 1.2 and 1.3, one can assume that the principal factor responsible for the observed changes of SB parameters is structural ordering in the heterosystems exposed to microwave treatments. This ordering improves semiconductor material and makes the disordered heterogeneous contact boundaries more uniform. The above conclusion is also supported by the results on the effect of high-power G-irradiation on the Au–Pt–Cr–Pt– n - n^+ –GaAs multilayer contact (Fig.1.18).

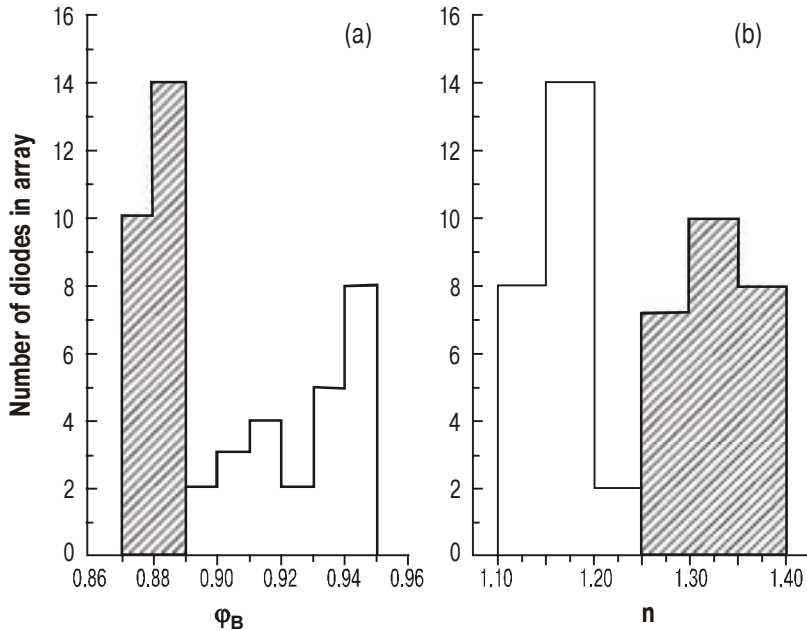


Fig.1.18. Barrier height ϕ_B (a) and ideality factor n (b) histograms for Au–Pt–Cr–Pt– n - n^+ –GaAs contact before and after (hatched area) microwave annealing [35].

One can see that a clear tendency exists toward decrease of parameter spread after microwave treatment for SB made on the same wafer [35]. In Table 3 the results for other contact pairs are given. From them one can conclude that G-irradiation either does not change the contact parameters or even slightly impairs them, with some decrease in spread of their values.

Below we summarize the most probable mechanisms that are responsible for the observed changes under microwave irradiation in properties of both semiconductor materials and contact structures based on them [15,19,20,24,25,27,34-45]:

Thermal mechanism that is related to heating of boundaries between phases by absorbed microwave energy. Our analysis of the Auger concentration depth profiles for the contact structure components taken before and after microwave irradiation, as well as their comparison with the results of the layer-by-layer analysis of contacts after thermal annealing, evidence that this factor is insignificant.

Electrostatic mechanism that is related to an actual drop in barrier voltage. It was shown in [2] that this mechanism can substantially affect spatial redistribution of the contact components through diffusion, even if there are no critical electric fields that determine mechanisms for avalanche and tunnel breakdowns. An intense interdiffusion between a metal and gallium arsenide begins when the absorbed energy level is as high as about 2/3 the critical value needed for avalanche breakdown to occur. However, according to estimations made in [2], this factor counts little in the used irradiation mode.

Electrodynanic mechanism that is related to a departure of the electron subsystem of a semiconductor from the state of thermodynamic equilibrium. This departure occurs due to ap-

pearance of hot charge carriers in the semiconductor near-surface layer that changes the impurity-defect composition of this layer [2]. The electrophysical parameters of the surface-barrier structures exposed to microwave treatment are close to those after ^{60}Co γ -irradiation [46] (and it is known that in the latter case the above mechanism is the governing factor). This fact indicates that it is the electrodynamic mechanism that plays a decisive role in the structural-impurity transformation under microwave actions.

Occurrence of non-steady-state stress gradients due to a practically instantaneous heating of disordered regions that appear in a semiconductor during the contact structure formation. In this case the concentration depth profiles for the contact pair components can be practically the same before and after microwave irradiation. However, taking into account the possibility for collective interactions in the stress fields, one can substantially decrease the barrier for defect annihilation or defect complex transformation [47].

1.4. EFFECT OF MICROWAVE RADIATION ON THE PARAMETERS OF RESONANT TUNNELING DIODES

1.4.1. GaAs tunneling diode with two δ -layers in SCR

In recent years many authors have been studying the tunnel diodes exposed to microwave actions. The emphasis was mainly on a search for ways to exert control over their $I-V$ characteristics. In this connection the works [48-59] should be recalled, to mention just a few. Along with technological problems, their authors considered some physical aspects concerning interaction between microwave radiation and degenerate semiconductors, as well as degradation mechanisms in the irradiated tunnel diodes. However, similar effects in more com-

plicated resonant-tunneling structures exposed to microwave irradiation practically have not been studied yet.

An attempt to fill in the gap in this area has been made in [60-63]. In the GaAs tunnel diodes studied the *p-n* junction width was $l_j = 10$ nm, spacing between two δ -layers $d_\delta \approx 5$ nm, impurity concentration in the δ -layers was $N_\delta \approx 10^{13}$ cm⁻², those in the p^+ - and n^+ -regions were 10^{20} and 10^{19} cm⁻³, respectively. The Fermi energy in n^+ -GaAs was $E_F \approx 0.023$ eV and the electric field in the *p-n* junction was $E_j = 2 \times 10^6$ V/cm.

We investigated *I-V* curves for the GaAs resonant tunneling diodes (RTD) with two δ -layers in SCR, both before and after microwave irradiation in the magnetron waveguide. The frequency of M-radiation was $f = 2.5$ GHz and the irradiance was $W = 3 \div 30$ W/cm². A strong anisotropy of the microwave field action has been observed. When the angle of incidence of the electromagnetic wave was 90° (glazing incidence), then *I-V* curves remained practically the same at time of exposure $t^M \leq 300$ s, while at normal incidence the changes occurred after $t^M = 10$ s.

The starting doses of microwave irradiation ($t^M = 10 \dots 20$ s, $W = 3$ W/cm²) have led to a shift (toward higher voltages) of the *I-V* curve peak related to the resonant-tunneling current flow via a level in the potential well formed by the δ -layers; besides, the excess current I_{ex} has somewhat dropped (Fig.1.19). The qualitative explanation for this might be as follows. The first δ -layer goes down under the counter electric field E_j i.e., this field induces the impurity diffusion from the δ -layer to SCR. In this case the potential well changes its form. A local level appears in the well that is responsible for the resonant-tunneling current: the wall of the potential well that is closer to the *p-n* junction becomes less abrupt, and the energy level (whose energy is measured from the well bottom) becomes shallower.

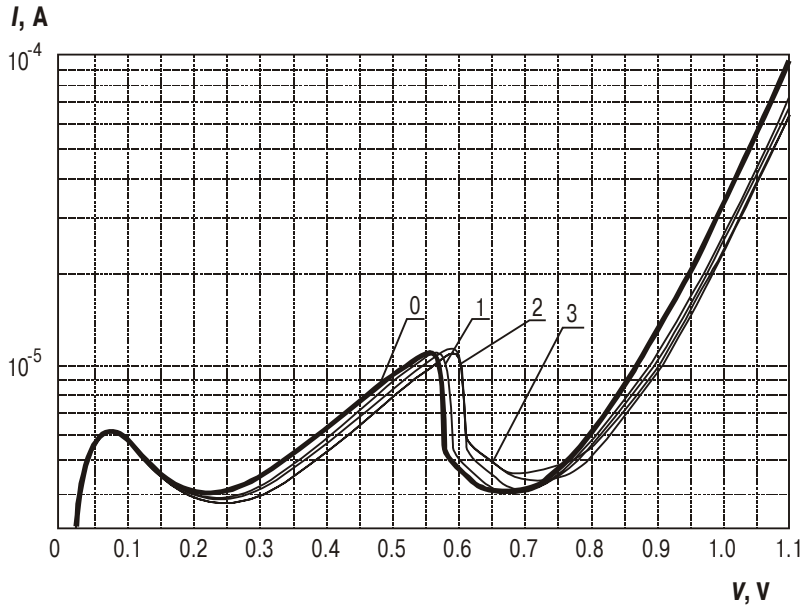


Fig.1.19. Forward branches of I - V curves for RTDs with a δ -layer before (0) and after microwave irradiation (irradiance $W = 10 \text{ W/cm}^2$, exposure time 20 s (1), 40 s (2), 60 s (3)).

Accordingly the depth of this level (counted from the conduction band bottom in the n^+ -layer) increases and the resonant-tunneling current peak somewhat shifts toward higher voltages.

Further microwave action does not shift this peak, thus evidencing that the form of the potential well does not change. This seems to be due to the fact that all impurities have left the δ -layer for SCR. In this case the excess current $I_{ex}(V)$ (defined as a diffusion current increase after irradiation: $I_{ex}(V) = I(V) - I_0(V)$, $V > 0.7 \text{ eV}$) grows with time of expo-

sure to microwave irradiation (Fig.1.20). An analysis of the obtained irradiation dose dependencies of I_{ex} enables one to get the following approximate expression:

$$I_{ex}(V) = i_1 \exp(a_1 V) + i_2 \exp(a_2 V). \quad (1.9)$$

Here V is the forward bias; the coefficients $a_1 = 0.58 \text{ V}^{-1}$ and $a_2 = 6.8 \text{ V}^{-1}$ do not change under irradiation, while the factors i_1 and i_2 are zeros at times of exposure below 90 s and then grow linearly with time of exposure, the corresponding coefficients being $0.178 \times 10^{-10} \text{ A/s}$ and $0.844 \times 10^{-10} \text{ A/s}$, respectively.

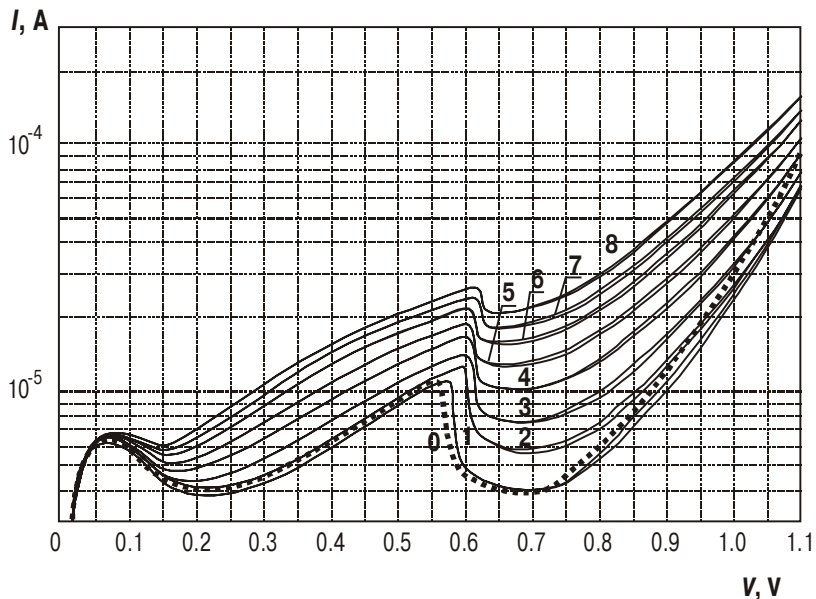


Fig.1.20. Forward branches of I - V curves for RTDs with two δ -layers before (0) and after microwave irradiation (irradiance $W = 3 \text{ W/cm}^2$, (1)-(8) – consecutive exposures 30 s each).

The excess current features seem to be related to impurity diffusion from the δ_l -layer into SCR. In this case some impurity levels appear in SCR via which interband tunneling can occur. Their energy does not change with time of exposure, while their concentration changes. This fact correlates with expression (1.9) in the case of two different levels (centers) in SCR. The coefficients a_1 and a_2 are determined by the level nature and electric fields (i.e., by the structure geometry); the factors i_1 and i_2 are proportional to the concentration of the centers responsible for interband tunneling.

Let us determine the conditions under which the above diffusion can occur. The problem of electrically enhanced diffusion from an infinitely thin layer into an unrestricted medium can be solved rather easily. It was shown in [64] that

$$\frac{\partial N_r}{\partial t} = D \frac{\partial^2 N_r}{\partial x^2} - V(t) \frac{\partial N_r}{\partial x}, \quad (1.10)$$

where

$$V = \mu E, \quad \mu = q_0 D / kT, \quad E = E_j + E_l \sin \omega t \quad (1.11)$$

(for $W = 3 \text{ W/cm}^2$ ($\lambda = 12 \text{ cm}$) the electric field amplitude $E_l \sim 10^7 \text{ V/cm}$).

$$N_r(x, t) = \frac{Q}{2\sqrt{\pi D t}} \exp \left\{ -\frac{1}{4D t} \left[x - \mu \left(E_0 t + \frac{E_l}{\omega} \cos \omega t \right) \right]^2 \right\}. \quad (1.12)$$

Here Q is the total electric charge in the δ_l -layer and $D = D_0 e^{-\frac{E_a}{kT}}$. In further estimation let us take for D_0 and E_a the values known from silicon diffusion in GaAs [65]: $D_0 = 4 \times 10^{-4} \text{ cm}^2/\text{s}$, $E_a = 2.45 \text{ eV}$.

When estimating the temperature T at which diffusion occurs that could be observed experimentally, the following considerations are used. The concentration of impurity centers

in a layer (whose thickness is Δx) located at a distance of $-x_0$ from $x = l_j$ should be comparable (i.e., of the same order) to the concentration n in the n^+ -region. Since $\Delta x \equiv \varepsilon_F/eE_j$, then

$$n(\Delta x, 0) \cong \frac{Q^{3/2}}{\Delta x} \left[\operatorname{erf}\left(\frac{x - \frac{D_e E t}{kT}}{2\sqrt{Dt}} \right) - \operatorname{erf}\left(\frac{x + \Delta x - \frac{D_e E t}{kT}}{2\sqrt{Dt}} \right) \right]. \quad (1.13)$$

The estimated temperature value turned out to be about 550 °C. Only at this (or higher) temperature diffusion can occur that leads to δ_l -layer flattening. However the experimentally observed diode temperature is considerably below the above value. This enables one to conclude that the diffusion is predominantly of non-thermal origin; it may be related to, say, a decrease in the activation energy E_a due to electric field. In this case a 0.5 eV drop in E_a value would result in sample heating up to $T = 200$ °C and δ_l -layer flattening; this does not disagree with the results of experiment.

When analyzing the results of the above estimation, one might assume that the following two processes occur in RTD exposed to high-power microwave irradiation. At first the quantum-sized well becomes broader because the δ_l -layer and SCR boundaries are flattened due to electrically enhanced diffusion. Later on the generation-recombination centers are gathered; this results in an increase of the excess diffusion current.

1.4.2. Two-barrier resonant tunneling diode

In [60,61] it was reported on the effect of microwave irradiation on $I-V$ curves of the Al-GaAs/GaAs two-barrier heterostructure. The authors studied MBE-grown two-barrier RTD (TBRTD) with $n^+ - n - p$ emitter and collector contacts. A reso-

nance peak was observed on I - V curves of initial (before microwave irradiation) samples for both voltage polarities. It was characterized by current density of 10^4 A/cm² and the ratio between the current values at and off the peak about 3 at a temperature of 300 K. Microwave treatments for 7 and 14 min. were performed using a magnetron with microwave signal power of 3 kW at a frequency of 2.45 GHz. It was found that such treatments improved the TBRTD characteristics: the ratio between the current values at and off the peak increased by a factor of 1.5–2.

1.5. THE FEATURES OF STRUCTURAL CHANGES IN GaAs SINGLE CRYSTALS UNDER MICROWAVE IRRADIATION

It was stated before that when single crystals and epitaxial layers of III–V semiconductors (GaAs, GaP, InP) are exposed to microwave irradiation, then a structural-impurity modification of near-surface layers may occur in them. One can detect it from the changes in PL spectra [15,19,20,25]. The reason for this modification is (as in other cases when the electron subsystem of a crystal is excited [32,45,64]) relaxation of intrinsic stresses [46,66,67]. It was found, however, that in this case the kinetics of intrinsic stress relaxation is of long-term type. This is an additional factor that intensifies degradation processes in semiconductor materials enhanced by microwave radiation [68–74]. This fact determined a need to consider in more detail the structural changes that occur in III–V semiconductors under microwave irradiation. A material that is most studied in this respect and can serve as a model is GaAs [68–74].

We investigated the commercial wafers of single-crystalline GaAs (100) doped with tin (the impurity concentra-

tion of $3 \times 10^{16} \div 10^{17} \text{ cm}^{-3}$). The dislocation density was $N_d \sim 10^4 \text{ cm}^{-2}$. Both wafer sides were exposed to the same chemical-dynamic treatment. The samples were irradiated in the magnetron chamber in a continuous mode. The irradiance at the place where the samples were positioned was 100 W/cm^2 .

The sample irradiation was performed in series 1 and 5 s long. The structural parameters of the substrates studied were checked between these series of irradiation. We used x-ray topography in Borrman geometry ($\text{Cu } K\alpha$ -line). The radii of curvature of atomic planes were found using x-ray diffraction (XRD). The above two methods enabled us to determine how the elastic strain fields are redistributed. The method of x-ray quasi-forbidden reflections (QFR) made it possible to characterize stoichiometry changes, i.e., redistribution of point defects and impurities.

The x-ray topography studies of the initial gallium arsenide wafers have revealed that they predominantly demonstrated a nonuniform cellular dislocation structure (the cell sizes being from 0.5 to 1.5 mm). The dislocation density distribution along the diameter was of a weakly pronounced W-type. The separate linearized aggregations of dislocations along the $\langle 110 \rangle$ direction, as well as single inclusions up to 0.1 mm in size (regions demonstrating no diffraction contrast) were observed. In some wafers (with charge carrier concentration $n = 3 \times 10^{16} \text{ cm}^{-3}$) there were regions with high density of $\langle 110 \rangle$ dislocation slipbands. This is most likely to result from the growth mode departures from the optimal one. The results on radius of curvature planar distribution enabled us to estimate the strain level in the initial samples. It was found to be as much as about 10^{-6} .

In the initial samples there were regions with different general contrast. This indicated at higher (lower) surface per-

fection level. It was not related to the cellular structure but was due to the impurity-defect composition and strain fields. Such fields manifested themselves as a light (dark) colored positive contrast. After microwave treatment for 1 s no changes in the substrate defect structure were observed on the x-ray topograms. After microwave treatment for 5 s the contrast has leveled off (see Fig.1.21). This occurred due to structural changes resulting in a more uniform distribution of the above defects. Both dislocation density and length increased in the peripheral wafer regions with dislocation slipbands, while the cellular dislocation structure remained unchanged.

Microwave irradiation of the wafers for 20 s resulted in considerable changes of their defect structure and, in some cases, even single crystal disruption (cracking) (see Fig.1.21). The cellular structure character held, but microinclusions began to dissociate, the dislocation slipbands penetrated from the sample edges into the crystal bulk along the $<110>$ directions, and the spiral dislocation bands (bridges at strain contrast) appeared.

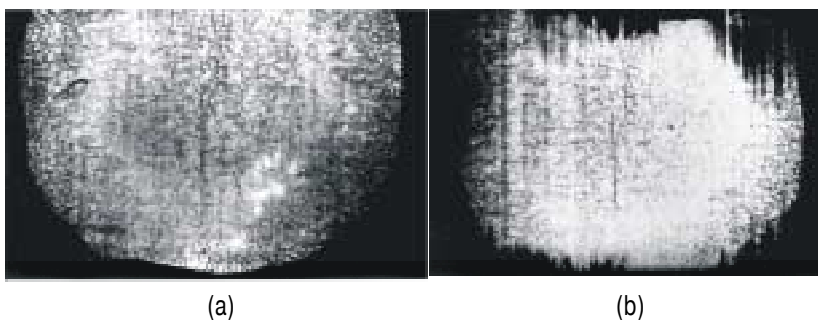


Fig.1.21. Topography of GaAs single crystal before (a) and after (b) microwave irradiation for 20 s [20].

The residual strain relaxation has been checked, both immediately following irradiation and in the subsequent keeping, from the profile changes for atomic planes of the sample surfaces. No defect structure changes have been observed (within the technique resolving ability) on the Borrman topograms obtained after sample exposure to microwave irradiation for 1 s. However, both atomic plane form and bending has changed. Either decrease or increase of bending was observed, depending on the initial curvature value. One can see from Fig.1.22a that for the samples whose initial bending was small, microwave irradiation for 1 s resulted in a small increase of stress whose value then changed at further irradiation stages.

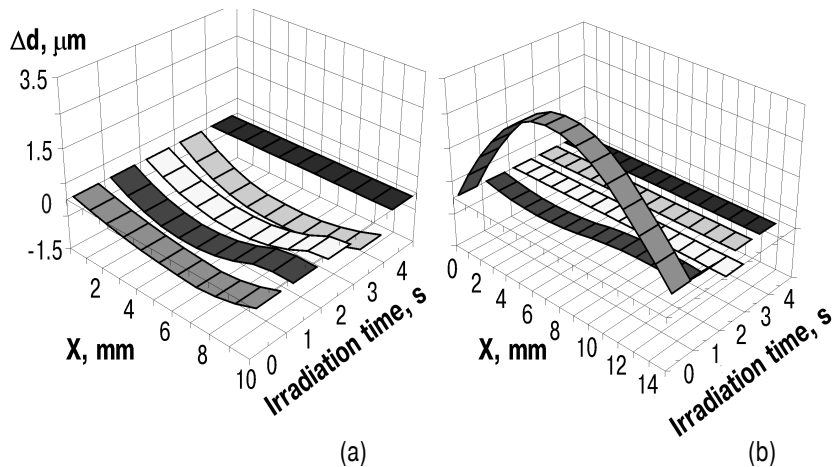


Fig.1.22. Changes of GaAs substrate surface profile along the wafer diameter due to microwave irradiation (consecutive exposures 1 s each) for samples with low (a) and high (b) stress level [74].

Contrary to this, in the samples with high initial stress level a considerable stress relaxation occurred at the first stage of microwave irradiation. Some small changes in the GaAs surface profile were detected for such samples (Fig.1.22b). After three or four irradiation sessions (each for 1 s) in all samples intrinsic stresses have relaxed completely [73].

After microwave treatment for 5 s the strain level in the crystal studied has dropped (see Figs.1.23, 1.24). Further irradiation sessions (each for 5 s) always increased the strain level; in several cases the strain field has reversed its sign. It should be noted that, as topograms evidenced, the dislocation slipbands have occurred in the sample regions of highest curvature.

The structural changes that have been observed in topograms and atomic plane profiles were accompanied with changes in the total intensity of QFR (TIQFR) (Fig.1.25). The ratio $\Delta R/R_r$ between the TIQFR change for the studied GaAs crystals due to a deviation from stoichiometry (ΔR) and TIQFR value for the stoichiometric (reference) sample (R_r) is determined by the concentrations and reflectivities of host and foreign atoms in the gallium and arsenic sublattices. One can see from Fig.1.25 (curve 1) that the initial GaAs substrates were characterized by the deviations from stoichiometry, namely, they had excess gallium atoms. After microwave irradiation TIQFR dropped by 1÷3 % for all the points measured. Its distribution became less uniform and followed the W-like dislocation structure distribution in the wafer (Fig.1.25, curve 2). Next irradiation session for 5 s resulted in a slight redistribution of the $\Delta R/R_r$ value along the wafer diameter (Fig.1.25, curve 3).

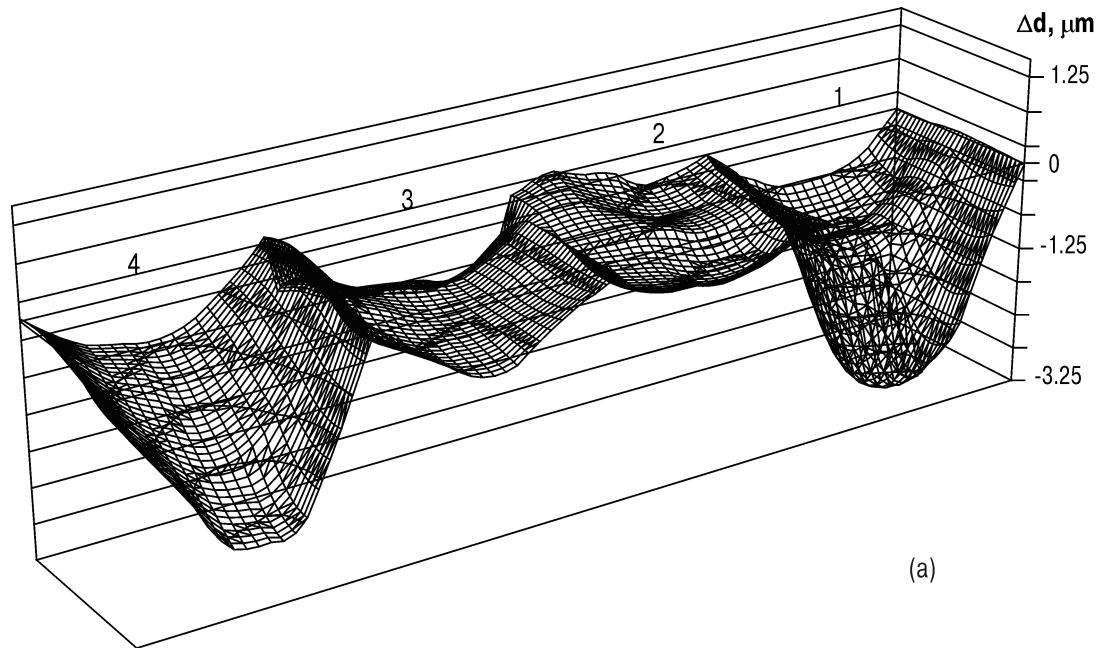


Fig.1.23. Change of the atomic plane form for GaAs substrate surface taken for samples *a* and *b* with different initial stresses: 1 – initial sample; 2 – after irradiation for 5 s; 3 – after keeping for 300 h; 4 – after second irradiation for 5 s (d characterizes departure from horizontal position) [20].

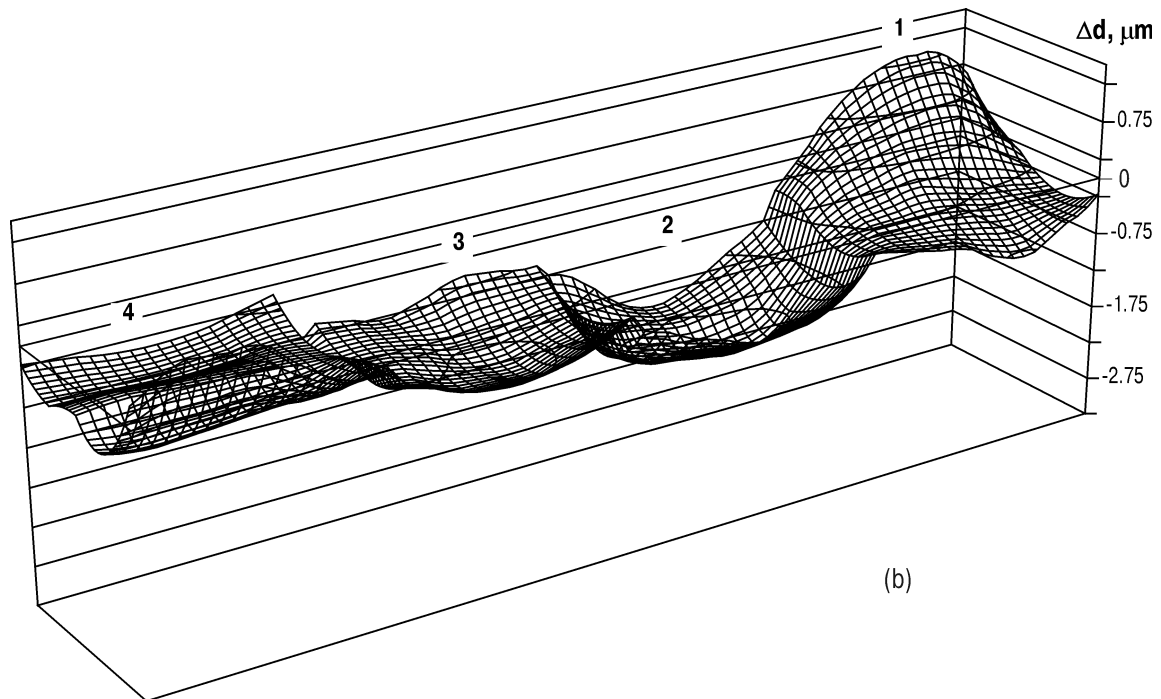


Fig.1.23. Change of the atomic plane form for GaAs substrate surface taken for samples *a* and *b* with different initial stresses: 1 – initial sample; 2 – after irradiation for 5 s; 3 – after keeping for 300 h; 4 – after second irradiation for 5 s (d characterizes departure from horizontal position) [20].

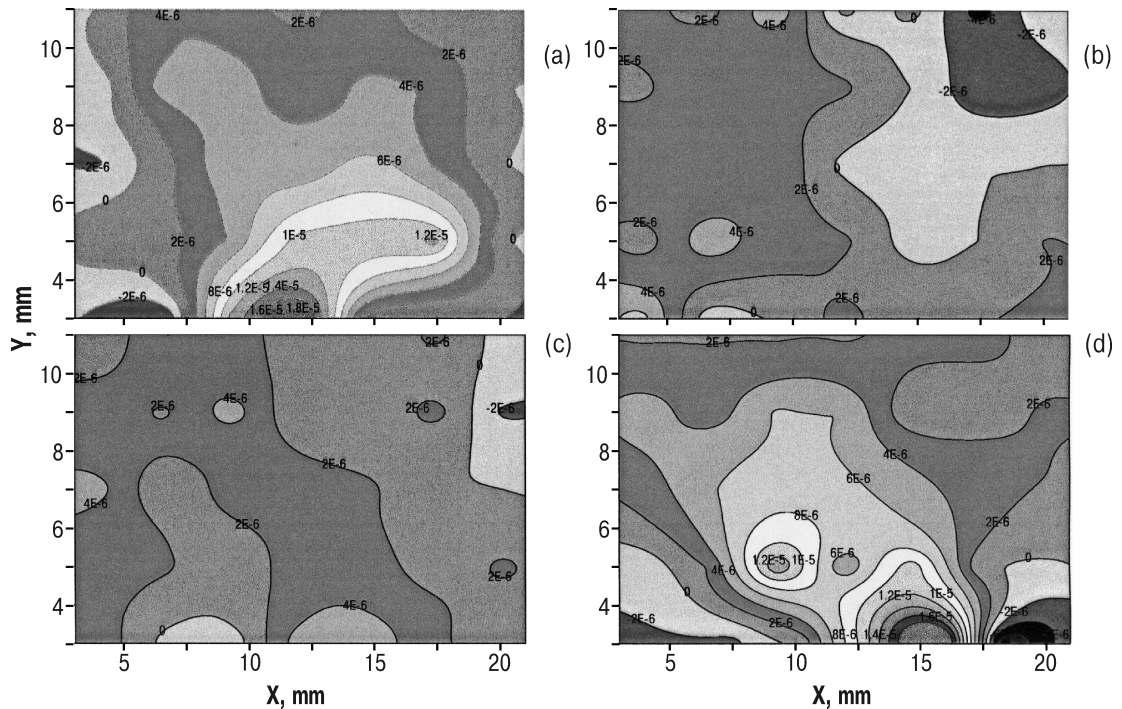


Fig.1.24. Change of the residual strain fields under microwave irradiation for the sample whose atomic plane form changes are shown in Fig.1.23: a – initial sample; b – after irradiation for 5 s; c – after keeping for 300 h; d – after second irradiation for 5 s.

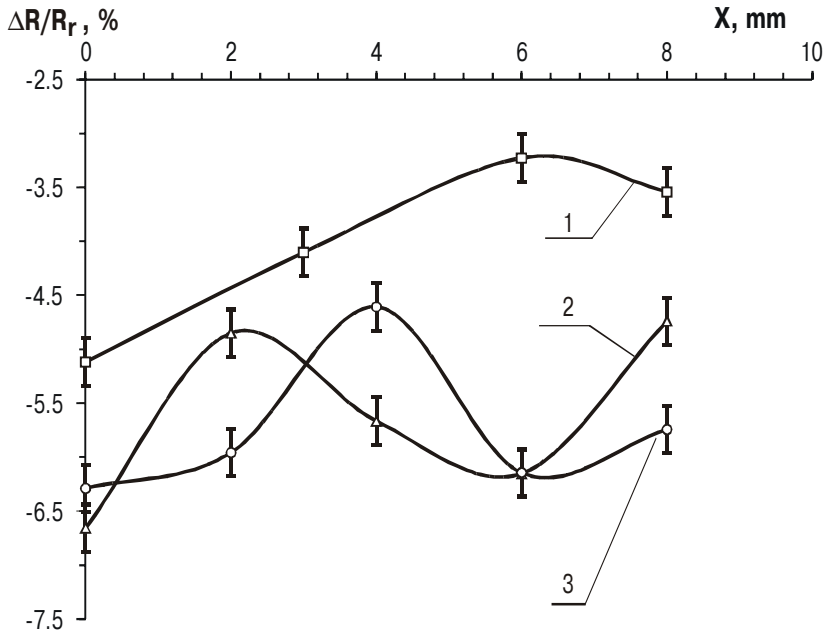


Fig.1.25. Relative departure of the total intensity of x-ray quasi-forbidden reflections taken along the wafer diameter (from edge to center): 1 – initial sample; 2 – after microwave irradiation for 5 s; 3 – after second irradiation for 5 s [74].

Such a behavior of TIQFR could be explained by a drop in the Ga vacancy concentration as a result of decay of the gallium microdefects that were observed on the topograms. Another factor that could take part in these processes is presence of Sn impurities. However one did not manage to separate a contribution from a possible redistribution of Sn impurities whose concentration was 10^{17} cm^{-3} .

The results of PL studies at low temperatures support the conclusion that microwave radiation stimulated trans-

formation of the impurity-defect complexes. This transformation manifests itself in changes of intensity, position and form of the PL band in the long-wavelength spectral region that is related to the recombination centers in the initial samples [68].

The following fact deserves particular attention. Contrary to the cases of thermal annealing and γ irradiation, no dislocation-impurity equilibrium appears in the subjects studied during microwave irradiation. One can see from Figs.1.23, 1.24 that further changes in the atomic plane form for the sample surfaces and strain field redistribution occur on keeping. These processes come to an end (judging from the results obtained when measuring the radius of curvature, the resolution being about 10^{-4} m) after keeping the samples at room temperature during 6÷7 months. The final curvature distribution in the samples is determined by the level of their structural perfection and irradiation modes. Microwave irradiation performed in sessions 1 s each presents a rather “soft” treatment. However after keeping for the above time the sample curvature can turn back almost to its initial level in the strongly stressed samples. At the same time microwave irradiation performed in sessions 5 s each provides better stability of sample curvature.

Shown in Fig.1.26 in more detail is the kinetics of the above process in a sample exposed to microwave irradiation for 20 s. The surface profile continued to change non-monotonically during 1000 h. However, as one can see from the topogram presented in Fig.1.21, such doses should not be used in technological procedures since a trend to sample failure is clear.

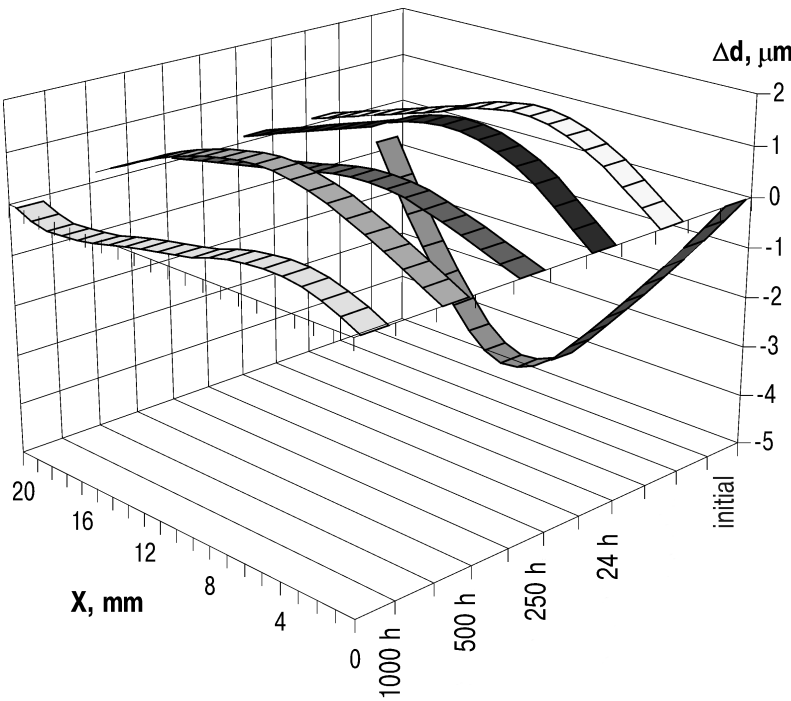


Fig.1.26. Change of the atomic plane profile for GaAs substrate surface after microwave irradiation for 20 s and keeping for 24, 250, 500 and 1000 h [20].

To perform an analysis of relaxation processes stimulated in the wafers by microwave irradiation, one should estimate a depth of electromagnetic field penetration Δ (this is the depth at which the electromagnetic wave amplitude drops by a factor of $e = 2.718$, i.e., an analog to the skin depth in metals). This depth strongly depends on the wafer conductance σ (see Fig.1.27). It was estimated from the known expression

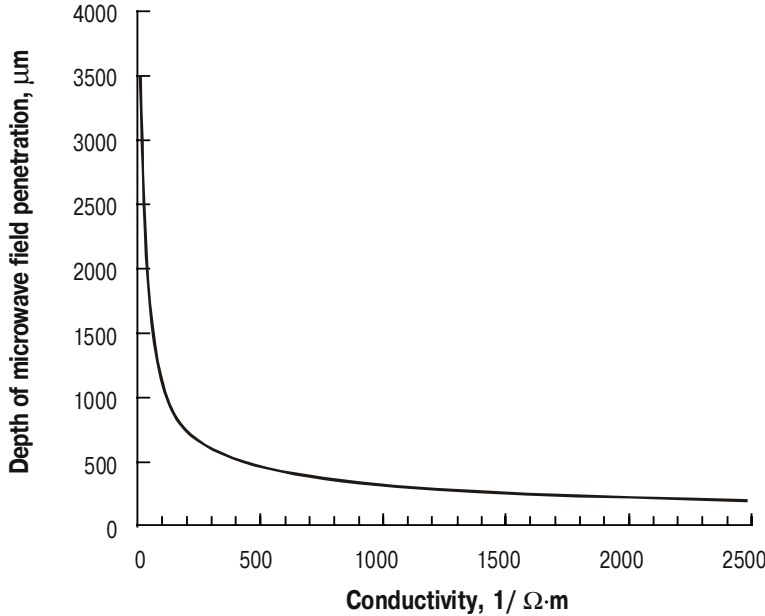


Fig.1.27. Depth of microwave field penetration into GaAs single crystal as function of its conductivity [74].

$$\Delta = \left\{ \omega \sqrt{\frac{\mu_0 \epsilon_0}{2}} \left[\sqrt{1 + \left(\frac{\sigma}{\omega \epsilon_0} \right)^2} - 1 \right] \right\}^{-1}. \quad (1.14)$$

Here ω is the microwave angular frequency; μ_0 and ϵ_0 are the material permeability and permittivity, respectively; $\sigma = q_0(n\mu_n + p\mu_p)$. For the samples studied with $n = 3 \times 10^{16} \div 10^{17} \text{ cm}^{-3}$ the above penetration depth was $230 \div 130 \mu\text{m}$.

The character of microwave power distribution in the sample with $\Delta = 230 \mu\text{m}$ is illustrated by Fig.1.28. The estimation was performed according to the following expression:

$W(t) = W_0 \exp(-2d/\Delta)$. Here W_0 is the irradiance at the sample surface and d is the depth measured from the sample surface exposed to irradiation. During experiments the samples were in a cavity resonator, and so they were exposed to both the incident and reflected electromagnetic waves (Fig. 1.28, curves 1 and 2, respectively). One can see that the total (incident + reflected) power distribution with sample thickness is nonuniform (Fig. 1.28, curve 3). Our estimation of the sample temperature has shown that it did not exceed 100 °C at the treatment modes used.

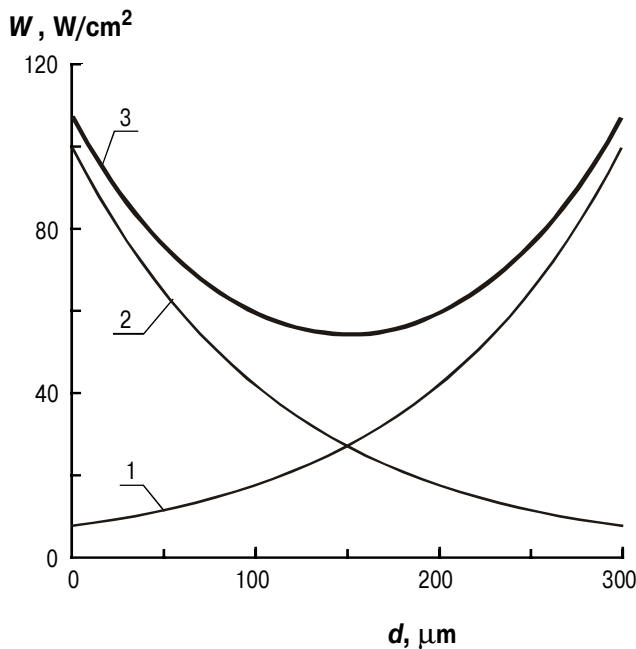


Fig.1.28. Microwave power depth profiles in GaAs single crystal doped with Sn ($n = 3 \times 10^{16} \text{ cm}^{-3}$) for: 1 – incident wave; 2 – reflected wave (the samples are in a cavity resonator); 3 – total power [74].

Interaction between microwave radiation and semiconductor leads to excitation of the electron subsystem, i.e., the electron gas density and temperature grow. Some below-threshold mechanisms for interaction between the excited electron subsystem and structural defects (dislocations, inclusions, impurity complexes) come into force. This results in appearance of temperature and stress gradients.

As mentioned above, there are inclusions in the GaAs wafers studied. These inclusions are Ga precipitates (drops) having metallic properties. The dielectric loss in these regions substantially grows under irradiation, so their temperature grows too. In [73] estimation was made for the time $\tau' \sim s_m^2/A$ that characterizes the dynamics of thermal processes in GaAs. Here s_m is the mean spacing between the local temperature sources; $A = \Lambda/C_p\rho_0$ (Λ is the thermal conductivity, C_p is the heat capacity and ρ_0 is the material density). For estimation the minimal spacing between the Ga inclusions was taken to be 1 mm. Using the known values for GaAs parameters, one obtains $A = 8.77 \times 10^{-5} \text{ cm}^2/\text{s}$. The estimated τ' value was found to be over 100 s. The duration of microwave treatment sessions was not greater than 5 s, thus being much below τ' . So the sample was heated nonuniformly and thermal gradients appeared in it. These were the reasons for intense diffusion and relaxation processes in bulky single crystals after irradiation that led to defect structure modification and redistribution of the elastic strain fields. Thus the mechanisms for interaction between microwave electromagnetic fields and semiconductors are strongly nonequilibrium.

Taking into account the piezoelectric properties of GaAs, one could advance the following mechanism for dislocation slipband generation at cleavage fractures, if in this region the surface electron states are present that are character-

istic of atomically-clean surface. Due to the limiting permittivity jump existing at a cleavage surface, an electric charge appears on it in electromagnetic field. This charge is oscillating with the frequency of the electromagnetic field. Such charge oscillations lead to appearance of inverse piezoelectric effect. The piezoelectric strains appearing due to this effect are propagating as a longitudinal or transverse high-frequency elastic wave (hypersonic vibrations). The type of such wave depends on the electric field orientation relative to the cleavage surface.

In our case a longitudinal hypersonic wave (wavelength of about 3 μm) seemed to appear. It propagated along the $<110>$ direction and was enhanced by the processes occurring at the cleavage surface (that was close to atomically-clean one). If the surface electron levels are only partially filled, then conductance and permittivity for thin (coverage degree of several tens of monolayers) semiconductor layers can be similar to those for metals. So considerable temperature and stress gradients are to appear. They are due to an essential difference between microwave radiation absorption at the surface and in the bulk.

From the above-said it follows that the processes of structural relaxation in GaAs stimulated by microwave electromagnetic field are determined (both during irradiation and after it) by a combined action of thermal, electric and mechanical phenomena. Interrelation between them, as well as their character, depends on the initial structural perfection of the material exposed to microwave irradiation, its morphological parameters and treatment conditions. The intense diffusion of host and foreign atoms, as well as structural relaxation processes, is not accompanied with considerable sample heating. The structural modification, as follows from [20,68,73,74],

could be related to a direct effect of microwave field on the charged defects in a semiconductor, growth of the electron gas density and temperature, as well as with local heating of defect regions via dielectric loss.

The kinetics of relaxation processes in substrates after considerable microwave irradiation demonstrates non-monotonic long-term character. This is evidence that some strongly nonequilibrium physical processes occur in them.

The results obtained show promise of using microwave treatment of semiconductor materials, under optimal conditions, in technological procedures of defect annealing to improve structural uniformity of substrates.

1.6. EFFECT OF MICROWAVE IRRADIATION

ON THE PROCESSES OF INTRINSIC STRESS RELAXATION IN GaAs EPITAXIAL STRUCTURES

Despite the high level of modern technological procedures used when manufacturing GaAs epitaxial layers, the residual intrinsic stresses are always present in them. These stresses have appreciable effect on the properties of epitaxial films. This is the reason why the specialists in materials science are permanently interested in the techniques for regulation of the intrinsic stress level. It was shown above that one of such techniques lies in microwave irradiation. The features of the effect of microwave irradiation on relaxation of intrinsic stresses proceeding in GaAs epitaxial structures of different types are considered below. The irradiation conditions are the same as those used for substrates, namely, frequency of 2.38 GHz, irradiance of 100 W/cm^2 , irradiation sessions 1 or 5 s each.

We investigated the GaAs $n-n^+$ epitaxial structures grown on GaAs (100) substrates 300 μm thick doped with Te

(the impurity concentration up to $2\times10^{18} \text{ cm}^{-3}$). The GaAs layers were grown using vapor-phase epitaxy. Their thickness d was from 6 to 8 μm . The dopant (Te) concentration in them was $2\times10^{15}\div1.5\times10^{16} \text{ cm}^{-3}$. We also studied the multilayer $i-n^-n^-n^+$ -GaAs structures ($n^+ = 3\times10^{18} \text{ cm}^{-3}$, $d_{n^+} = 0.25 \mu\text{m}$, $n^- = 4.5\times10^{17} \text{ cm}^{-3}$, $d_{n^-} = 0.35 \mu\text{m}$, $n^- = 10^{14} \text{ cm}^{-3}$, $d_n = 0.8 \mu\text{m}$) on semi-insulating GaAs substrate and Au-Ti- n^-n^+ -GaAs test structures ($n^+ = 2\times10^{18} \text{ cm}^{-3}$, $d_{n^+} = 300 \mu\text{m}$, $n^- = 2\times10^{16} \text{ cm}^{-3}$, $d_n = 2.5 \mu\text{m}$, $d_{\text{Ti}} = 50 \text{ nm}$, $d_{\text{Au}} = 50 \text{ nm}$).

By and large the processes of structural relaxation in the above GaAs-based epitaxial films resembled those in the substrates. There were some specific features, however, related to the presence of boundaries between phases and distinctions in elastic stress levels as compared to those in bulky GaAs samples. As to the multilayer $i-n^-n^-n^+$ -GaAs structures, the results of our studies have proved that, at the treatment modes used, even a short-term (1 s) session of microwave radiation leads to catastrophic changes in them resulting in material failure.

Microwave irradiation for 5 s leads to appearance of some changes in the dislocation structure of substrates that could be observed on the Borrmann topograms. These changes, however, are not observed for the regions near the film-substrate interface when using Bragg geometry. The changes in the dislocation structure of substrates are accompanied with intense stress fields redistribution over the whole system studied.

For the samples with different initial stress levels the surface form modification under M-irradiation for 5 s is shown in Fig.1.29. One can see that, depending on the initial degree of surface perfection, processes of intrinsic stress relaxation may proceed in noticeably different ways.

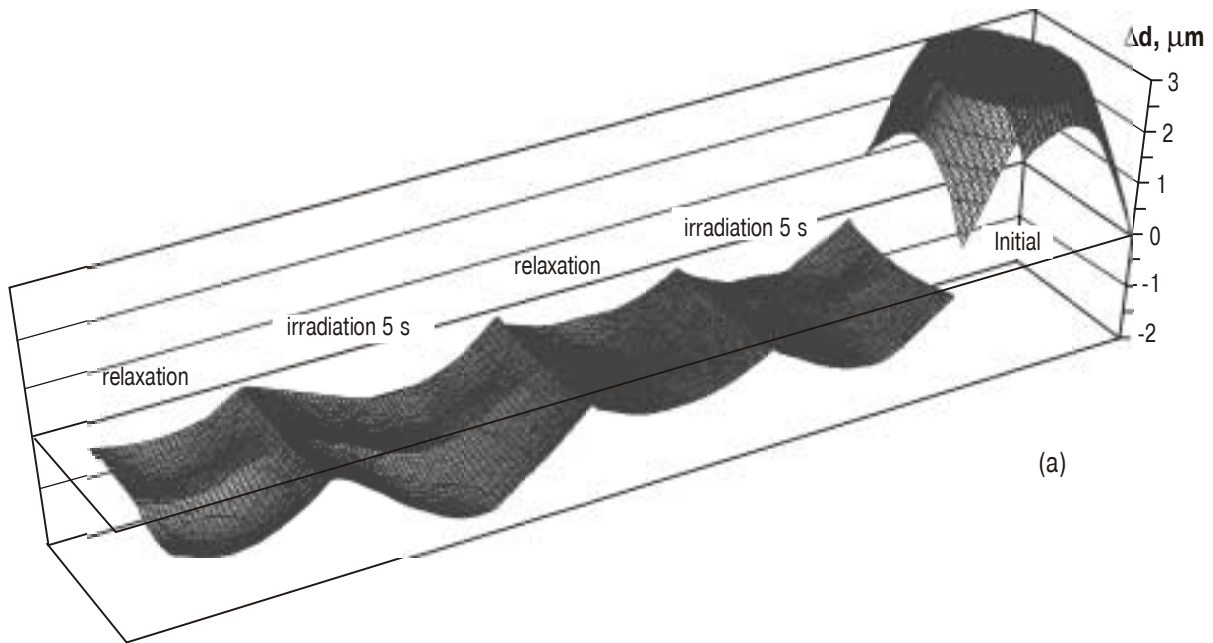


Fig.1.29. Change of the surface form for $n-n^+$ -GaAs epitaxial structures under microwave irradiations for 5 s;
a, b – samples with high and low stress level, respectively.

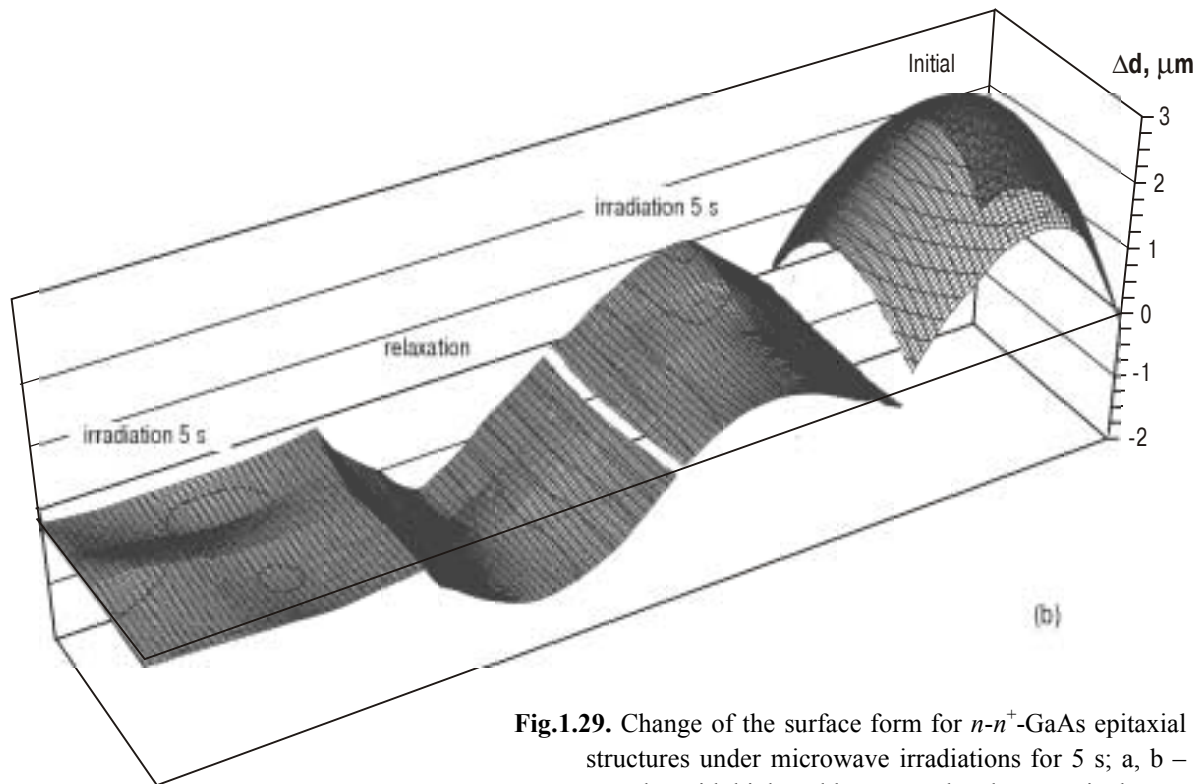


Fig.1.29. Change of the surface form for $n-n^+$ -GaAs epitaxial structures under microwave irradiations for 5 s; a, b – samples with high and low stress level, respectively.

These processes in epitaxial structures are long-term and non-monotonic, as in the case of substrates. However the intensity of relaxation processes that do not need activation is higher for epitaxial structures, as compared to those in substrates. Another distinction is that repeated microwave irradiation of the $n-n^+$ -GaAs structures for 5 s leads, as a rule, to bigger stress relaxation. Shown in Fig.1.30 are the changes in the residual elastic strain fields for those epitaxial structures whose form modifications are shown in Fig.1.29b.

The initial level of the sample structural perfection determines proceeding of the structural modification processes also at the point defect level. The TIQFR values attained at the first stage of microwave irradiation of the samples with higher stresses remained almost the same during further irradiation sessions (see Fig.1.31a). At the same time for the samples whose surface profiles are shown in Fig.1.31b the TIQFR values gradually approached those in a stoichiometric crystal.

For the Au–Ti–GaAs structures exposed to microwave irradiation sessions 5 s each, the elastic strain fields changed approximately in the same way as those in the above-mentioned $n-n^+$ -GaAs structures. The latter, however, demonstrated lower levels of elastic stresses than the Au–Ti–GaAs structures (Fig.1.32), for which microwave treatment for 5 s resulted in partial removal of these stresses. Further microwave irradiation did not lead to complete removal of elastic stresses in the systems studied. Structures with maximal relaxation could be obtained at microwave treatment for 25 s.

Thus presence of a metal film on the GaAs surface, as well as interactions between phases in the metal–GaAs contacts, make an additional impact on the effects of structural modification under microwave irradiation.

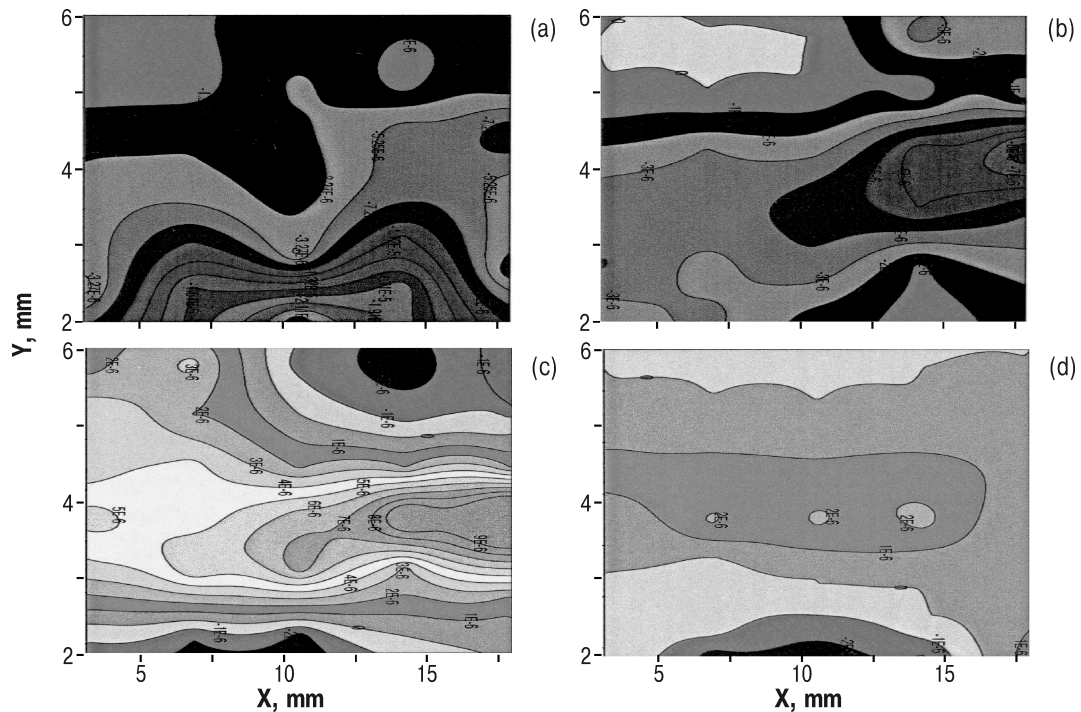


Fig.1.30. Change of the residual strain fields under microwave irradiation for the sample whose atomic plane form changes are shown in Fig.1.29b: a – initial sample; b – after irradiation for 5 s; c – after keeping for 300 h; d – after second irradiation for 5 s.

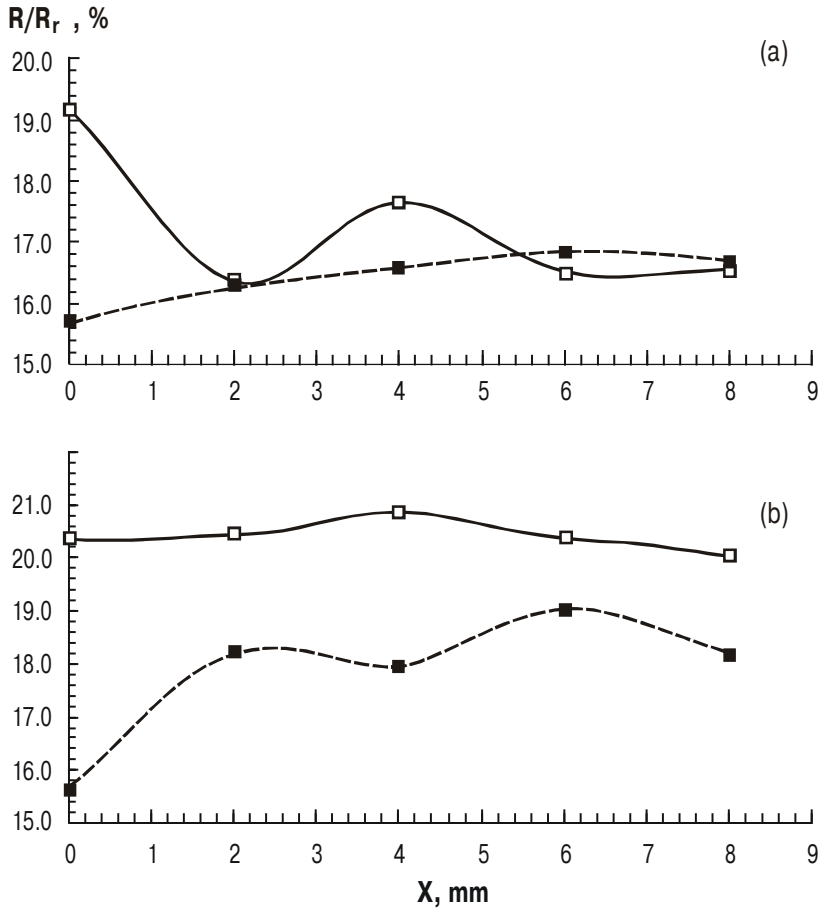


Fig.1.31. Changes of the total intensity of x-ray quasi-forbidden reflections for the samples with different initial stresses after the first (full curve) and second (broken curve) microwave irradiations (each for 5 s); a, b – the samples with high and low stress level, respectively.

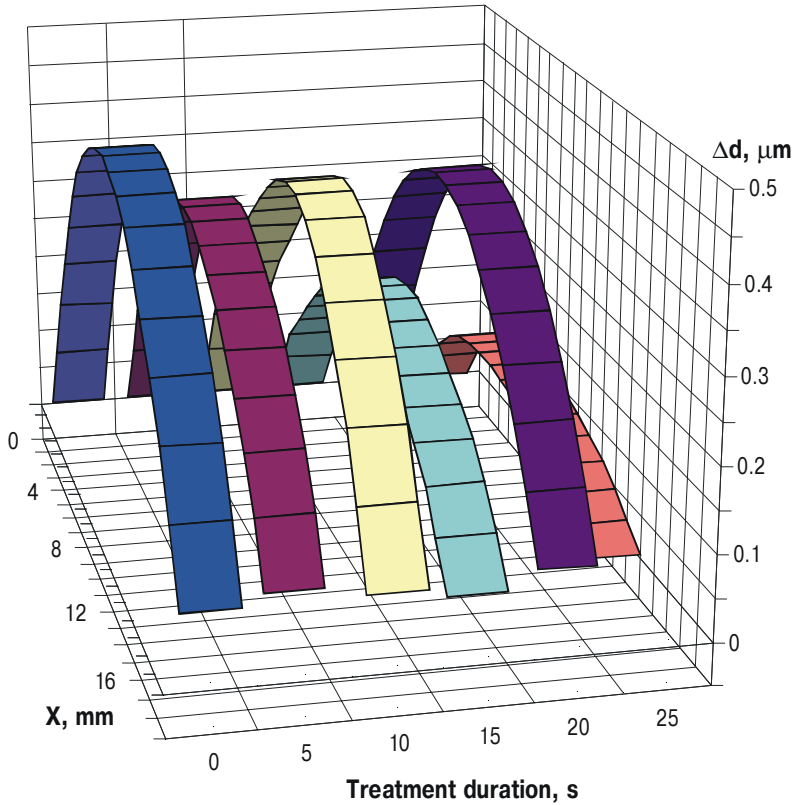


Fig.1.32. Change of the surface profile for Au–Ti– $n-n^+$ –GaAs structure during microwave irradiation.

1.7. EFFECT OF MICROWAVE RADIATION ON THE GaAs MESFET CHARACTERISTICS

Many authors have studied the influence of high-power microwave irradiation on the GaAs metallized semiconductor field-effect transistors (MESFETs) in the context of development of highly reliable element base for microelectronic de-

vices. In particular, the mechanisms for both reversible and catastrophic failures in MESFETs have been investigated rather comprehensively [2-4]. At the same time the initial stages of such actions on the technological GaAs MESFET wafers still remain far from being understood.

The above problem has been touched on in [75,76]. The subjects of investigation were GaAs MESFETs whose design has been described in [77-79]. The technological route for such transistor manufacturing was advanced and discussed in [80] where MESFETs on the wafer were investigated. The SB gate was formed using the Au-Ti metallization, while both the drain and source were formed using AuGe eutectics with further Au metallization.

A magnetron served as source of microwave radiation of frequency $f = 2.45$ GHz and irradiance $W = 1.5$ W/cm². The structures studied were placed on a rotating table to provide uniform, as well as anisotropic, irradiation. Both before and after microwave treatment for 1–300 s we measured the stationary I - V curves of MESFETs and SB gate. From them the following MESFET parameters were determined: transconductance S , initial drain current I_d (at source-drain voltage of 2 V), cutoff voltage V_c , SB height φ_B , ideality factor n .

Shown in Figs.1.33a,b are transconductance and initial drain current vs time of exposure curves for MESFETs on the GaAs wafer. One can see that considerable changes in the MESFET parameters occur at initial radiation doses. In this case both S and I_d values go down, while the cutoff voltage V_c remains practically the same. Further increase of microwave treatment duration leads to growth of S and I_d values but does not affect V_c .

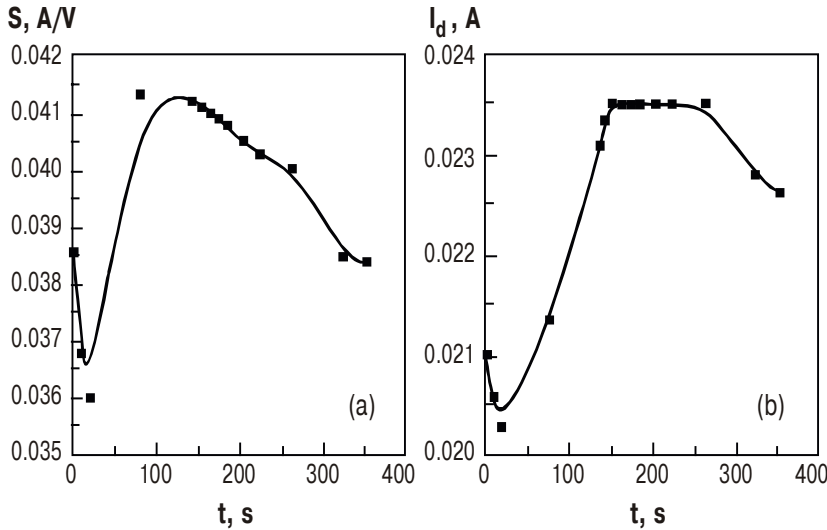


Fig.1.33. Transconductance (a) and initial drain current (b) as function of time of exposure to magnetron irradiation ($f = 2.45$ GHz, irradiance of 1.5 W/cm^2) for GaAs MESFET on wafer [76].

The MESFET stationary I - V curves taken before and after microwave irradiation for 80 s are presented in Fig.1.34. One can see that such microwave treatment improves I - V curves. This is related to the structural-impurity ordering of a near-surface layer in the MESFET channel.

The above changes of MESFET characteristics presented in Figs.1.33 and 1.34 could occur if microwave treatment leads to relaxation of intrinsic stresses. Initially this process leads to the structural defect production accompanied with drop in S and I_d values. At further increase of processing duration the defect gettering stimulated by microwave radiation occurs in the contact near-surface region.

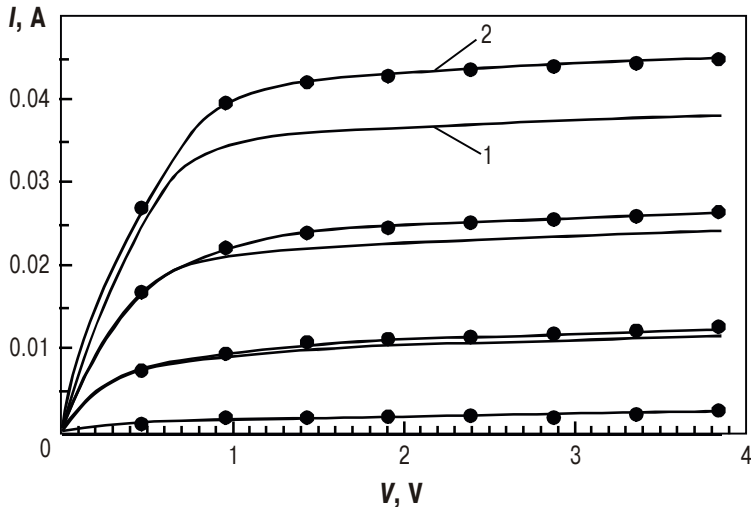


Fig.1.34. Static I - V curve for GaAs MESFET taken at different gate voltages: initial (1) and after exposure to microwave irradiation ($f = 2.45$ GHz, irradiance of 1.5 W/cm^2) for 80 s (2) [76].

Indeed, for MESFET GaAs wafers rather high levels of residual intrinsic stresses are observed after all the technological procedures. The intrinsic stress distribution over the wafers is nonuniform [79]. There are also stress concentrators (another phase inclusions, metal inclusions and points, etc.) at the MESFET wafers. During microwave treatment energy is absorbed in the regions with stress concentrators. This gives rise to the conditions for triggering mechanisms of intrinsic stress relaxation. At further microwave actions the produced defects are draining down to the boundaries between phases of which that between a metal and GaAs is the nearest.

Similar redistribution of structural defects occurs in the MESFET GaAs wafers exposed to ^{60}Co γ -irradiation [78-85]. In [20] it was shown that intrinsic stress relaxation followed with

defect gettering is observed in GaAs test structures, both initial and metallized (Au–Ti–GaAs contact), after exposition to short-term M-irradiation. The diode structure mockups with various metal barrier-forming contacts were irradiated in the same modes as MESFETs. In that case their parameters related to defect gettering were improved: both minority charge carrier diffusion length L_p and SB height φ_B increased, while the ideality factor n , as well as the reverse current I_R , dropped.

We considered intrinsic stress relaxation stimulated by M-irradiation (frequency $f = 2.45$ GHz, output power of 160 W, irradiance $W = 1.5$ W/cm²) immediately on the GaAs samples with MESFET wafer pattern. It was shown for these wafers that their transconductance was an oscillating function of the microwave treatment duration. Besides, it was found that both curvature magnitude and sign changed during M-irradiation. At the time of exposure range from 100 to 500 s some wafers demonstrated absence of stresses (i.e., their radius of curvature equaled to ∞). It was just this time of exposure range for which the MESFET parameters were improved.

An analysis of I – V curves for the Au–Ti– n -GaAs diode structures exposed to microwave irradiation for 1–300 s was performed in [75,76]. It was shown that their parameters φ_B , n and I_R depended on irradiation dose and demonstrated minima (n and I_R) or peak (φ_B) in the time of exposure range from 120 to 180 s. The ideality factor n dropped from 1.06–1.07 (initial value) down to 1.03–1.02 after microwave irradiation, while the SB height φ_B grew from 0.76–0.78 eV (initial value) up to 0.81–0.82 eV after microwave treatment. These results enable one to assume that growth of the transconductance S and initial drain current I_d might be due to the processes of intrinsic stress relaxation discussed above. In the case of structural defect gettering these processes may lead to an increase in the

charge carrier mobility μ_n in the MESFET channel. Indeed, it is known that the channel current $I_{ch} \sim q_0 N_t \mu_n E a b$ and transconductance $S \sim q_0 N_t a b / L_{ch}$ (Here N_t is the dopant concentration in the channel that is equal to the majority charge carrier concentration N_D ; E is the electric field strength; a is the active layer thickness; b and L_{ch} are the channel width and length, respectively.) From these estimation expressions it follows that S and I_{ch} growth might be related to some μ_n increase, since no change in the majority charge carrier concentration has been detected under such microwave irradiation. This conclusion is supported also by an analysis of the capacitance vs voltage curves for Schottky-barrier diodes from which it follows that the doping profile for test structure did not change at times of exposure to microwave irradiation considered in [75,76].

1.8. EFFECT OF MICROWAVE RADIATION ON THE PARAMETERS OF DISCRETE DEVICES AND INTEGRATED CIRCUITS

In previous sections we considered some primary phenomena that appear in semiconductor materials and metal–semiconductor test structures immediately exposed to high-power microwave irradiation. These phenomena intensify inter-phase diffusion and chemical interaction at boundaries between phases, as well as change the generation-recombination processes in both single-phase materials and structures based on them. In the long run the above effects may serve as reasons for degradation of electrophysical parameters of such subjects. These physical effects seem to occur in finished discrete devices and integrated circuits (IC) exposed to high-power microwave fields [91-103].

The investigations dealing with the element base for diodes and transistors have shown that the effect of high-power microwave radiation may be characterized by the following three stages of device operation changing, namely, short-duration failure, performance degradation and catastrophic failure [1-4,91,92,94]. The efficiency of microwave radiation action depends on both the irradiation parameters (frequency, power, frequency band and duration) and device characteristics (material, package and lead geometry, orientation relative to the electric field), as well as on the circuitry features. So an analysis of regularities in the device failures and revealing of information-carrying parameters that characterize the device serviceability make a complicated problem.

The authors of [3,92,93] investigated how short-term microwave irradiation affects the discrete devices. They found that in this case a field mechanism for device degradation was predominant. That mechanism was characterized by presence of some threshold. It was shown in [3,92] that the device degradation appears only when the electric field exceeds certain threshold value. The field mechanism for device degradation causes numerous injuries even during a single session of microwave irradiation. The distribution of these injuries over the surfaces of complex electronic devices is nonuniform.

The threshold values W_{th} and E_{th} characterizing the thermal and electric mechanisms for degradation of diodes and transistors that are used when developing microwave electronic equipment are given in Table 1.4. One can find the W_{th} and E_{th} values for other types of discrete devices and ICs in [3]. It is apparent that the information-carrying parameters W_{th} and E_{th} are macroscopic and do not require detailed knowledge of subject structure for their determination. Such thermal and field threshold parameters for microprocesses oc-

curing in the materials and heterostructures exposed to microwave irradiation remain to be determined.

Table 1.4. Thermal (W_{th}) and electric (E_{th}) degradation thresholds for discrete electronic devices [3].

Device type	W_{th} , J	E_{th} , kV/cm	Failure character	Degradation features
diodes	$(1\text{--}3)\times 10^{-7}$	0.1÷3	catastrophic failure	$p\text{-}n$ junction breakdown
transistors	$(1\text{--}2)\times 10^{-5}$	1÷5	catastrophic failure	breakdown, fusion, metallization burn*

*The injuries are localized in the peripheral near-contact region.

The effect of electromagnetic fields on the IC tolerance was considered in [98-103]. The degradation effects in IC (threshold processes) were shown to essentially depend on the relative orientation of IC and electromagnetic field. It was experimentally found that about 90% bipolar ICs and 70% CMOSICs (complementary metal-oxide-semiconductor ICs) demonstrated catastrophic failures related to metallization melting-down and burning-out (the so-called burn-through). Further development of the above investigations was made in [102] where the authors studied the effect of the higher-type waves on the electromagnetic field distribution near nonuniformities. The model advanced in [102] makes it possible to study interrelation between the permittivity of nonuniformities in discrete devices or ICs and the electromagnetic field structure. The results obtained enable to predict tolerance of the solid-state electronic components to such external actions.

The threshold-like character was found in [95] for IC (in particular, the digital microelectronic devices of serial numbers 133, 533) failures caused by r.f. pulse trains. In this case the IC behavior obeyed the probabilistic law. According to [95], the failure probability W_f is described by the following expression:

$$W_f = \left[(p_c - \langle p(t) \rangle) / \sqrt{2\sigma(t)} \right], \quad (1.15)$$

where $\langle p(t) \rangle$ and $\sigma(t)$ are the mean value and distribution variance of a random variable p_c . Shown in Figs. 1.35, 1.36 are probabilistic characteristics of IC failure as function of r.f. pulse number and intensity. The computer processing of the results obtained in [95] has shown good agreement between the values calculated from expression (1.15) and experimental ones.

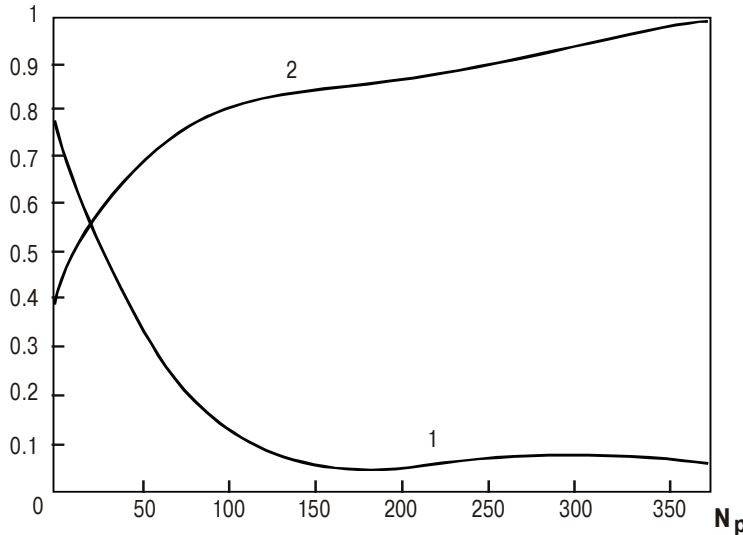


Fig.1.35. Probability density (1) and probability (2) for IC failure as function of r.f. pulse number [96].

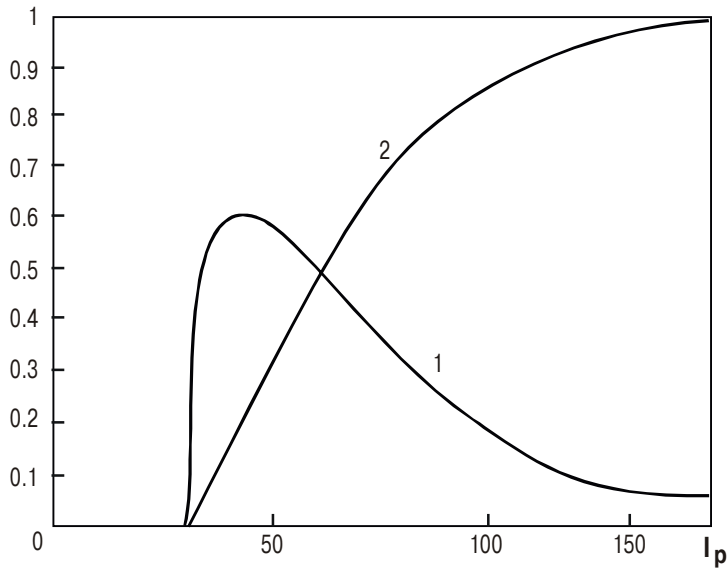


Fig.1.36. Probability density (1) and probability (2) for IC failure as function of r.f. pulse intensity [96].

An analysis of failures in complex microwave facilities and PC caused by ultrashort electromagnetic pulses was performed in [93,104]. It was shown that degradation of complex systems made from solid-state components is due to appearance of a state of dynamic chaos (specific nonlinear response). The authors of [104] believe that the nature of this state is related to the fact that conditions of signal propagation and transformation in microwave transmission lines are non-monotonic and nonstationary. This effect is most clearly pronounced when ultrashort electromagnetic pulses act on analog facilities. The state of “chaos” in them that determines duration of equipment blocking may be several orders of magnitude over the signal duration.

The existence of the effect of “chaos” has been proved in [93,104-106] and now seems to cast no doubt. An interest in this effect, however, has not ceased but transferred to a pragmatic area. A problem arises concerning how probable is its appearance in electronic facilities. One of possible answers has been formulated using statistical simulation. It states that the phenomenon of “chaos” by itself rarely occurs in standard electronic components but probability of its appearance grows with the degree of integration. One could recollect the known principle stating that a workable system can counteract variety of external actions only via variety of its reactions.

* * *

The results presented above show that microwave treatments leading to changes in the electron subsystem state are promising for control over electrophysical properties of spatially-nonuniform semiconductor structures. Action of microwave radiation on the gallium arsenide wafers and epitaxial layers, as well as on the $\text{Cd}_x\text{Hg}_{1-x}\text{Te}$ -based solid solutions, changes the impurity-defect composition and intrinsic stress level in these materials, as well as improves tolerance of their electrophysical parameters to plastic deformation.

The results of a number of experiments dealing with the effect of microwave treatment on the properties of spatially nonuniform systems involving metal contacts to III-V structures are equally promising. It was found that one could reduce leakage currents for both forward and reverse I - V curve branches, as well as spread of the electrophysical parameters for surface-barrier structures. The effect of defect gettering at microwave treatment has been found. It leads to growth of

both lifetime and diffusion length for minority charge carriers, as well as changes the intrinsic stress level in heterosystems (in particular, in metal–semiconductor contacts). Such effects are observed in the tunnel diodes with δ -layers in SCR and MESFETs.

Thus one would expect that, provided the proper irradiation mode is chosen, it would be possible to solve such technological problems as homogenization of properties and removal of undesired defects in semiconductor materials, as well as improve the device structure parameters. To realize these promising prospects in practice, it is necessary, first of all, to investigate various mechanisms for interaction of high-power microwave radiation with semiconductors and device structures. These mechanisms are still far from being understood.

Part 2. LASER METHODS FOR DIAGNOSTICS AND MODIFICATION OF SEMICONDUCTOR COMPOUNDS (GaAs, InSb, SiC), AS WELL AS FORMATION AND DIAGNOSTICS OF STABLE OHMIC CONTACTS

INTRODUCTION

The present-day trends in semiconductor opto- and microelectronic technologies lie in the intense mastering of submicron (in particular, nanometer) range of device element sizes. One of the promising lines on this way is the use of short high-power laser pulses. They provide high rates of lattice heating, as well as local character of their action. Laser modification (LM) of electric and optical parameters of semiconductors is used in micro- and optoelectronics to form irregular structures, such as *p-n* junctions [1], buried layers [2], conducting layers and electric contacts [3,4], as well as for annealing of ion-implanted layers [5] and in technological procedures for production of precipitation centers [6].

Considerable advances have been made in the laser technology applications for semiconductors, especially elemental (Si, Ge). However, the problem of controlled LM of binary compounds, such as III–V (GaAs, InSb) and SiC, still remains unsolved. The reason is that the binary compounds (contrary to elemental semiconductors) are characterized by a

considerably wider spectrum of defect structures, as well as of the mechanisms for their modification and impurity diffusion. In addition, a short-term high-power laser irradiation (LI) leads to considerable gradients of heat and strain fields. This may result in an increase of impurity concentration — a factor that in most cases is unacceptable at modification. At the same time, under certain conditions nanosecond LI can substantially improve the surface parameters for a binary compound (for instance, InSb surface after chemical etching [7]). A mechanism for this effect still remains far from being understood.

The application efficiency of a wide class of semiconductor materials is determined, to a large extent, by the level of methods for control over such important NCC parameters as concentration, lifetime, diffusion coefficient, mobility and surface recombination velocity. The severe requirements on operating speed give impetus to investigations of the direct-gap materials like GaAs, other III–V compounds, ternary compounds, etc. These materials are promising for optoelectronics because they provide rather high operating speed and higher quantum efficiency. The NCC lifetimes (diffusion lengths) in them are by five (three) orders of magnitude below, and surface recombination velocities are by a factor of several hundreds over the corresponding values in Si and Ge.

In recent years of special interest are high potentialities offered by SiC for use under extreme external actions (radiations, electromagnetic fields, high temperature). Determination of NCC parameters in this case is complicated because one has to deal with nonequilibrium processes occurring for ultra-short time intervals (radiative and Auger recombination, charge carrier heating, etc.). In this case it is profitable to use laser excitation of high intensity. This makes it possible to simulate the operating conditions for a wide range of semi-

conductor devices that are functioning at high NCC concentrations. Among them are semiconductor lasers, modulators, detectors of laser radiation, etc.

Considerable progress has been made in manufacturing technology for α -SiC single crystals that are suitable for production of heat-tolerant ICs. In this connection the requirements on formation of high-melting ohmic contacts to submicron layers of α -SiC have become more severe. Such contacts must meet all the standard requirements on ohmic contacts used in semiconductor devices. They have to provide minimal contact resistance and I - V curve linearity over a wide range of operating current and temperature. Their interface, when forming ohmic structure, has to be thin and have an even front. The latter requirement is of special importance for submicron layers used in ICs.

When developing heat-tolerant ohmic contacts to p -GaAs, the central problem appears at transition to submicron sizes. Traditionally the Au–Ge eutectics are used in thin layers, and compositions formed by Ga and Au are chemically unstable. As a result, the unstable interfacial and surface relief nonuniformities (vertical and horizontal irregularities of 0.2–0.3 μm) appear. They are quite undesirable for submicron technology. The use of traditional techniques for contact formation involves rather high temperature and long duration of thermal annealing. These factors result in diffusion of undesired impurities and mass transport of contact components both to and from the structure used. Besides, surface wetting for semiconductor–metal transition layers is impaired and high-resistance compounds formed by the metals involved may appear.

To meet the present-day requirements on contacts, purposeful development of pulse laser techniques for structure formation and control is needed. The advantages of such

techniques are their local character, short duration of high-power technological action and nondestructive testing action. Below are presented the results of theoretical and experimental studies of defect modification in III-V compounds (GaAs and InSb are examples) and development of ohmic contact structures to α -SiC and p -GaAs, under nanosecond laser pulses, as well as nondestructive laser-thermal diagnostics.

2.1. MODEL FOR DEFECT PRODUCTION IN III-V SEMICONDUCTOR COMPOUNDS BY NANOSECOND LASER PULSES

By now it has been found that when a semiconductor absorbs energy from laser pulses whose duration is at least several tens nanoseconds, then dissipation of this absorbed energy proceeds according to the thermal model [8]. However the results of laser action on semiconductors have some quantitative distinctions from the case of traditional thermal treatment. These are anomalously high values of impurity concentrations in modified layers and depths of these layers. They essentially depend on the experimental conditions: laser radiation wavelength λ , pulse duration t_p and radiation intensity I . Under LI defect concentration may decrease or increase, and sample surface may become more even or degraded (usually the changes begin to appear at the surface).

It was noted above that presence of considerable temperature and strain field gradients at LM of semiconductors [9] does not inevitably result in defect production. To illustrate, the effect of decreasing surface recombination activity at I values below threshold (I_{th}) is known to occur in InSb [7,10], InP [11] and GaP [12]. At the same time such effect does not appear in GaAs with low doping level [13]. The reason for such distinction in the LM effect remains unclarified.

It is known that nanosecond LI of GaAs in the intrinsic absorption region results in appearance of high-resistance layers with elevated defect concentrations [14,15]. The authors of [14] relate high resistance of laser-modified GaAs layers to production of intrinsic defects in the near-surface layers. These defects are interstitial atoms I_{As} and I_{Ga} , gallium (V_{Ga}) and arsenic (V_{As}) vacancies, antisite atoms — Ga in arsenic sublattice (Ga_{As}) and As in gallium sublattice (As_{Ga}), as well as their complexes. Absence of a "window" for defect-free LM of GaAs was stated in a number of papers.

At the same time for another III-V compound, InSb, the conditions have been experimentally determined under which the surface recombination velocity substantially drops [7]. These are as follows: irradiation with a Q -switched ruby laser, $\lambda = 0.69 \mu\text{m}$, $t_p = 30 \text{ ns}$, $W_{th} \sim 1.5 \text{ MW/cm}^2$. Similar results have been also obtained using the yttrium-aluminum-garnet laser (YAG:Nd³⁺) [10] or CO₂ laser (whose radiation is weakly absorbed) [16].

The explanations for the results obtained by different authors do not correlate with each other. The authors of [16] relate the above effect to surface melting and intense oxidation, while the authors of [10] explain it within the frameworks of structural modification (the type of this modification being undetermined). It seems to us that the nature of laser-stimulated defect production in III-V compounds (using InSb as an example) could be understood taking into account the following. LI produces in InSb many interstitial In and Sb atoms (I_{In} and I_{Sb}), as well as vacancies (V_{In} and V_{Sb}). Under rapid heating these vacancies and interstitial atoms are diffusing in the bulk with different velocities, since they have different diffusion coefficients: $D(I_{\text{In}}) > D(I_{\text{Sb}})$ and $D(I_{\text{In}}), D(I_{\text{Sb}}) \gg D(V_{\text{In}}), D(V_{\text{Sb}})$ [17]. This fact breaks the equilibrium distribution of interstitial atoms

and vacancies near the surface. It is known that I_{In} (I_{Sb}) serves as donor (acceptor) [18] and the interstitial In atoms move opposite the temperature gradient [19,20]. As a result, a spatial redistribution of I_{In} occurs in the near-surface layer, thus giving rise to a layer of n -type. The I_{In} concentration depth profile can be calculated from the nonstationary diffusion equation [19]

$$\frac{\partial N_v}{\partial t} = \frac{\partial}{\partial x} \left[D_0 e^{-E_a/kT} \left(\frac{\partial N_v}{\partial x} - N_v F \right) \right]. \quad (2.1)$$

Here N_v is the V_{In} concentration; F is the force acting on an indium vacancy due to a temperature gradient: $F = -\frac{Q^*}{T} \cdot \frac{\partial T}{\partial x}$, where Q^* is the heat of I_{In} migration; E_a is the activation energy; the coordinate x grows from the surface ($x = 0$) into the bulk. From the microscopic theory [21] one can get the following expression for Q^* in the case of I_{In} : $Q^* = akT$ where $a \approx 3.5$.

The meaning of Q^* could be qualitatively explained with the help of the expression $Q^* = H_0 - H_f$ where H_0 (H_f) is the energy of the initial (final) atomic configuration corresponding to an elementary displacement act. The sign of Q^* (and, correspondingly, the direction in which an atom moves) depends on the sign of parameter a . The latter is determined by the interrelation between covalent radii and covalent bonding energies for diffusing atoms and host atoms involved in the diffusion process, as well as by the type of their movement in the lattice. At $a > 0$ the force F is oriented opposite the temperature gradient. If $a < 0$, then F reverses its orientation and atoms move from the cold region to the hot one.

The calculations were performed for a semiconductor sample placed in the temperature field $T = \Delta T \exp(-x/x_0) + T_0$. Let us introduce the dimensionless coordinate $\xi = x/x_0$ and di-

mensionless time $\tau = tD_0 / x_0^2$. Then the equation (2.1) takes the following form:

$$\frac{\partial N_v}{\partial \tau} = \frac{\partial}{\partial \xi} \left[D_0 e^{-E_a / kT} \left(\frac{\partial N_v}{\partial \xi} + \frac{N_v a}{T} \cdot \frac{\partial T}{\partial \xi} \right) \right], \quad (2.2)$$

where $T = \Delta T \exp(-\xi) + T_0$. The following values were used for calculation: $T_0 = 300$ K; $E_a = 1.2$ eV; $\Delta T = 500$ and 400 K. The boundary condition was $\left(\frac{\partial N_v}{\partial \xi} + \frac{N_v a}{T} \cdot \frac{\partial T}{\partial \xi} \right) \Big|_{\xi=0} = 0$, ac-

cording to the law of conservation for the total number of I_{In} and I_{Sb} [22]. The initial distributions of the interstitial In and Sb atoms near the surface were taken as initial conditions.

One can see from Fig.2.1 that the I_{In} concentration depth profiles (corresponding to the same τ values) spread with temperature. They have peaks $N_v(\delta) \Big|_{\xi=\delta} = N_{v\max}$ in the semiconductor bulk. The calculated peak position δ is 0.5 μm at laser radiation intensity of 3 MW/cm 2 .

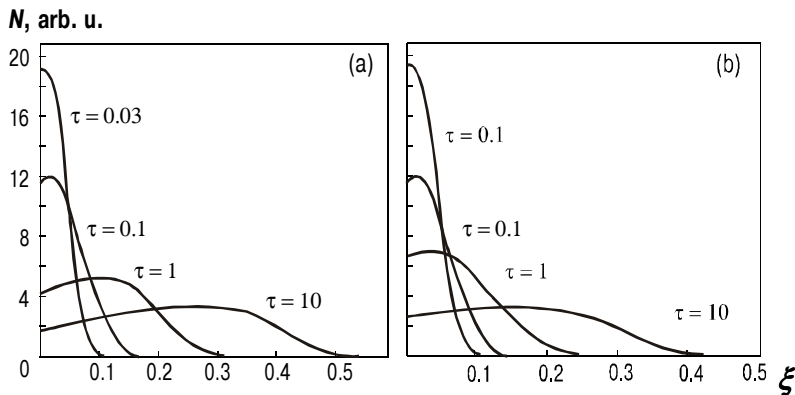


Fig.2.1. Change of the interstitial In atom concentration I_{In} depth profile with time: a – $T = 800$ K; b – $T = 700$ K.

2.2. TECHNIQUES AND EQUIPMENT

2.2.1. A plant for laser pulse sputtering

The experimental plant (see Fig.2.2) involved: *Q*-switched YAG:Nd³⁺-laser (1) (wavelength $\lambda = 1.06 \mu\text{m}$, pulse duration $t_p = 2 \times 10^{-8} \text{ s}$, repetition frequency of 12–100 Hz, pulse energy $E_p = 0.3 \text{ J}$); pulse energy meter ИМО-2H (2); pulse amplitude and form meter ФЭК-09 (3); focusing system (4); standard vacuum chamber (5) (pressure of about 10^{-4} Pa). The plant was equipped with the automatic scanning systems (to scan laser beam over the target and substrate), system for substrate temperature control and vacuum system with two nitrogen traps. Automation of laser beam scanning over the target surface enabled to follow the required mode of laser evaporation by synchronizing the laser pulses with the evaporated target movement and control the relationship between the LI repetition frequency and scan velocity.

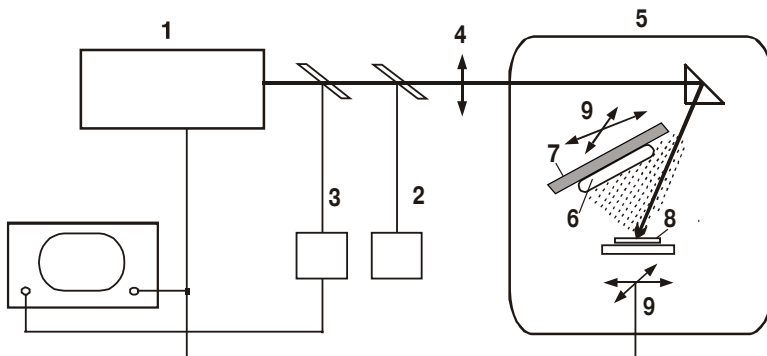


Fig.2.2. Diagram of the plant for pulse laser sputtering. 1 – YAG:Nd³⁺-laser; 2 – laser pulse energy meter ИМО-2M; 3 – coaxial photocell ФЭК-09; 4 – focusing system; 5 – vacuum chamber; 6 – sample onto which sputtering is made; 7 – substrate with electric heating; 8 – target; 9 – automatic scanning systems.

The contact layers were deposited through the Kovar masks (made using laser cutting) to provide the required layout of the deposited structure (e.g., for the four-probe technique for contact resistivity measurements). The deposition rate was controlled by the laser pulse repetition frequency and power. It was determined using a reference film whose thickness d_f (≥ 250 nm) was sufficient for measurement with a МИИ-4 microinterferometer.

2.2.2. A plant for laser modification of semiconductors

When studying modification of semiconductor materials and structures under LI, one has need for a control over the temperature of active area. To allow electrophysical and PL investigations of the modified layer parameters, the sample surface area S_s should be large enough (≥ 0.5 cm 2). In experiments the laser beam cross section S_b may be as small as ≤ 0.35 cm 2 and the irradiance W_0 in case of unfocused LI is < 0.1 J/cm 2 . The solution of the problem of performing measurements under the above conditions has become possible with the use of an automated system for focused LI scanning (with regulated degree of laser spot interception) concurrently with pyroelectric facility to control the temperature [23] in active area.

The plant for LM on the basis of a laser scriber ЭМ-210 has been upgraded (as concerning the section for detection of thermal emission), supplemented by a high-power pulse quantron K-107 (YAG:Nd $^{3+}$ -laser), power supply unit, synchronization unit and PC. The diagram of the plant is presented in Fig.2.3.

The plant operation proceeds as follows. First the fixation of position of the two-coordinate table with the sample studied is program-stimulated. Then signals for starting the

pump lamp of the laser quantron and (with a time lag) the electrooptical modulator are generated. Thermal emission from the laser-irradiated sample area is collected by the pyroelectric (lithium niobate) detecting system. From it a signal is applied (via a preamplifier) to the broadband amplifier Y3-33 and the screen of the storage oscilloscope C8-12. The system to control the laser radiation parameters is similar to that used in the plant for pulse laser sputtering (section 2.2.1).

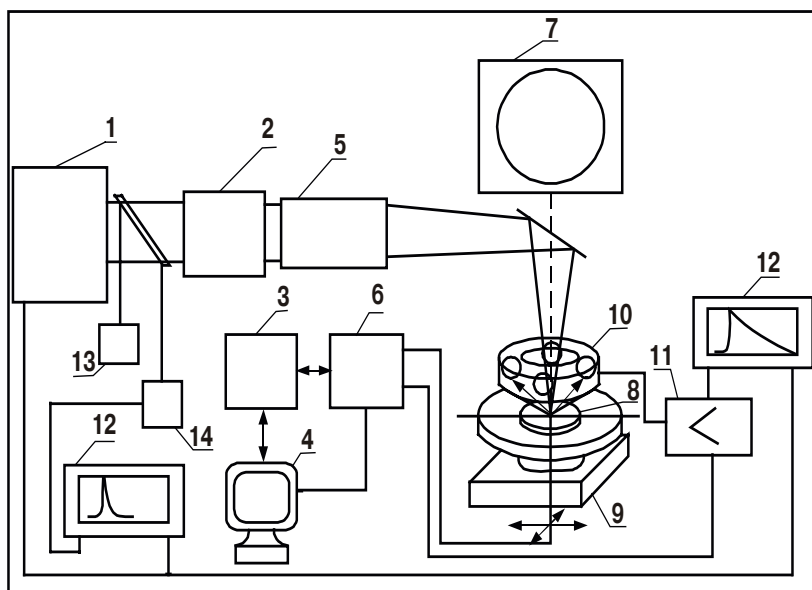


Fig.2.3. Diagram of the plant for laser modification. 1 – YAG:Nd³⁺-laser (pulse quantron K-107); 2 – focusing system; 3 – PC; 4 – monitor; 5 – homogenizer; 6 – controller; 7 – visualizer; 8 – sample; 9 – positioner; 10 – pyroelectric system; 11 – amplifier; 12 – oscilloscope; 13 – calorimeter ИМО-2Р; 14 – coaxial photocell ФЭК-19К.

2.3. LASER MODIFICATION OF GaAs AND InSb

To study the LI effect on the spatial distribution of recombination centers in III-V binary compounds, we used the magnetoconcentration effect (MCE) [24]. It is known that when a semiconductor is placed in crossed electric **E** and magnetic **H** fields, then a transverse drift of charge carriers (both equilibrium and nonequilibrium) occurs. The direction of this drift depends on the Lorentz force orientation. If the Lorentz force is directed towards the sample surface, then the bipolar conduction component (characterized by the charge carrier concentration n_{bp}) decreases because the surface recombination centers come into force. And vice versa, if the Lorentz force is directed from the sample surface, then the sample conductance increases since in this case the n_{bp} value is determined by the charge carrier lifetime in the bulk (τ_b).

GaAs has a wide gap E_g . So at room temperature the concentration of intrinsic charge carriers n_i (about 10^7 cm^{-3}) may be less than that of the uncompensated impurity by several orders of magnitude. Therefore at room temperature it is more convenient to study the bipolar component of conduction provided by NCC. That is why we studied the laser-modified GaAs layers using MCE on charge carriers excited with a He-Ne laser ($\lambda = 0.63 \mu\text{m}$). Contrary to this, in InSb at room temperature $n_{bp} \equiv n_i \sim 10^{16} \text{ cm}^{-3}$ (the residual impurity concentration is about 10^{14} cm^{-3}). So to study MCE in InSb, it was quite sufficient to use the intrinsic dark conduction.

Let us consider LM of GaAs and InSb surfaces. To study the defect transformation in GaAs, we chose the GaAs (100) samples ($l \times h \times w = 0.7 \times 0.3 \times 0.3 \text{ cm}$) with the minimal initial lattice disordering and not too high compensation degree (resistivity $\rho \sim 10^4 \Omega \cdot \text{cm}$). Just before LM the samples were etched in two sessions: 1) in a solution $\text{H}_2\text{SO}_4:\text{H}_2\text{O}_2:\text{H}_2\text{O} = 3:1:1$ at 70°C for 1 min. and 2) in a dilute solution of HCl to remove the re-

mains of oxide. The irradiation was performed in the air at room temperature with the first and second harmonics of the YAG:Nd³⁺-laser ($\lambda_1 = 1.06 \mu\text{m}$, $\lambda_2 = 0.53 \mu\text{m}$, $t_p = 10 \text{ ns}$). For some samples TiO₂ capsulating layers have been sputtered onto their irradiated surfaces to study the effect of volatile component evaporation.

We took I - V curves in the crossed electric and magnetic fields ($\mathbf{E} \times \mathbf{H}$) at irradiation from a He-Ne laser, and also the stationary PL spectra. The contacts to the Czochralski-grown semi-insulating GaAs samples were made using pulse laser sputtering of multilayer GaAs/Si/W/Ni structure followed by laser annealing. Shown in Fig.2.4 is the typical evolution of dark I - V curves at different stages of laser annealing.

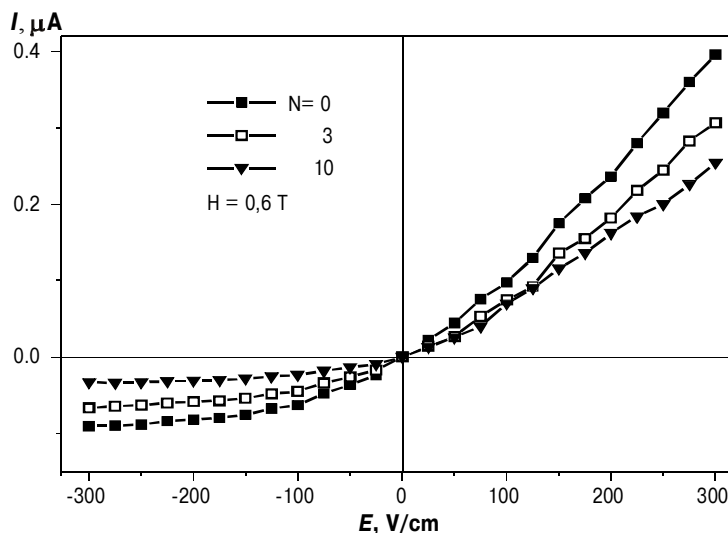


Fig.2.4. Evolution of I - V curve for Czochralski-grown semi-insulating GaAs/Si/W/Ni system during laser annealing (YAG:Nd³⁺ laser; $\lambda = 0.53 \mu\text{m}$; pulse duration $t_p = 10 \text{ ns}$). Number of pulses N_p : 1 – $N_p = 0$; 2 – $N_p = 1$; 3 – $N_p = 3$; 4 – $N_p = 8$.

One can see that, within the electric field range used, the contacts remained sufficiently ohmic. A typical set of photo- I - V curves taken under MCE is presented in Fig.2.5. One can see that LI resulted only in a decrease of I - V curve slope for both orientations of the Lorentz force and, consequently, to a drop of photocurrent as against the initial value. The surface recombination velocity S_r as function of the number N_p of laser pulses for Czochralski-grown semi-insulating GaAs is shown in Fig.2.6. The S_r values were calculated from PC in crossed $\mathbf{E} \times \mathbf{H}$ fields according to the procedure advanced in [25]. The threshold irradiance values at which the irreversible changes (I_i) and visually observed damage (I_d) of GaAs and InSb sample surfaces occurred are presented in Table 2.1.

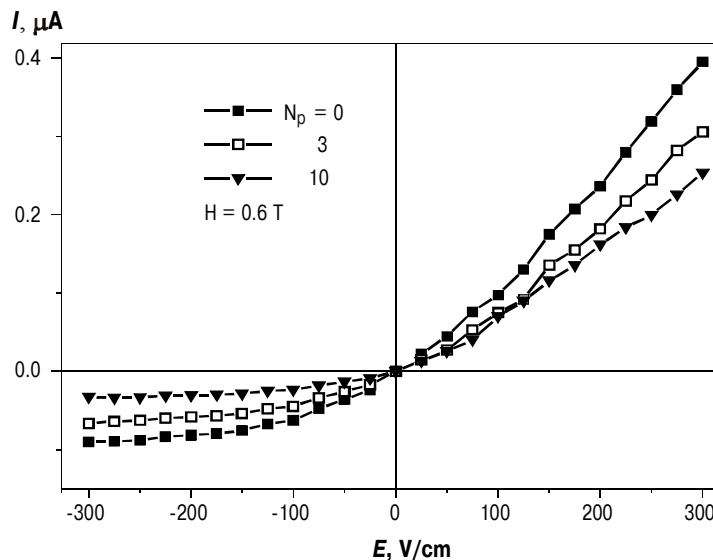


Fig.2.5. Dependence of the luminous I - V curve for GaAs in crossed $\mathbf{E} \times \mathbf{H}$ fields on the number of pulses (YAG:Nd³⁺ laser; $\lambda = 0.53 \mu\text{m}$; pulse duration $t_p = 10 \text{ ns}$).

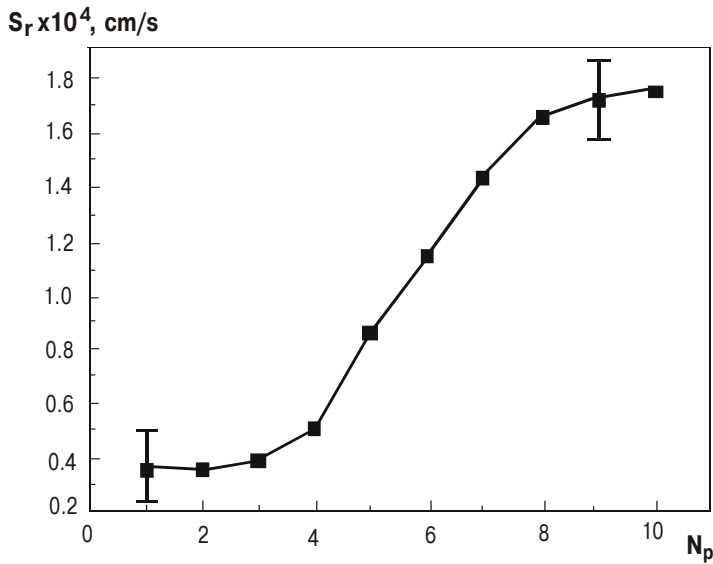


Fig.2.6. Dependence of the surface recombination velocity S_r for GaAs in crossed $\mathbf{E} \times \mathbf{H}$ fields on the number of pulses (YAG:Nd³⁺ laser; $\lambda = 0.53 \mu\text{m}$; pulse duration $t_p = 10 \text{ ns}$).

The above results agree with those obtained by us from the PL spectra of GaAs. Considerable changes in the PL bands after LM are of only one character, namely, the total intensities of PL decrease. These results evidence that there is no indication at a "defectless" modification "window" for GaAs under the experimental conditions used. It should be noted that no drop of recombination activity was observed for etched GaAs surface exposed to laser pulses of nanosecond duration at other wavelengths ($\lambda = 1.06, 0.53$ and $0.31 \mu\text{m}$). This is in agreement with the results obtained in [26,27]. Use of a capsulating TiO₂ layer did not qualitatively change the results of LM under the conditions of the above experiment.

Table 2.1. The threshold values of laser irradiation intensity for irreversible changes (I_i) and visually observed damage (I_d) of GaAs and InSb sample surfaces.

Material and impurity	Type of laser and threshold value of laser irradiation intensity, MW/cm ²			
	YAG:Nd ³⁺ ($\lambda = 0.53 \mu\text{m}$, $t_p = 10 \text{ ns}$)		XeCl ($\lambda = 0.31 \mu\text{m}$, $t_p = 120 \text{ ns}$)	
	I_i	I_d	I_i	I_d
Czochralski-grown semi-insulating GaAs (Cr_2O_3)	2.3	6.2	0.8	1.6
Czochralski-grown semi-insulating GaAs (Cr_2O_3)/ TiO_2	2.0	5.6	0.5	1.4
GaAs:Si	1.9	5.2	0.8	1.5
InSb	1.5	3.5	0.5	1.2
InSb/ SiO_2	1.3	3.4	0.2	0.8

To study the defect transformation in InSb, we chose the p -type samples with uncompensated acceptor concentration; $N_A - N_D \approx 10^{14} \text{ cm}^{-3}$. The sample size was chosen using the following considerations. The sample length l should be such as to provide illumination uniformity. The sample thickness d was taken to fulfill the condition $d \geq L$ to enable determination of changes in the effective thickness d_e for a sample with bipolar conduction using MCE. (Here L is the bipolar diffusion length for NCC; at a temperature of 200 K $L \approx 30 \mu\text{m}$.) The peak of the sample conductance as function of its thickness d should be expected at $d_e = 1.4 L$ [28]. The illuminated sample surface was etched in CP-4A to obtain the minimal

surface recombination velocity ($S_{r\min} \approx 10^3$ cm/s). The opposite sample face was mechanically polished to obtain the maximum surface recombination velocity ($S_{r\max} \approx 10^5$ cm/s). Such asymmetric surface treatment was required to improve the efficiency of the technique that depended on the d_e value.

The dynamics of the laser donor centers production was studied from I - V curves in crossed $\mathbf{E} \times \mathbf{H}$ fields ($E \leq 400$ V/cm, $H = 0.1$ T). The controlled p - n junction depth was determined from I - B (current vs magnetic induction) curves at transverse magnetic fields up to 0.3 T (see Fig.2.7). To perform LM, we used a Q -switched YAG:Nd³⁺-laser ($\lambda = 1.06$ μm, $t_p = 10$ ns, energy of 0.1 J).

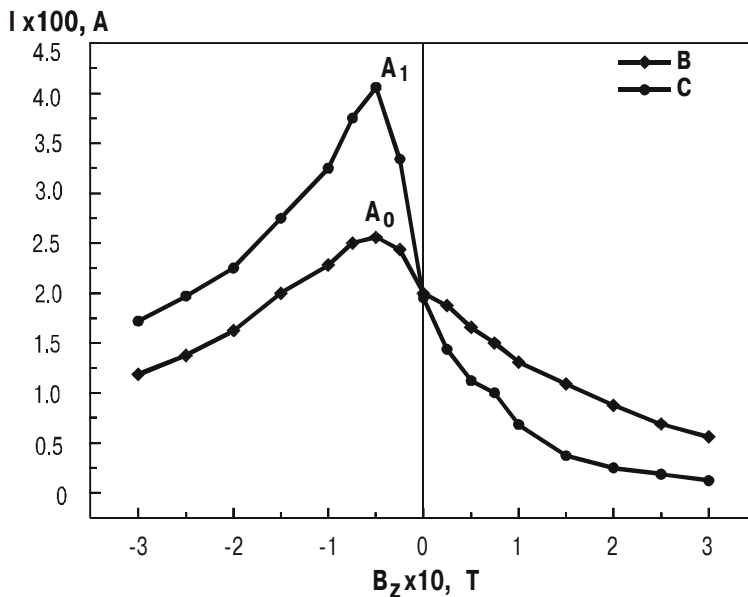


Fig.2.7. Current I vs magnetic induction B curve for p -InSb sample before (B) and after (C) laser irradiation (irradiance $W = 3.5$ MW/cm²).

The samples were exposed to LI in the air at room temperature. The surface morphology was studied, both before and after the laser treatment, with atomic force microscopy. We have determined the threshold irradiance values for the laser donor centers production and InSb surface melting. They were about 1.5 and 3.5 MW/cm², respectively.

After exposure to LI with irradiance of 1.5 MW/cm² (when the activation threshold is reached) the conductivity of the illuminated sample surface becomes of *n*-type. In this case the centers of at least the following two types are observed: (i) those that remain stable at temperatures up to $T = 670$ K and (ii) unstable at room temperature. From the temperature measurements we obtained for the stable centers the activation energy $E_a = 1.1$ eV. This value correlates well with the activation energy for vacancies V_{In} . It is known [17] that in the high-temperature region ($T > 400$ K) the In vacancies are annealed quicker than V_{Sb} . When $\nabla T \neq 0$ exists, the above fact substantially violates the equilibrium distribution of I_{In} and V_{In} . The diffusion coefficients $D(I_{\text{In}})$ and $D(V_{\text{In}})$ are different. Therefore at rapid cooling the frozen interstitial In atoms and vacancies are separated in space. Having opposite electric charges, they remain in a polarized state, thus leading to appearance of a *p-n* junction. The threshold character of the observed effect seems to be related to temperature gradient growth up to a threshold value ∇T_{th} (due to nonuniform heating of a crystal). This enhances migration of interstitial In atoms. At several sessions of exposure an accumulation effect occurs. It is due to formation of a potential barrier. Presence of a *p-n* junction near the semiconductor surface under MCE is equivalent to absence of surface recombination ($S_r = 0$). In this case crystal conductance change is determined by a decrease of the effective thickness d_e of the sample region with

bipolar conductivity (i.e., the thickness of *i*-layer with intrinsic conductivity). The above decrease results from growth of the controlled *p-n* junction depth. The *p-n* junction spreading into the crystal bulk with LI intensity begins at the initial thickness *d* of the sample that is somewhat over the diffusion length *L* (see Fig.2.8, point A₀). Owing to this fact, the sample conductance grows and then flattens out. An estimation of the controlled *p-n* junction depth *x_j* made from *I-B* curve (Fig.2.7, point A) using the criterion $d_e \cong 1.4 L$ gives $x_j = 8 \mu\text{m}$ (the initial thickness *d* of the sample being 50 μm).

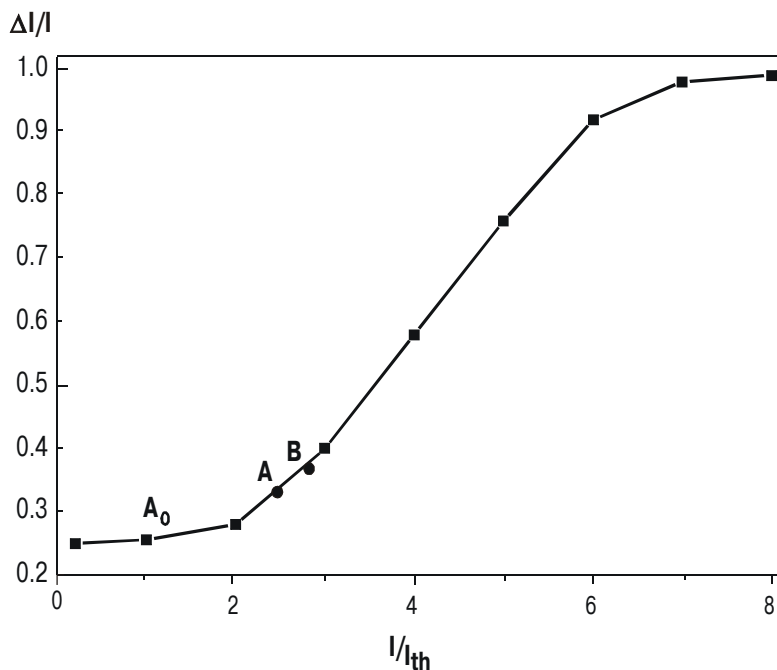


Fig.2.8. Relative change of the InSb sample conductance as function of laser irradiation intensity [21].

A considerable disagreement with the result of theoretical calculation ($x_j = 0.5 \mu\text{m}$) could be explained by existence, during LM, either of a metastable state of matter (that is characteristic of binary compounds [29]) or a liquid phase for which the atomic diffusion coefficients are essentially bigger than those in solid phase. The atomic force microscopy studies of *p*-InSb surface morphology changes under LI have revealed appearance of drop-shaped objects (see Fig.2.9) similar to those observed at InSb surface irradiation with a CO₂-laser [16]. Besides, an increase of surface damage at irradiances over 3.5 MW/cm² has been detected (see Fig.2.8, point B) [21].

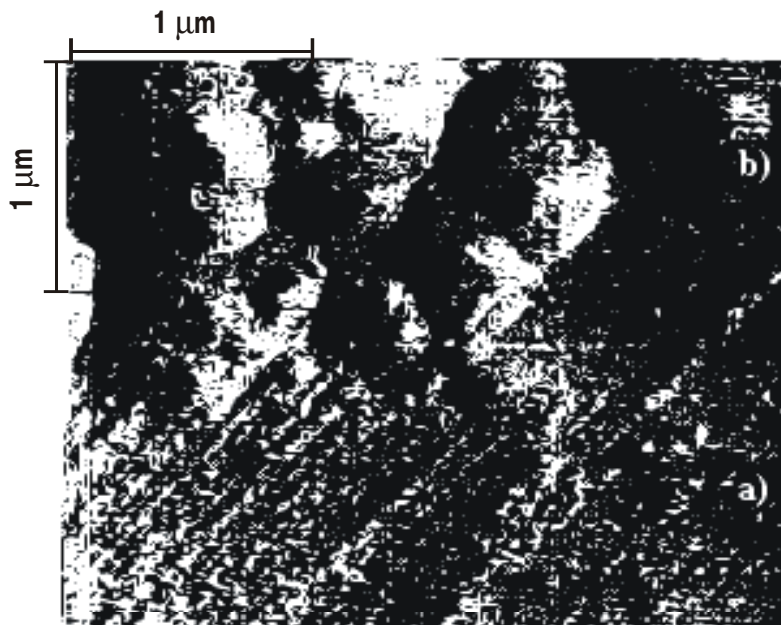


Fig.2.9. InSb surface morphology before (a) and after (b) laser irradiation (irradiance $P = 6.0 \text{ MW/cm}^2$).

A probability of existence, for some time, of a metastable state of InSb crystal lattice is known to be high [29,30]. So one could assume that at irradiances lying in the 1.5– 3.5 MW/cm² range a degree of dissociation for In–Sb pairs in the InSb liquid phase is insufficient to obtain high defect concentration after recrystallization (Fig.2.9, section a). The section b in the upper part of Fig.2.9 that is observed at irradiances over 6.0 MW/cm² seems to be caused by recrystallization from the stable (overheated) state that leads to a considerable increase in the lattice defect concentration. This conclusion is supported by the fact of current drop after LI of the above irradiances under transverse drift of charge carriers toward the exposed surface. It should be noted that, as in the case of GaAs, the capsulating insulator layers (TiO_2 , SiO_2) did not qualitatively change the results obtained. Therefore one may state that for both materials the observed effects did not result from the laser-enhanced formation of surface oxides or other factors related to photochemical surface reactions, as well as from possible stoichiometry violation due to noncongruent evaporation from the InSb liquid phase.

For GaAs LI substantially increases concentration of structural defects, such as vacancies, interstitial atoms and antisite defects Ga_{As} and As_{Ga} . Contrary to InSb, deep lying centers appear in the GaAs gap. They increase the recombination rate [11,13,14]. A material layer of higher resistivity is produced due to self-compensation [27]. This fact seems to be the principal reason why no barrier structures (similar to those in InSb) are formed in high-resistance GaAs. One should also take into account that the degrees of GaAs and InSb melt dissociation differ fundamentally. According to [30], liquid GaAs is much more dissociated (due to absence of a metastable state) than liquid InSb. So a probability to find Ga–As pairs in GaAs melt is substantially lower than in the case of InSb melt. This serves as an

additional factor favoring formation of more perfect InSb lattice at cooling.

Thus the results obtained for GaAs and InSb using the determined criteria within the developed model may be of use when applying the controlled laser techniques to solve the following problems:

- choosing of diffusing atoms (foreign and host) for semiconductor materials;
- development and fabrication of irregular structures of prescribed configurations for a wide range of semiconductors;
- obviation of the need in such technological procedures as previous ion implantation and impurity diffusion when dealing with specially undoped semiconductors.

2.4. LASER DIAGNOSTICS OF NONEQUILIBRIUM CHARGE CARRIERS IN SEMICONDUCTORS

It is known that nonlinear effects appear in semiconductors at considerable NCC concentrations. These effects are due to many-particle recombination, charge carrier degeneration, nonparabolicity of the conduction band, electron-hole scattering. In GaAs and InSb such effects occur even at moderate NCC concentrations. In addition (as was noted above) the NCC diagnostics is complicated because it is necessary to take into account charge carrier diffusion from the illuminated surface to crystal bulk.

2.4.1. A contactless technique for determination of bipolar diffusion coefficient for nonequilibrium charge carriers

It is rather difficult to take into account the above effects when determining the NCC characteristics. To do this, one has to solve the continuity equation that is nonlinear because

the bipolar diffusion coefficient D , as well as the bulk (r) and surface (S_r) recombination rates, depends on the charge carrier concentration n . For a bipolar ($n = p = n_s$) semiconductor such problem has been solved in [31-33]. The authors considered the following nonlinear stationary equation:

$$\frac{d}{dx} D(n) \frac{dn}{dx} = r(n). \quad (2.3)$$

The boundary condition at the plane $x = 0$ was

$$\left[D(n) \frac{dn}{dx} - n S_r(n) + I \right]_{x=0} = 0. \quad (2.4)$$

Here $I = I_0(1 - R)\eta$ is the rate of charge carrier generation due to LI; R is the reflection coefficient; η is the quantum efficiency of photoionization; I is the excitation intensity; I_0 is the LI intensity.

For etched surfaces the surface recombination velocity S_r often is low ($\frac{S_r L}{D} \ll 1$). In this case the bipolar diffusion coefficient D is of the following form [31]:

$$D = \frac{I}{N_s} \cdot \frac{\partial N'}{\partial n_s}, \quad (2.5)$$

where the total number of charge carriers is

$$N' = \frac{1}{\sigma_p} \left[\left| \frac{\Delta T}{T} \right| + \left| \frac{\Delta R}{R} \right| \cdot \frac{q^2 - 1}{4q} \right] \quad (2.6)$$

and the surface electron concentration n_s is to be determined from the following equation:

$$\frac{\Delta R}{R} = \frac{8\pi e^2 n_s}{q (q^2 - 1) \omega^2 m^*}. \quad (2.7)$$

Here σ_p is the cross-section of the hole IR absorption; $\frac{\Delta T}{T}$ ($\frac{\Delta R}{R}$) is the relative change of IR transmission (reflection); q is the refractive index of the ambience; ω is the angular frequency of the probing radiation; $\frac{1}{m^*} = \frac{1}{m_n^*} + \frac{1}{m_p^*}$ where m_n^* , m_p^* are the so-called optical effective masses for electrons and holes, respectively. They are defined in the following way:

$$m_{opt}^* = m_c^* \left(1 + \frac{6\pi^2 \hbar^3 n_s^{2/3}}{m_c^* E_g} \right). \quad (2.8)$$

Here \hbar is the Planck's constant; m_c^* is the m_{opt}^* value at the bottom of conduction band.

Thus one can determine both N' and D values and their concentration dependencies when the nonlinear recombination, electron-hole scattering and conduction band nonparabolicity are present simultaneously. To do this, one should measure IR reflection and transmission as function of the intensity of surface excitation by a laser. This is well illustrated by the example of InSb for which an anomalous growth of bipolar diffusion coefficient with excitation level has been found (Fig.2.10).

2.4.2. A complex technique for diagnostics of electron-hole plasma

The nonlinear effects (that show themselves at relatively low NCC concentrations in narrow-gap semiconductors — say at $n \geq 3 \times 10^{16} \text{ cm}^{-3}$ for InSb — and at high NCC concentrations in wide-gap materials) lead to complicated nonlinear concentration dependencies of such important NCC parameters as life-

time τ , mobility μ , bipolar diffusion coefficient D , surface recombination velocity S_r . In [32,33-35] a corresponding nonlinear

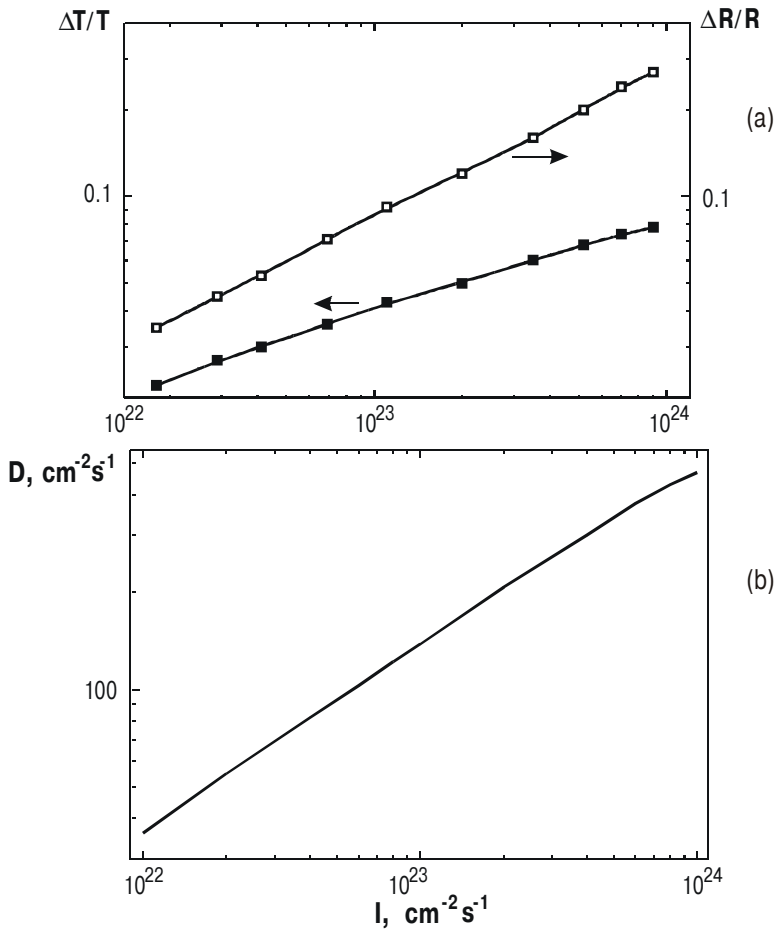


Fig.2.10. Relative transmission $\Delta T/T$ and reflectivity $\Delta R/R$ (CO_2 laser radiation) (a) and NCC bipolar diffusion coefficient (b) as function of intensity of InSb excitation with ruby laser.

stationary problem has been considered. The power approximations were used for the bipolar diffusion coefficient $D = An^\alpha$, bulk recombination rate $r_b = Bn^\beta$ and charge carrier mobility $\mu = Cn^\delta$ (A , B and C are constants). The NCC spatial distribution, $n(x)$, was determined, as well as the following expressions for estimation of the surface electron concentration n_s , total charge carrier number N' and average photoconductivity $\Delta\sigma$ as a function of excitation intensity:

$$n_s \sim I \frac{2}{\alpha + \beta + 1}, \quad (2.9a)$$

$$N' \sim I \frac{\alpha - \beta + 3}{\alpha + \beta + 1}, \quad (2.9b)$$

$$\Delta\sigma \sim I \frac{\alpha - \beta + 2\delta + 3}{\alpha + \beta + 1}. \quad (2.9c)$$

After representing the corresponding experimental dependencies as

$$n_s(I) = n_{s1} \left(\frac{I}{I_1} \right)^a, \quad (2.10a)$$

$$N'(I) = N'_1 \left(\frac{I}{I_1} \right)^b, \quad (2.10b)$$

$$\Delta\sigma(I) = \Delta\sigma_1 \left(\frac{I}{I_1} \right)^c, \quad (2.10c)$$

(where a , b , c are the slopes of curves plotted on double-logarithmic scale) and setting the corresponding exponents in expressions (2.9) and (2.10) equal to each other, one obtains a set of algebraic equations. By solving these equations, one gets the exponents α , β , δ and the following expressions for the desired NCC parameters:

$$\tau(n) = b \frac{N'_1}{I_1} \left(\frac{n_s}{n_{s1}} \right)^{\frac{b-1}{a}}, \quad (2.11)$$

$$D(n) = \frac{b}{a} \cdot \frac{N'_1 I_1}{n_{s1}} \left(\frac{n_s}{n_{s1}} \right)^{\frac{b-2a+1}{a}}, \quad (2.12)$$

$$L(n) = \frac{b}{a} \cdot \frac{N'_1}{n_{s1}} \left(\frac{n_s}{n_{s1}} \right)^{\frac{b-a}{a}}, \quad (2.13)$$

$$\mu(n) = \frac{cd\Delta\sigma_1}{bN'_1\epsilon_0} \left(\frac{n_s}{n_{s1}} \right)^{\frac{c-b}{a}}. \quad (2.14)$$

The efficiency of such technique could be well demonstrated by the example of InSb. The experimental curves $\frac{\Delta T}{T}(I)$, $\frac{\Delta R}{R}(I)$ and $\Delta\sigma(I)$ measured at $T = 300$ K, as well as the calculated functions $\tau(n)$, $D(n)$, $L(n)$ and $\mu(n)$, are presented in Fig.11a, b.

The above expressions that give NCC parameters as function of the charge carrier concentration enabled to reveal that the recombination rate r slowed down ($r \propto n^{2.3}$ - cf. the case of Auger recombination for which $r \propto n^3$) while the diffusion coefficient anomalously grew ($D \propto n$). These effects are due to electron degeneration and shielding of the Coulomb interaction between NCC. The principal advantages of the discussed technique are as follows. It enables to predict the NCC properties when several nonlinear effects occur. There is no need in knowing the exact model for semiconductor: it could be refined from the experimentally measured microscopic parameters. In addition, there is no need in unique equipment for measurements.

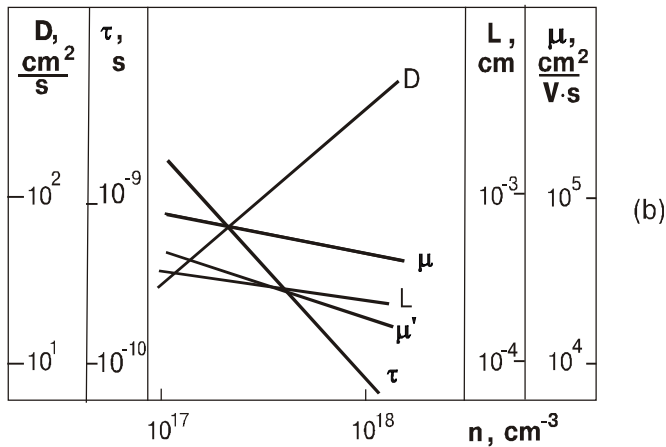
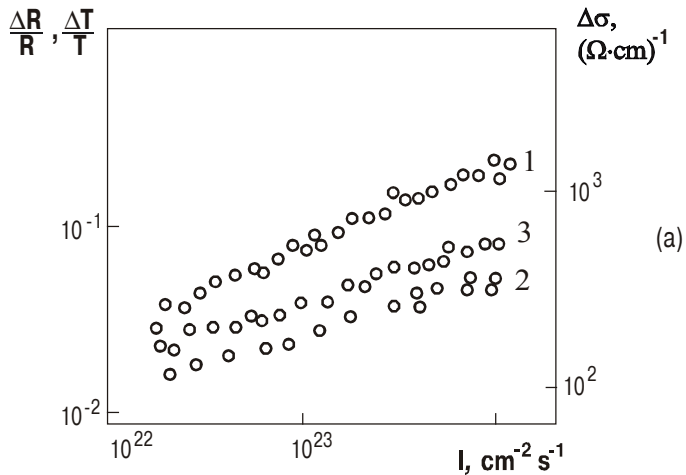


Fig.2.11. a – experimental relative transmission $\Delta T/T$ (1), relative reflectivity $\Delta R/R$ (2) and photoconductivity $\Delta\sigma$ (3) vs excitation intensity I curves for InSb (etched surface; $T = 300$ K); b – NCC lifetime τ , bipolar diffusion coefficient D , length L and mobility μ vs concentration n curves for etched InSb surface ($S_r L/D \ll 1$) at $T = 300$ K (μ' is electron mobility as function of n -InSb doping level).

Further decreasing of diffusion length under nonlinear recombination at even higher ($\Delta n \geq 10^{18} \text{ cm}^{-3}$) NCC concentrations can also lead to violating the ray optics approximation $\frac{\lambda}{2\pi q l} \ll 1$. In this case the plasma resonance (PR) technique is more advantageous. It enables to determine the plasma parameters at extreme concentrations from the depth and position of minimum in the reflection curve (2.6).

In one of the first experimental studies where the PR technique has been used [36] estimations of the NCC in InSb have been made. A theoretical consideration of the PR technique in the case when the above ray optics approximation does not hold, with allowance made for charge carrier degeneration and nonlinear recombination, has been made in [37]. However, the reflection curve has been calculated for the exponential distribution profile only, when the NCC diffusion is absent. Besides, the authors of [36,37] have not taken into account the intraband V_1-V_2 transitions in the valence band, as well as the conduction band nonparabolicity.

A more elaborate modification of this technique that is not subject to the above drawbacks has been advanced in [33]. The NCC distribution profile was set from the solution of the continuity equation (2.3), while the reflection of IR radiation was calculated using decomposition in layers and a matrix feasible for any NCC distribution profile:

$$R = \left| \frac{A_{21}}{A_{11}} \right|^2. \quad (2.15)$$

Here $A_{21} = a_1, a_2, \dots, a_s; a_j$ is a matrix involving the refractive index q_j of the j -th layer. By choosing a large enough number j one can obtain, to sufficient accuracy, the reflection coefficient for a semiconductor whose refractive index q is a

preset function of coordinate x . If q slowly varies with x , then one can ignore the reflection from nonuniformities. In this case the ray optics approximation is valid.

The Kane dispersion law was accounted for in expression (2.8) for the electron effective mass. From comparison between the experimental reflection curves and theoretical ones (Fig. 2.12) plotted at different values of the nonlinear recombination exponent β ($r = Bn^\beta$) and bipolar diffusion coefficient exponent α ($D = An^\alpha$) we determined the Auger recombination coefficient $B_3^A = 2.9 \times 10^{-39} \text{ m}^6 \text{s}^{-1}$, lifetime $\tau = 10^{-11} \text{ s}$ and diffusion length $L = 4.3 \times 10^{-6} \text{ m}$.

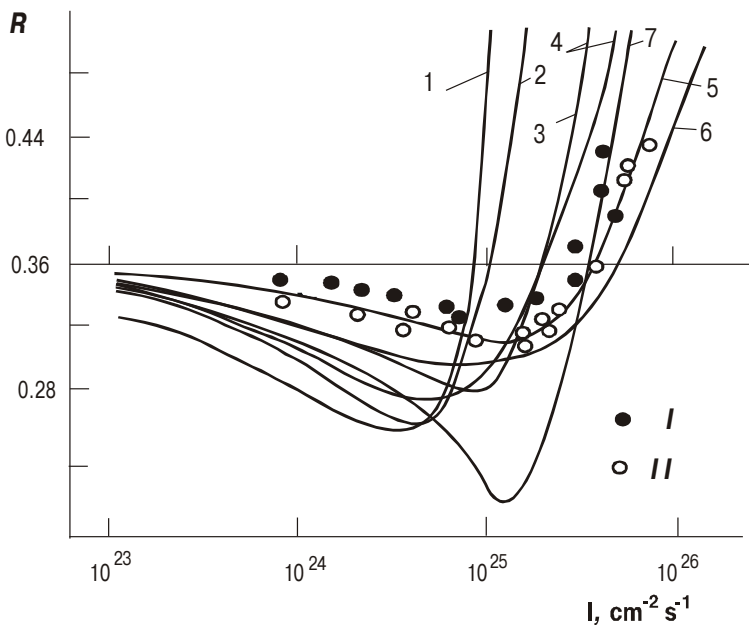


Fig.2.12. Theoretical and experimental reflection coefficient R (probing radiation wavelength $\lambda = 1.06 \mu\text{m}$) vs excitation intensity I curves [34].

The new regularities in NCC recombination and diffusion that have been revealed for InSb using the PR technique were supported by the results of [35,38-42]. The authors of [35] obtained their results from complex diagnostics using the direct method for measuring PC kinetics; the InSb samples were excited with picosecond pulses from a mode-coupled YAG:Nd³⁺-laser [38]. The authors of [39-42] dealt with nonstationary PR at even higher ($\Delta n \geq 10^{19} \text{ cm}^{-3}$) NCC concentrations and picosecond excitation.

2.4.3. Photoconductivity of InSb under picosecond excitation

When studying rapid processes with light ultrashort pulses (USP), the researchers come up against a number of side effects and peculiarities of crystal excitation. These factors affect the results of measurements [43]. In both optical (self-diffraction technique and measurement of transmittance) and electrical investigations (measurement of conductivity) a signal detected is determined by the total NCC number in the volume of the crystal studied; under nonlinear recombination this signal is determined by a whole set of instantaneous NCC lifetimes.

Judging from the estimations made in [44,45], thermalization of an electron whose energy is 1 eV occurs during $\tau_E \approx 10^{-12}-10^{-11} \text{ s}$. This value corresponds to the duration t_p of the exciting light pulse. As a result, when a semiconductor is exposed to light USP whose energy $h\nu$ far exceeds the crystal gap E_g ($h\nu \gg E_g$) and $t_p \approx \tau_E$ then the semiconductor plasma is not in thermal equilibrium. The distributions of NCC concentration and electron temperature become essentially non-uniform in depth. Both factors can affect the value of the ambipolar diffusion coefficient D [46,47].

The characteristic times of nonlinear recombination processes depend on the NCC concentration n . Therefore, if the crystal thickness exceeds the diffusion length, then the diffusion flow of charge carriers from the crystal surface into the crystal bulk slows down the PC signal decay. On the other hand, when the NCC concentration in a semiconductor (and, especially, in InSb) decreases, then the role of Auger recombination grows [32]. The action of this factor on the PC signal is opposite to that of the above factor. During the rise time integration of all the above effects into the PC signal occurs.

At room temperature the NCC lifetime τ_A in intrinsic InSb is known to be determined by Auger recombination. At low excitation levels, when $n \approx 10^{16} \text{ cm}^{-3}$, this time is about several tens of nanoseconds [48,49]. The theoretical estimations of τ_A that have been made for this case taking into account the conduction band nonparabolicity [50], transitions to the light-hole band and shielding of Coulomb potential [51], gave values considerably below the experimental ones. In [52] it was found that $B_3^A = 6.5 \times 10^{-26} \text{ cm}^6 \text{s}^{-1}$. In [32,35,53] it was shown that at $n > 10^{17} \text{ cm}^{-3}$ the concentration dependence of Auger recombination becomes weaker due to strong electron degeneration and approaches the quadratic one. The kinetics of PC relaxation in InSb samples excited with picosecond laser pulses at injection levels $n = 10^{16}-10^{18} \text{ cm}^{-3}$ was studied in [38].

For most of modern lasers that operate in the nano- and picosecond ranges $h\nu \approx 1 \text{ eV}$. The absorption coefficients K for radiation of such energy in narrow-gap semiconductors are very high, while the pumping region is small (about 1 μm). The diffusion coefficients in such semiconductors are high because the effective masses of electron-hole pairs are small. Therefore adequate allowance for true NCC distribution in

depth is of particular importance when studying recombination processes in the nano- and picosecond ranges.

The authors of [38] used a neodymium-doped silicate glass laser with mode self-synchronization as excitation source. An ethanol solution of polymethyl dye 3274 was used for Q switching and mode synchronization. The USP duration was 5–7 ps; an interval between the pulses in the train was 12 ns. All optical elements of the system were mounted on the wedge substrates or positioned at Brewster's angle to the incident beam.

The USP contrast relative to the radiation between pulses was increased with a discrimination amplifier. It involved an optical amplifier and a dish with a passive filter (ethanol solution of dye 3955) whose transmittance was about 5% [54]. Then the radiation was split into three beams and passed to a coaxial photocell ФК-19 and oscilloscope C7-10Б, to a calorimeter ИМО-2H and (after a telescope-expander) to the InSb sample studied. If required, the radiation frequency could be doubled using a LiIO_3 crystal 3 mm thick.

The n -InSb samples ($N_D - N_A = 10^{14} \text{ cm}^{-3}$ at $T = 300 \text{ K}$) were prepared as dumbbell-like plates and treated with the standard etchant CP-4A. The linearity and speed of response of the recording circuit were checked by passage of electric USP (Fig.2.13a) from the coaxial photocell ФК-19 exposed to light USP, with concurrent measurement of energy with the calorimeter ИМО-2H. The PC signal was registered with the second oscilloscope C7-10Б (Fig.2.13b).

Shown in Fig.2.14 is a typical PC amplitude vs excitation intensity I curve for InSb samples exposed to light USP. One can see that the linear luminous-current characteristic becomes sublinear at $I = 5 \times 10^{24} \text{ quant/cm}^2 \cdot \text{s}$.

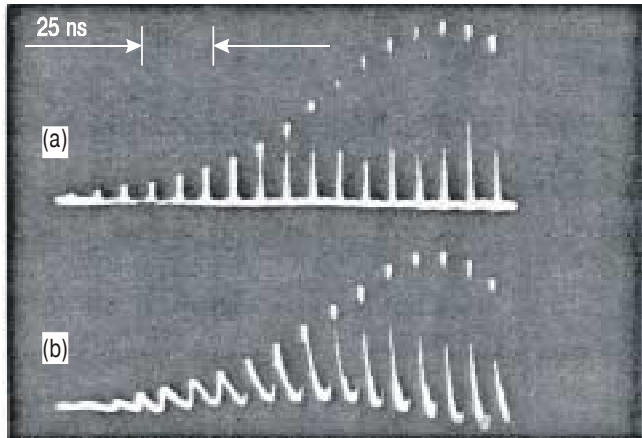


Fig.2.13. Oscillogram of a picosecond pulse train (wavelength $\lambda = 1.06 \mu\text{m}$, pulse duration $t_p = 5 \div 7 \text{ ns}$) registered with coaxial photocell $\Phi\text{K}-19$ (a) and InSb sample (b).

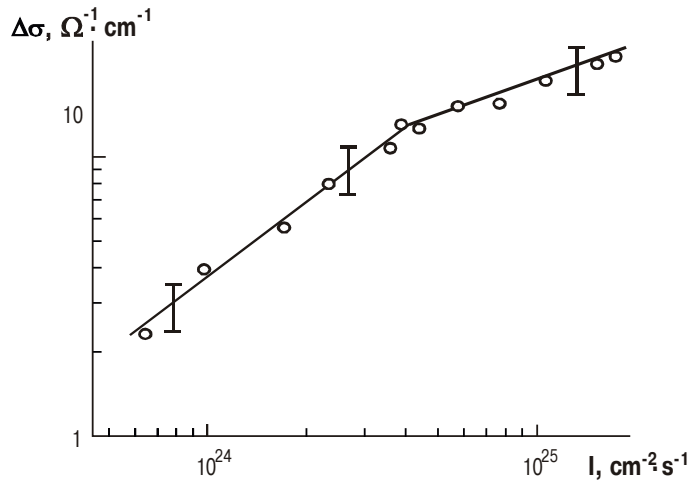


Fig.2.14. Photoconductivity amplitude $\Delta\sigma$ vs excitation intensity I curve for InSb sample.

Tentative lifetime estimations from the plasma reflection [33] have shown that the PC mode remained nonstationary over the whole concentration range. The observed deviation of luminous-current characteristic from linearity at the above intensity of exciting radiation is due to the fact that at $n = 3 \times 10^{17} \text{ cm}^{-3}$ the PC relaxation time τ_r becomes less than the rise time (τ_{rise}) of the equipment that registers the signals. In this case the observed signal amplitude becomes to depend not only on the amplitude of the input PC signal but also on its duration. In the $10^{16}\text{--}10^{17} \text{ cm}^{-3}$ concentration range the diffusion process during time interval τ changes local n value several times quicker than recombination process. The size $L_{rise} = \sqrt{Dt}$ of the region of NCC penetration into the crystal depth after irradiation grows with time t , but the rate of this growth decreases with t . Since diffusion does not change the total number of NCC in the crystal bulk, one may consider, in rough approximation, that the rate of PC signal decrease is determined by the n_{rise} value that has been reached as a result of diffusion. So the measured PC signal amplitude in the case of cubic Auger recombination is proportional to PC:

$$\Delta\sigma \sim \int_0^\tau \frac{n_{rise} dt}{\sqrt{1 + 2n_{rise}^2 B_3^A t}} = \frac{1}{B_3^A n_{rise}} \left(\sqrt{1 + 2n_{rise}^2 B_3^A \tau} - 1 \right). \quad (2.16)$$

For sufficiently small $n_{rise} \ll 1 / \sqrt{2B_3^A \tau}$ one can obtain (by expanding the subradical expression in (2.16) in series) that the integral in expression (2.16) is $n_{rise} \tau$. This means that the PC signal amplitude is proportional to the NCC concentration or irradiance W . At $n_{rise} \geq 1 / \sqrt{2B_3^A \tau} \approx 2 \times 10^{17} \text{ cm}^{-3}$ the curve $\sigma(W)$ flattens out which is what one observes in experiment (see Fig.2.14).

Shown in Fig.2.15 is the instantaneous PC relaxation time τ_r as function of n in the region where $\Delta\sigma$ linearly depends on I . One can see that the curve $\tau_r(n)$ plotted at double logarithmic scale cannot be characterized by a single constant slope. In the initial portion τ_r almost does not depend on n (as it must be at low excitation levels). Then $\tau_r \sim n^{0.8}$ at $n \approx 10^{17} \text{ cm}^{-3}$, and at $n \geq 3 \times 10^{17} \text{ cm}^{-3}$, $\tau_r \sim n^{-1.2}$. The concentration was estimated from the total number of NCC under the surface unit area $N' = \eta W(1 - R)$ using the following expressions: $n_{rise} = N'/L_{rise}$, $L_{rise} = \sqrt{Dt}$.

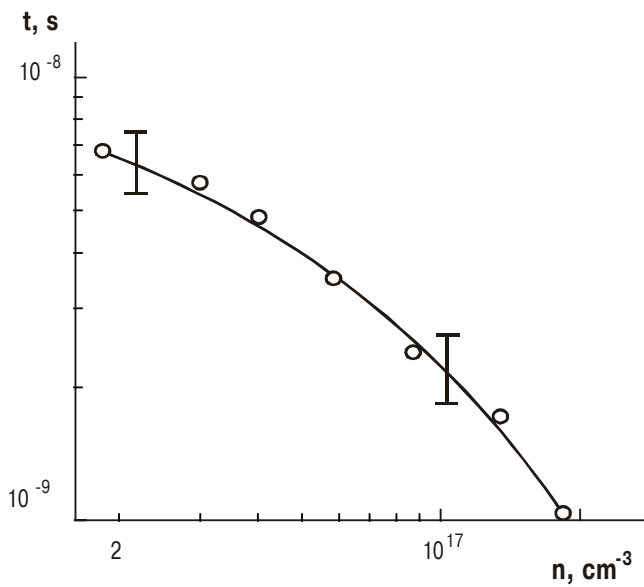


Fig.2.15. Photoconductivity instantaneous relaxation time τ vs NCC concentration n for InSb sample.

Here η is the photoionization quantum efficiency and R is the reflection coefficient of the crystal surface. If one neglects the surface recombination effect and, by analogy with [52], assumes that excitation occurs in the bulk (i.e., identifies τ_r with τ_A), then the concentration dependence of τ_r will be weaker than in the case of the cubic recombination law; it will be closer to the quadratic recombination law.

There may be several reasons for the above effect, namely, (i) mobility decrease with charge carrier concentration in the absorption region and lifetime increase at nonlinear recombination processes; (ii) recombination rate drop due to electron degeneration; (iii) NCC diffusion that results in charge carrier concentration decrease in the absorption region and lifetime increase at nonlinear recombination processes. Let us consider these reasons in more detail.

It is known that at room temperature in intrinsic InSb charge carrier scattering occurs predominantly on the optical lattice vibrations, while at $n > 10^{17} \text{ cm}^{-3}$ the electron-hole scattering prevails. Therefore the charge carrier mobility μ changes rather weakly ($\mu \sim n^{-0.2}$) at concentrations under consideration [55] and affects the $\tau_r(n)$ dependence but slightly.

In [56] it was shown that decrease of the Auger recombination rate in a semiconductor requires strong (chemical potential equal to about half gap E_g) charge carrier degeneration. But in the case considered the Fermi level E_F did not exceed 0.032 eV. So, as it was shown in [57], for $E_F \ll E_g$ one should expect recombination rate growth rather than decrease.

It seems that it is diffusion that has a dominant role in changing the $\tau_r(n)$ dependence. Indeed, the calculations made in [53] show that in the case of degeneration the diffusion length L in InSb very weakly decreases with n because D considerably grows ($D \sim n^\beta$, $\beta \geq 2/3$). So the condition $KL \gg 1$ for

surface absorption at excitation with the neodymium laser is well obeyed in a wide range of injection level. The allowance for bulk character of excitation [52] should be considered invalid; the actual values of instantaneous lifetimes are considerably less than the experimental τ_r values.

When the exciting radiation wavelength (and consequently the absorption coefficient K) changes, then the absorption depth changes abruptly (and consequently the initial n value) at the same pulse energy. In the case of bulk excitation this has to result in distinctions between the characteristic PC relaxation times. In [38], along with PC measurements using the first harmonic of the neodymium laser radiation (wavelength $\lambda = 1.06 \mu\text{m}$, absorption coefficient $K = 3.9 \times 10^4 \text{ cm}^{-1}$), the authors studied the effect of the second harmonic ($\lambda = 0.53 \mu\text{m}$, $K = 4.9 \times 10^5 \text{ cm}^{-1}$) on the crystal. In both cases the magnitudes of relaxation times and their dependencies on the NCC concentration were the same (to within experimental error). This fact serves as additional confirmation of an appreciable role of diffusion process in the PC kinetics formation.

One should note that the peak value $\tau_r = 9 \times 10^{-9} \text{ s}$ (obtained at minimal illumination levels) turned out to be somewhat below the values given in [48,53]. Let us take, for estimations, the surface recombination velocity S_r at low excitation level to be $2 \times 10^4 \text{ cm/s}$ [58] and assume that $S_r = \text{const}$. Then we get $S_r L/D \approx 0.3$. This serves as evidence that one should take into account both surface recombination and its possible dependence on n when performing a quantitative analysis of the PC kinetics relaxation. At $n = 2 \times 10^{16} \text{ cm}^{-3}$ a limiting value $B_3^A = 2 \times 10^{-25} \text{ cm}^6 \text{s}^{-1}$ was obtained that is close to the results of [59]; at $n = 3 \times 10^{17} \text{ cm}^{-3}$ $B_3^A = 1.5 \times 10^{-26} \text{ cm}^6 \text{s}^{-1}$. Investigation of nonstationary PC in InSb crystals excited with picosecond light pulses enabled to reveal an essential role of diffu-

sion in kinetics formation for relaxation processes and make estimations of limiting NCC lifetime values, as well as Auger recombination constant, at $n = 2 \times 10^{16}$ and $3 \times 10^{17} \text{ cm}^{-3}$.

Thus one or the other of the features of different diagnostic techniques turns out to be preferable, depending on the goal sought. During scientific investigations information on the magnitudes of the greatest number of parameters is most often required. Just another situation is when one is checking the NCC parameters under the manufacturing conditions. In this case information (obtained with minimal sample degradation) on the relative values of one or two parameters that are of importance for a given production cycle is most likely required. Sensitivity of photoelectric techniques is relatively low for narrow-gap materials due to low resistance of the samples. Reliability of these techniques applied to wide-gap materials is reduced due to the well-known difficulties encountered in the ohmic contact formation. That is why the contactless techniques that use optical probing and excitation are preferred.

2.5. DEVELOPMENT OF STABLE OHMIC CONTACTS TO n - α -SiC AND p -GaAs USING LASER TECHNOLOGY

2.5.1. Contacts to n - α -SiC

One of the biggest advantages of the SiC-based devices is their high thermal stability. Both 6H α -SiC and β -SiC have wide gap. So the free charge carrier concentrations in these materials do not exceed 10^{14} cm^{-3} even at such high temperatures as 1300 K for 6H α -SiC and 1100 K for β -SiC [60,61]. Therefore p - n junction can exist in both materials at temperatures up to the named above. This fact imposes heavy demands on stability and strength of ohmic contacts to SiC over a wide temperature range.

Several researchers have made efforts to apply the laser technology for formation of contacts to SiC. For instance, in [62] the authors studied how exposure to the picosecond laser changed the resistance of Cr–n-SiC ohmic contacts that were thermally sputtered onto a heated substrate. The metal layer thickness was 0.1–0.2 μm . The contacts were annealed with a single pulse (duration of 30 ns) of the YAG:Nd³⁺-laser ($\lambda = 1.06 \mu\text{m}$) in the passive synchronization mode. A 30–40% reduction of the contact resistance was observed in the 0.4–1.2 J/cm² emittance range. Besides, it was found that this effect did not depend on the substrate temperature during contact sputtering. The authors of [62] believed that such decrease of the contact resistance was related to doping of the SiC near-surface layers with Cr atoms.

In [63] ohmic contacts to SiC were formed as a result of the contact material diffusion under exposure to a millisecond YAG:Nd³⁺-laser. Such long pulse durations, however, led to a considerable heating of the samples to a depth of about several tens of microns. This effect is unwanted when treating the submicron structures.

It is also known that formation of ohmic contacts to SiC is related primarily to the metallurgic factor, i.e., formation of metal silicides at high temperatures and, as a result, degradation of mechanical properties of contacts. In addition, it is impossible to predict properties of the final ohmic structure from the parameters of the initial barrier structure that was intended for further formation of the ohmic contact. The reason for this is spread of work function χ values for different SiC polytypes and refractory metals, such as W, Mo and Ti. Therefore it is desirable to provide conditions for realization of the tunneling mechanism of current flow in order to reduce the contact resistance R_c .

This end may be accomplished by increasing doping level in the α -SiC near-surface layer. In [64] refractory contacts to α -SiC:Ni were formed using laser sputtering in a vacuum of (W/Si₃N₄/W/Ni) nanometer layer sequence onto α -SiC followed by laser-enhanced diffusion and annealing (YAG:Nd³⁺-laser: $\lambda = 1.06 \mu\text{m}$, $t_p = 30 \text{ ns}$; $\lambda = 0.53 \mu\text{m}$, $t_p = 10 \text{ ns}$; $P = 0.05 \text{ J}$). The Si₃N₄ layer was used as source of Ni impurity, with Si in it serving to compensate for possible silicon evaporation from SiC due to high temperature of laser annealing. The upper W layer served as (i) a contact metallization layer in the structure, (ii) an additional contributor of structure heating due to strong absorption of laser radiation, and (iii) a screen to prevent evaporation of the substrate and Si₃N₄ components at their dissociation (the melting temperatures T_m for W and Si₃N₄ are different, namely, 3420 and 1900 °C, respectively [65]). The W layer that was sputtered immediately onto SiC served for stabilization of the interface front during annealing.

The authors of [64] studied the n - α -SiC samples grown with modified Lely technique at the Special Bureau for Design and Technology (SBDT) of the Institute of Semiconductor Physics of the National Academy of Sciences of Ukraine. The impurity (nitrogen) concentration was $\sim 2 \times 10^{18} \text{ cm}^{-3}$. Before sputtering the SiC sample was chemically cleansed for 2–3 s in HF, washed in distilled water, dried and then placed into a vacuum chamber of the plant for laser pulse sputtering (see section 2.2.1). The working pressure was about 10^{-4} Pa . During structure sputtering the substrate temperature was about 200 °C.

Further laser-enhanced diffusion of nitrogen impurity and laser annealing were performed using the plant for LM (see section 2.2.2). Both processes (laser-enhanced diffusion and annealing) were checked in the real-time mode using py-

roelectric thermal technique and microscopic visualizer. It was found that if laser pulse annealing was performed using a YAG:Nd³⁺-laser ($\lambda = 1.06 \mu\text{m}$), then the *Q*-switching mode with the following parameters is optimal: pulse duration $t_p = 10 \text{ ns}$, repetition frequency $f_r = 25 \text{ Hz}$, average rate of target surface scanning with a laser beam 6 mm/s and irradiance of $3 \times 10^9 \text{ W/cm}^2$. These parameter values correspond to the pile-up mode of laser sputtering and minimal density of tear-shaped clusters on the substrate surface.

Evolution of *I*-*V* curve of $\alpha\text{-SiC}/\text{W}/\text{Si}_3\text{N}_4/\text{W}$ contact structure from diode- to ohmic-type during LM is shown in Fig.2.16. The contact resistivity ρ_c was measured using the four-probe technique.

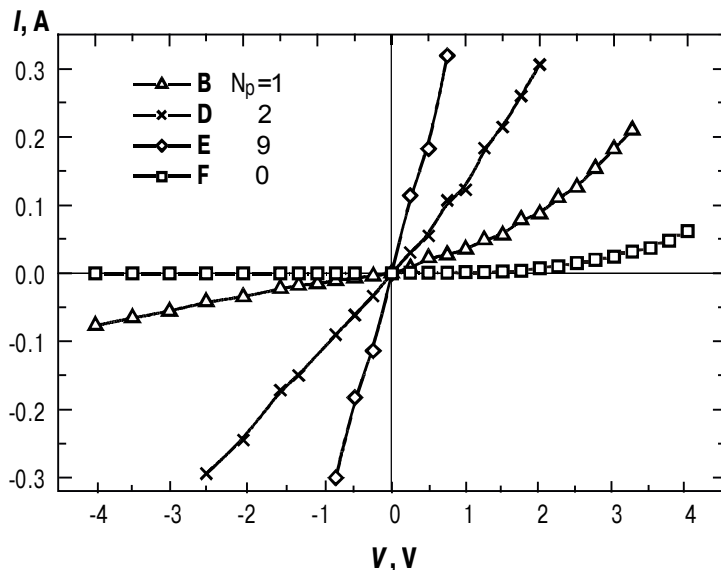


Fig.2.16. Evolution of the *I*-*V* curve for $\alpha\text{-SiC}/\text{W}/\text{Si}_3\text{N}_4/\text{W}$ contact structure during laser annealing; N_p is the number of pulses. (Concentration of nitrogen in $\alpha\text{-SiC}$ is $(1\div 3) \times 10^{18} \text{ cm}^{-3}$.)

The contact resistance R_c vs Si_3N_4 layer thickness curve is presented in Fig.2.17. Its initial portion is determined by the island-like character of the Si_3N_4 layer formation, while the increasing portion is due to growth of the interface imperfection level resulting from incomplete dissociation of the Si_3N_4 layer followed by its thickness increasing under nanosecond pulses of laser annealing. It was experimentally determined that laser-enhanced diffusion was most efficient when combining radiation at two wavelengths ($\lambda = 1.06 \mu\text{m}$ and $\lambda = 0.53 \mu\text{m}$) in the Q -switching mode; the pulse duration t_p was 10 ns and radiation intensity lied between 10^7 and 10^9 W/cm^2 , depending on the deposited layer thickness. The intensity threshold value at which irreversible changes of I - V curves occurred in the 10^7 – $2.8 \times 10^8 \text{ W/cm}^2$ irradiance range also depended on thicknesses of nanometer layers of the structures studied.

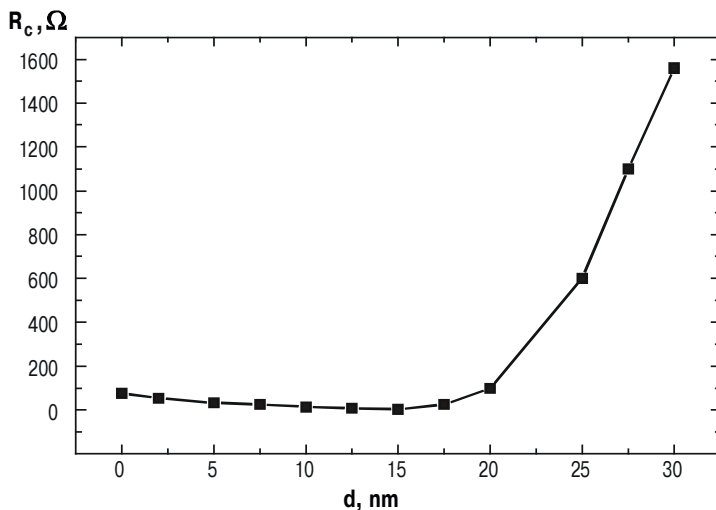


Fig.2.17. Contact resistance R_c of $\alpha\text{-SiC}/\text{W}/\text{Si}_3\text{N}_4/\text{W}$ structure as function of Si_3N_4 layer thickness.

Shown in Fig.2.18 are the results of investigations of surface morphology during ohmic contact formation. One can see that surfaces of "clean" SiC and W/Si₃N₄/W/n-SiC structures before and after laser annealing differ substantially from each other (see Fig.2.18a, b and c, respectively). The fact of this distinction after contact sputtering and annealing evidences that during LM a phase transition occurs.

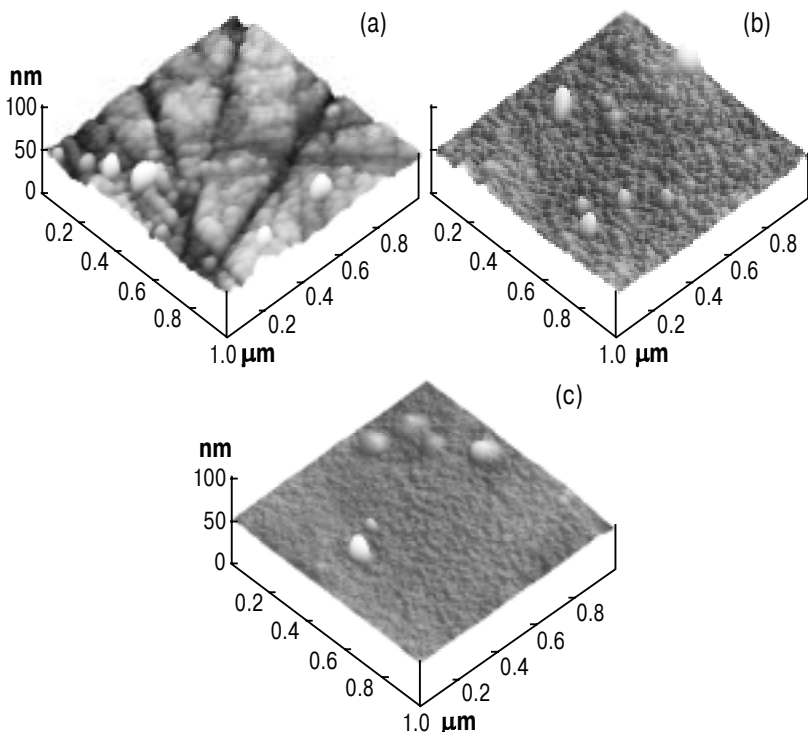


Fig.2.18. α -SiC surface morphology at different stages of laser modification of the α -SiC/W/Si₃N₄/W structure: a – before LM; b – after metallized structure formation using LM; c – after laser annealing.

Higher conductivity values were obtained for those W/Si₃N₄/W/*n*-SiC structures where the Si₃N₄ layer thickness was about 18 nm, while that of the first W layer was about 8 nm. Resistivity of contacts formed after laser annealing was (3–5)×10⁻⁴ Ω·cm². This value did not change for check samples through which current (density of about 4×10³ A/cm²) was flowing for 100 h.

The ohmic contacts based on the W/Si₃N₄/W/*n*-SiC system have several advantages over those based on gold, palladium or platinum [66,67]. These are as follows: (i) absence of elements whose chemical activity toward the basic material substantially changes with temperature at thicknesses of Si₃N₄ and the first W layers about 18 and 8 nm, respectively; (ii) contact formation requires no fusion; (iii) presence of tungsten does not require additional metallization to provide interconnections; (iv) high stability of resistance at submicron contact layers.

Further reduction of contact resistivity could be achieved by using laser radiation with much higher absorption coefficient (say, that from excimer lasers) capable of production of essentially bigger temperature gradients. This problem requires additional studies of microstructure modifications occurring in crystal lattices.

2.5.2. Contacts to *p*-GaAs

Traditionally widely used in practice low-resistance contacts to GaAs are formed by fusion or welding with Au-based metallizations, namely, AuGe for *n*-GaAs and AuZn for *p*-GaAs [68–71]. In these cases a thin heavily doped semiconductor layer appears after cooling. This makes it possible to obtain contact resistivity ρ_c of about 10⁻⁶ Ω·cm² due to tunneling of charge carriers. In this case the thermal and thermal-field mechanisms for barrier conduction are realized. The advan-

tages of contacts obtained in the above way are as follows: (i) low ($\rho_c \leq 10^{-6} \Omega \cdot \text{cm}^2$) ohmic resistivity at relatively low ($N_A - N_D \leq 10^{18} \text{ cm}^{-3}$) doping level; (ii) high (about $3 \times 10^2 \Omega/\square$) contact layer resistivity; (iii) compatibility of technological operations (sputtering and photolithography); (iv) high corrosion-resistance and strength.

The above advantages are undeniable for the discrete electronic elements whose sizes are no less than several μm . However, if the contact sizes lie in the submicron range, then the barrier height nonuniformities (due to instability of Au-Ga compositions) and resulting from this developed interfacial microrelief lead to appearance of regions with SBs that bypass ohmic contacts [72]. In addition, a considerable difference in amounts of Au and Zn saturated vapors, as well as low adhesion of zinc toward GaAs, result in moderate reproducibility of contact resistance.

Currently searches for alternative (free of the above flaws) ohmic contacts were carried out. Such contacts (where gold was replaced with other metals) were fabricated without welding, using either electron (ion) beams or magnetron sputtering followed with thermal annealing [70,71,73]. It was detected that ohmic resistance essentially depended on the sputtering technique, annealing duration and thicknesses of metallization layers. The lowest values of ohmic resistance were observed at magnetron sputtering and small duration of thermal annealing.

As mentioned above, refractory ohmic contacts can be made using the laser technique [4]. To illustrate, let us consider some technological aspects of W/Zn/W/GaAs contact formation. The nanometer W/Zn/W films were prepared with pulse laser spraying using the plant described in section 2.1.2. The *p*-GaAs material doped with Zn ($N_A - N_D = 2 \times 10^{18} \text{ cm}^{-3}$)

was used as substrate. Its surface was etched with the $\text{H}_2\text{SO}_4:\text{HNO}_3:\text{H}_2\text{O} = 1:1:1$ solution. Then the substrates were washed with distilled water and placed into a vacuum chamber. The contact area was about $4 \times 10^{-3} \text{ cm}^2$. After spraying the multilayer structures were exposed to the YAG:Nd³⁺-laser radiation ($\lambda = 1.06$ and $0.53 \mu\text{m}$) using different laser annealing modes. The laser-enhanced diffusion was checked (as in the case of SiC) using visualization of surface imperfections with a microscope and pyrometer technique for surface temperature determination from the thermal pulse amplitude and form in the real-time mode.

The resistance R_c of ohmic contacts was found from $I-V$ curves taken at different layer thicknesses, emittances and numbers of laser pulses. The contact resistance R_c as function of layer thickness is presented in Fig.2.19. One can see that R_c values corresponding to different thicknesses of W and Zn layers may differ by more than an order of magnitude. The initial decrease of R_c values is related to formation of a continuous film. This process restricts arsenic losses stemming from As diffusion out of GaAs bulk. On the other hand, the above process results in an increase of concentration of gallium vacancies V_{Ga} , i.e., in an increase of concentration of activated Zn_{Ga} impurities [74]. The concentration of Zn atoms (that was determined from surface conductivity measured at layer-by-layer etching) exceeded the value $N_{\text{Zn}} \cong 2 \times 10^{21} \text{ cm}^{-3}$ corresponding to natural Zn solubility in GaAs. As a result, a p^+ -GaAs layer was formed. Further increase of contact resistance with thicknesses of W and Zn layers is due to appearance and relaxation of intrinsic stresses in the contact structure.

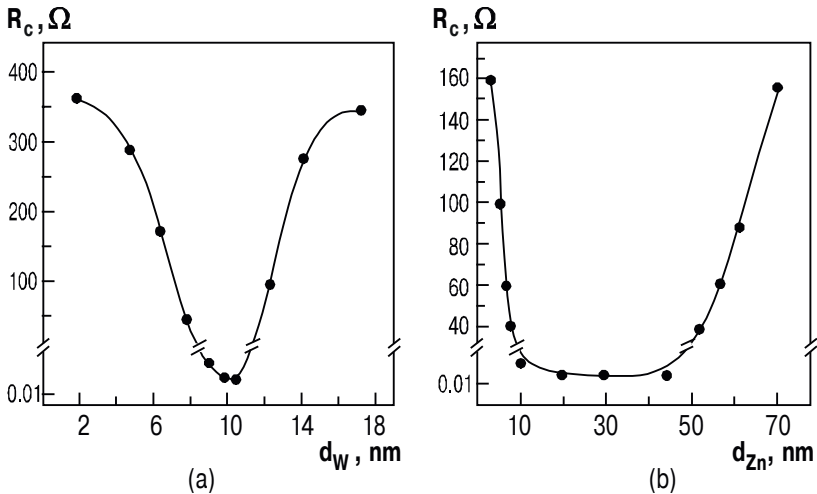


Fig.2.19. Contact resistance R_c of W/Zn/W/GaAs structure as function of W (a) and Zn (b) layer thickness.

Evolution of I - V curves (for a contact structure with optimized thicknesses of W and Zn layers) depending on the number N_p of laser pulses is shown in Fig.2.20. One can see that transformation of diode-like curves into ohmic ones tends to flatten out and depends on the number N_p of laser pulses: further increase of N_p over 10–12 does not change the form of I - V curves. As in the case of SiC, the most reproducible results have been obtained when using combined irradiation from a YAG:Nd³⁺-laser at two wavelengths: $\lambda = 1.06$ and $0.53 \mu\text{m}$.

The contact resistivity ρ_c was measured, as in the case of SiC, using the four-probe technique. The typical value $\rho_c = 2 \times 10^{-4} \Omega \cdot \text{cm}^2$ obtained for the W/Zn/W/GaAs contact structure has remained unchanged after thermal annealing at a temperature of 400°C and flow of testing current (150 mA) for 100 h.

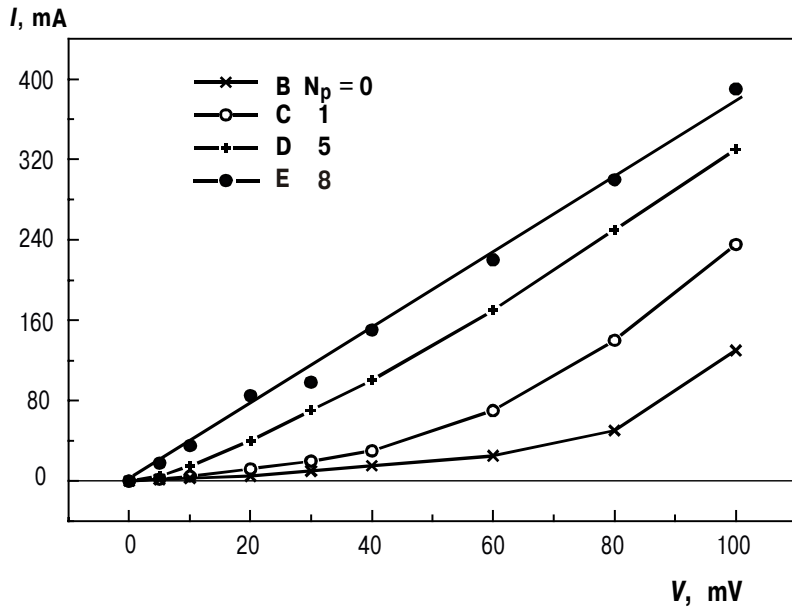


Fig.2.20. Evolution of the I - V curve for W/Zn/W/GaAs structure during laser annealing; N_p is the number of pulses.

The advantages of the W/Zn/W/GaAs-based ohmic contacts are as follows: (i) they require no welding and do not involve Au; (ii) presence of tungsten needs no additional metallization to provide interconnections; (iii) contact resistance demonstrates high thermal and current stability at submicron sizes of contact layers; (iv) it is possible to make ultra-shallow contacts using efficient and rather simple laser technique that in some cases can serve as alternative to expensive MBE [75].

2.6. LASER-THERMAL DIAGNOSTICS OF METAL-SEMICONDUCTOR CONTACT STRUCTURES

Reliability of ohmic contacts to semiconductor structures depends to a great extent on the quality of metal–semiconductor interfaces, uniformity of structures, temporal stability and metal layer adhesion to semiconductor surface. Nonuniformity of contact microstructure (especially of interfaces) determines nonuniformity of thermal resistance and thus affects its temperature field. Correlation between the temperature field of an object and its physical (thermal, mechanical, electrical) properties is determined using thermal flaw detection [76].

The laser-thermal diagnostics seems to be most preferable from the viewpoint of properties prediction for metal–semiconductor contact structures. This technique involves measurement of thermal radiation from an area of a contact structure exposed to focused pulse laser radiation whose intensity is much below the threshold at which irreversible structural changes appear. It is a contactless nondestructive technique that demonstrates high locality and low inertness, as well as potentialities to register wide range of both heating temperature and its changes. High sensitivity of this technique results from the fact that, according to the Stefan–Boltzmann law, the total energy radiated from a blackbody is proportional to the fourth power of the temperature of the body; the same approximately holds for radiation close to that from a blackbody. The advantage of the laser-thermal technique, as compared to other contactless techniques (say, that of time-resolved reflectivity), is that it does not need an additional laser probe, so its experimental realization is easier.

The first attempts to develop the laser-thermal diagnostics and apply it for study of semiconductors and semiconduc-

tor structures have been made in [77-82]. This technique has been successfully applied, in particular, to check quality of soldered connections. The authors of [83,84] have studied with the laser-thermal technique the metal-Al_xGa_{1-x}As contacts to detect potentially unreliable ones.

This section deals with investigation of thermal radiation flow from a model contact structure. The objective is to determine regularities in the influence of structure parameters and LI mode on the thermal radiation flow.

Let us consider the model metal-semiconductor contact structure suggested in [85] (see Fig.2.21) exposed to laser excitation. A feature of this structure is presence at the metal-semiconductor interface of a defect layer whose thermal conductivity is smaller than that of semiconductor. The above structure has been made from a circular plate (diameter of 80 mm, thickness $z_1 = 0.5$ mm) of single-crystalline silicon.

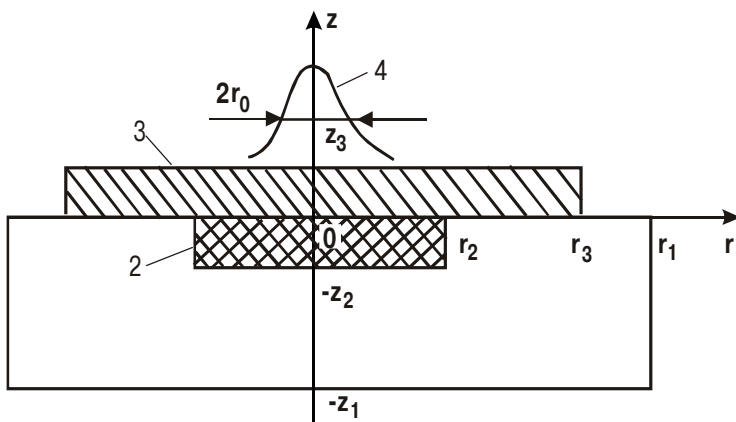


Fig.2.21. Cross section of a model axially symmetric contact structure. 1 – semiconductor layer; 2 – defect layer; 3 – metal layer (electrode); 4 – spatial distribution of laser radiation intensity.

The recesses whose diameters $2r_2$ were from 15 up to 100 μm and depth of about 20 μm were made in this plate. These recesses were filled with a heat insulator. A copper layer (electrode) was deposited using either thermal evaporation in a vacuum or electrodeposition. The electrode thickness z_3 was varied from 0.1 up to 12 μm . Special (without recesses) structures were made on the same single-crystalline silicon plate using deposition of a copper layer, either with or without additional sputtering of chromium. Different degrees of metal–semiconductor interface imperfection were simulated by changing copper layer adhesion to silicon. Thermal radiation flow was measured using a plant for LM whose diagram is presented in Fig.2.3.

A YAG:Nd³⁺-laser operated in the quasi-continuous mode. The electromechanical shutter placed in the resonator provided pulse duration of 10–25 μs . Diameter of the laser spot on the structure surface was changed from 30 up to 120 μm by focusing with the optical unit and replacement of a diaphragm in the laser resonator. The structure surface could be observed through a 30-power visualizer.

A detector of IR thermal radiation ПМ-4 had spectral characteristic close to bolometric one in the 2–10 μm range. We measured (i) kinetics of thermal radiation excited by laser action on the semiconductor–imperfect layer–metal structure and (ii) intensity I_t of the total heat flow, and also made estimation of the ratio P_2/P_1 between intensities of radiation at the moment $t = t_i$ from the imperfect and “perfect” structure areas exposed to LI. It was found experimentally that at $t_i = 20 \text{ ms}$ the P_2 and P_1 values differed from the stationary value no more than by 10–20%; their ratio was practically independent of time at $t_i \geq 10 \text{ ms}$. We studied how the intensities P_2 and P_1 depended on the excitation mode (energy E of

laser radiation, diameter $2r_0$ of laser spot) and model structure parameters: metal layer thickness z_3 (the imperfect layer diameter being fixed), imperfect layer diameter $2r_2$ (metal layer thickness being fixed), etc. We chose such LI mode that structure heating remained below 100 °C.

Let us consider thermal field excited by local action on a model contact structure of axial symmetry (see Fig.2.21). At the metal–semiconductor interface there is a local circular imperfect layer with reduced heat conductivity. Let us search for a solution of the equation (in cylindrical coordinates r, θ, z) of nonstationary heat conduction

$$c_i \rho_i \frac{\partial T_i}{\partial t} = \lambda_i \left[\frac{1}{r} \frac{\partial}{\partial r} \left(r \frac{\partial T_i}{\partial r} \right) + \frac{\partial^2 T_i}{\partial z^2} \right] - q_i(r, z, t) \quad (i = 1, 2, 3) \quad (2.17)$$

with the following initial condition

$$T_i|_{t=0} = 0 \quad (i = 1, 2, 3) \quad (2.18)$$

and boundary conditions:

$$T_1|_{z=-z_1} = 0, \quad (2.19)$$

$$\lambda_3 \frac{\partial T_3}{\partial z} \Big|_{z=z_3} + \alpha T_3 \Big|_{z=z_3} = 0, \quad (2.20)$$

$$\frac{\partial T_i}{\partial r} \Big|_{r=0} = 0 \quad (i = 1, 2, 3), \quad (2.21)$$

$$\frac{\partial T_i}{\partial r} \Big|_{r=r_i} = 0 \quad (i = 1, 3). \quad (2.22)$$

Besides, at joint boundaries Γ_{ij} of the i -th and j -th regions the conditions for thermal field matching should hold. This means that both temperature and normal component of the heat flow are to be continuous:

$$T_i|_{\Gamma_{ij}} = T_j|_{\Gamma_{ij}}, \quad \lambda_i \frac{\partial T_i}{\partial n}|_{\Gamma_{ij}} = \lambda_j \frac{\partial T_j}{\partial n}|_{\Gamma_{ij}}; \quad i, j = 1, 2, 3 \quad (i \neq j) \quad (2.23)$$

Here the indices 1, 2 and 3 apply to the parameters of the semiconductor layer, imperfect layer and electrode, respectively; z_1, z_2, z_3 (r_1, r_2, r_3) are the thicknesses (radii) of the corresponding regions; the functions $T_i = T_i(r, z, t)$ describe distribution of the difference of temperatures of a body and ambience; λ_i are the heat conductances of the corresponding regions; c_i are the specific heats at constant pressure; ρ_i are the densities; α is the coefficient of heat transfer from the electrode surface to the ambience; t is time. The function $q_3(r, z, t)$ describes distribution of the density of absorbed energy. For the metal layer this function was set in the following form:

$$q_3(r, z, t) = Q_0 \exp(-kr^2)[1 - \exp(-K_1(z_3 - z_1))], \quad (2.24)$$

where

$$\xi(t) = 1 \text{ at } 0 < t \leq t_p, \quad \xi(t) = 0 \text{ at } t > t_p. \quad (2.25)$$

Here Q_0 is the absorbed energy density at $r = 0, z = z_3$; $k = \ln 2 / r_0^2$ where r_0 is the laser beam radius at the $Q/2$ level; K_1 is the light absorption coefficient for metal; t_p is the laser pulse duration; $q_1 = q_2 = 0$.

Analytical solution of the above problem is known for some particular cases only [86]. To get solution in the general case, we have applied the numerical method of finite elements [87,88]. After multiplying both sides of equation (17) by r and carrying out replacements

$$\lambda_i^* = \lambda_i r, \quad c_i^* = c_i r, \quad q_i^*(r, z, t) = q_i(r, z, t)r \quad (i = 1, 2, 3) \quad (2.26)$$

we obtain:

$$c_i^* \rho_i = \frac{\partial T_i}{\partial l} \left[\frac{\partial}{\partial r} \left(\lambda_i^* \frac{\partial T_i}{\partial r} \right) + \frac{\partial}{\partial z} \left(\lambda_i^* \frac{\partial T_i}{\partial z} \right) \right] - q_i^*(r, z, l) \quad (i = 1, 2, 3). \quad (2.27)$$

One can see that after the above transformations the equation (2.17) for heat conduction (that has been written using the cylindrical coordinates) has took the form (2.27) that is characteristic of a planar problem (with parameters λ_i^* and c_i^* being functions of r). Therefore one can apply the well-known algorithm for solution of planar problems of heat conduction [87,88] in the convenient version advanced in [89]. To estimate the accuracy of the algorithm applied, we have made a comparison between the results of numerical calculation and the known analytical solution of the problem dealing with heating of a cylindrical region by heaters uniformly distributed within it. For the number of points of division equal to 21×11 it was found that the two solutions (exact and numerical) differed by no more than 0.4%.

From the temperature difference distribution in the structure considered that was determined in the above way we calculated an excess of the heat radiation from the structure over that from the ambience according to the Stefan–Boltzmann law:

$$P_T = \varepsilon_g \sigma_0 \int_0^{2\pi} d\theta \int_0^{r_3} \{[T(r) + T_0]^4 - T_0^4\} dr. \quad (2.28)$$

Here ε is the degree of grayness of the structure considered ($\varepsilon_g = 0, 1$); σ_0 is the Stefan–Boltzmann constant; $T(r)$ is the temperature difference distribution over the metal layer surface ($z = z_3$); T_0 is the absolute temperature of the ambience.

Shown in Fig.2.22 are temporal dependencies of heat radiation from three structures, both with and without an imperfect layer. One can see that structure heating and cooling rates, as well as heat radiation intensities, strongly depend on the imperfect layer size. Therefore one can detect imperfect layer from the ratio P_{T_2} / P_{T_1} between the “thermal signal” amplitudes for structures with and without this imperfect layer.

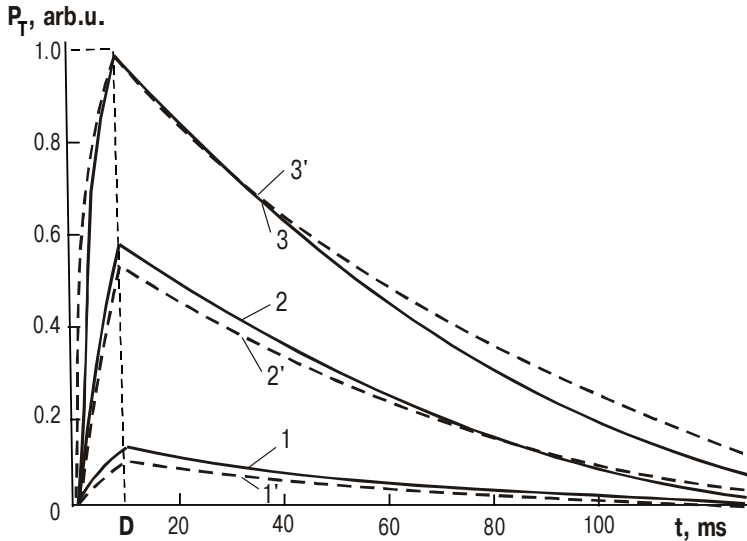


Fig.2.22. Heat emission kinetics for three Si–Cu structures with different values of the defect layer radius r_2 : 1 – 0 (without defect layer); 2 – 20 μm ; 3 – 75 μm . Metal layer thickness $z_3 = 0.13 \mu\text{m}$. Full (broken) curves are the experimental (calculated) ones. Chain curve corresponds to a laser pulse (duration of 10 μs).

The P_{T_2} / P_{T_1} vs metal layer thickness z_3 and laser action energy E curves are shown in Fig.2.23. One can see that the ratio P_{T_2} / P_{T_1} drops when z_3 grows and E decreases. At the indicated irradiation mode parameters the imperfect layer manifests itself (when $P_{T_2} / P_{T_1} = 1.05$) at metal layer thicknesses $z_3 = 2.05\text{--}4.5 \mu\text{m}$ and $E = 2\text{--}10 \text{ mJ}$. From the inset (Fig.2.23) one can see that when the excitation energy grows, then the value of metal layer thickness at which one can still detect the imperfect layer grows too; when (at a fixed laser radiation energy) the metal layer thickness decrease, then it becomes possible to detect imperfect layers of smaller sizes.

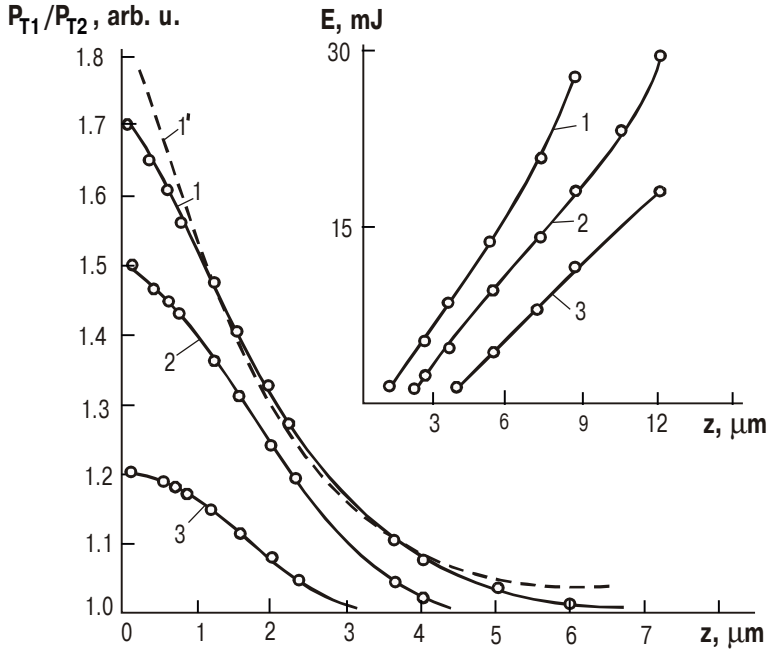


Fig.2.23. Ratio P_{T2}/P_{T1} (between heat emission intensities for excitation of Si–Cu structure areas with and without a defect layer) as function of the metal layer thickness z_3 at different laser excitation energies E : 10 mJ (curves 1, 1'); 5 mJ (curve 2); 2 mJ (curve 3). (Curve 1' is a calculated one.) Inset: E vs z_3 curves for structures with defect layer size 20 (1), 30 (2) and 50 μm (3).

Shown in Fig.2.24 are the total thermal radiation from the Si–Cu structure vs the “defect” radius curves taken at different sizes of the laser spot. (Here by “defect” is meant the imperfect layer whose parameters are those proposed for the model described in [84].) A laser beam was incident at the “defect” center. The beam diameter could be changed by focusing; in this way the excitation intensity was varied. One

can see from Fig.2.24 that the thermal radiation intensity P_T increases with "defect" size. The $P_T(r_2)$ curve has an inflection point at $r_2 = r_0$: at small ($r_2 \leq r_0$) "defect" sizes the $P_T(r_2)$ curve is sloping, while at big ($r_2 \geq r_0$) "defect" sizes it flattens out. From the above behavior of the $P_T(r_2)$ dependence it follows that one can estimate the "defect" size from the inflection point position. It also follows from the presented $P_T(r_2)$ curves that the minimal size of the detectable "defect" is about one third that of the laser spot for the conditions used.

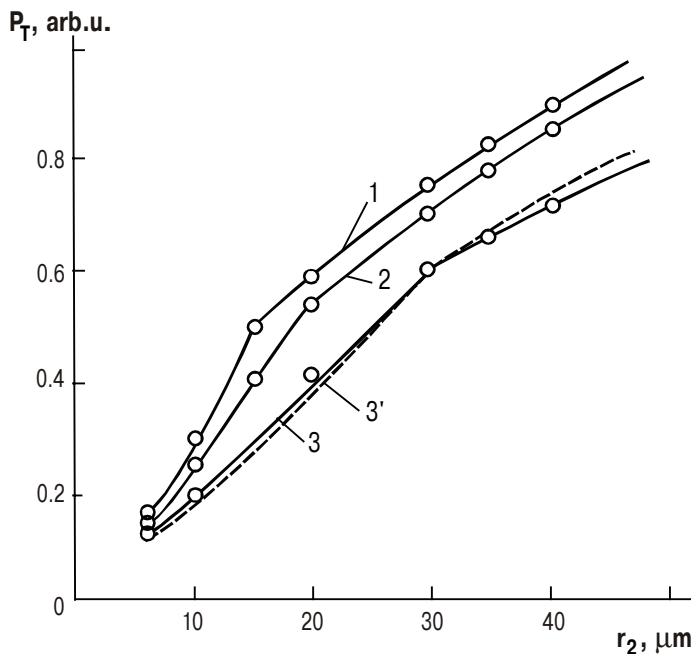


Fig.2.24. Heat emission intensity P_T vs "defect" size r_2 curves at different laser beam radii r_0 : 15 (1), 20 (2) and 30 μm (3). Laser excitation energy $E = 10$ mJ; laser pulse duration $t_p = 10$ ms. Broken curve 3' is the calculated one.

Shown in Fig.2.25 are the total thermal radiation vs metal thickness curves, $P_T(z_3)$, for two types of tailor-made structures that differ in adhesion between the metal layer and semiconductor. One can see that (as for the model structure) P_T decreases when z_3 grows. At small metal layer thicknesses the total thermal radiation is bigger for those structures that demonstrate lower metal adhesion. So one can judge adhesion of structure layers from the measurement of thermal radiation.

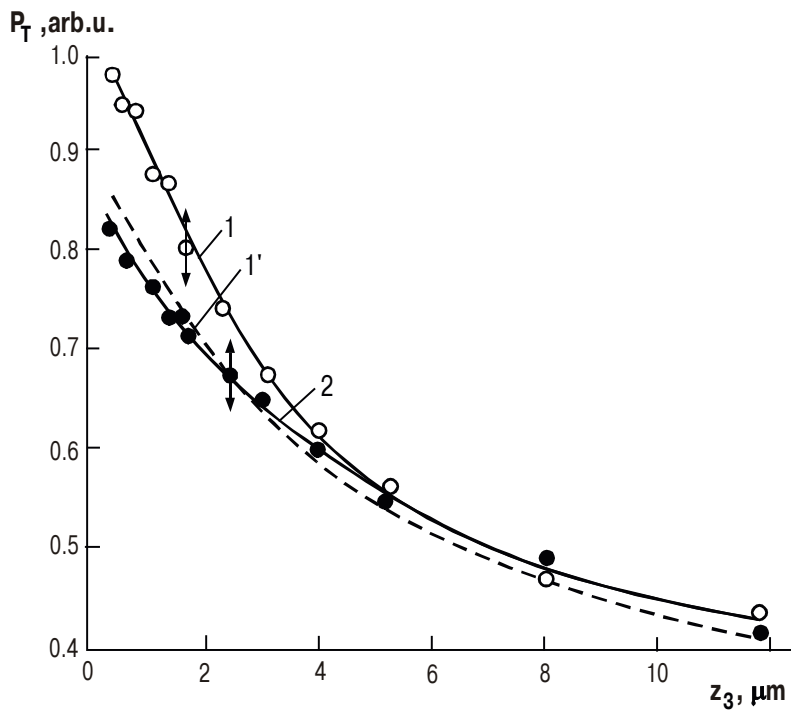


Fig.2.25. Heat emission intensity P_T vs metal layer thickness z_3 curves for Si–Cu structures of two types: with improved Cu adhesion (curves 1, 1') and initial (2). Broken curve 1' is the calculated one.

A comparison between the values of metal layer thickness obtained from the calibrated $P_T(z_3)$ dependence and from the results of independent measurement showed that measurement of the total thermal radiation P_T makes it possible to estimate the metal layer thicknesses lying in a certain range (say, up to 10 μm , judging from Fig.2.25). One can conclude from Fig.2.25 that for the chosen structure the accuracy of thickness z_3 measurement varies from 0.3 μm (in the 0.5–4 μm thickness range) to 0.5 μm (in the 4–10 μm thickness range).

Figure 2.26 illustrates isotherm distribution in the transverse cross-section of the model structure considered. This distribution was calculated using the numerical method of finite elements for the following cases: (i) without imperfect layer (Fig.2.26a); (ii) imperfect layer with heat conductivity $\lambda_2 = 1 \text{ W/m}\cdot\text{K}$ (Fig.2.26b); (iii) the same as (ii) but with $\lambda_2 = 10^{-2} \text{ W/m}\cdot\text{K}$ (Fig.2.26b). When there is no imperfect layer (Fig.2.26a), then heat is removed from the maximal heating point (that corresponds to the laser beam center) into the structure bulk. Presence of a metal layer results in a lateral heat flow whose fraction in the total heat removal increases with metal layer thickness. Figure 2.26b illustrates the case when a "defect" with low heat conductivity retards heat removal into the semiconductor bulk under it. This results in an increase of temperature difference. In this case most of the heat flow (whose lines are normal to the isotherms) passes around the "defect" through the metal layer over it. The rest of the heat flow is removed immediately through the "defect" ("semitransparent defect"). Figure 2.26c corresponds to the case when the "defect" is practically "nontransparent" for the heat flow lines. In this case the "defect" edge serves as a secondary heat source from which heat is taken away in the structure depth. This is evidenced by the form of the corresponding isotherms that are concentric semicircles similar to those presented in Fig.2.26a.

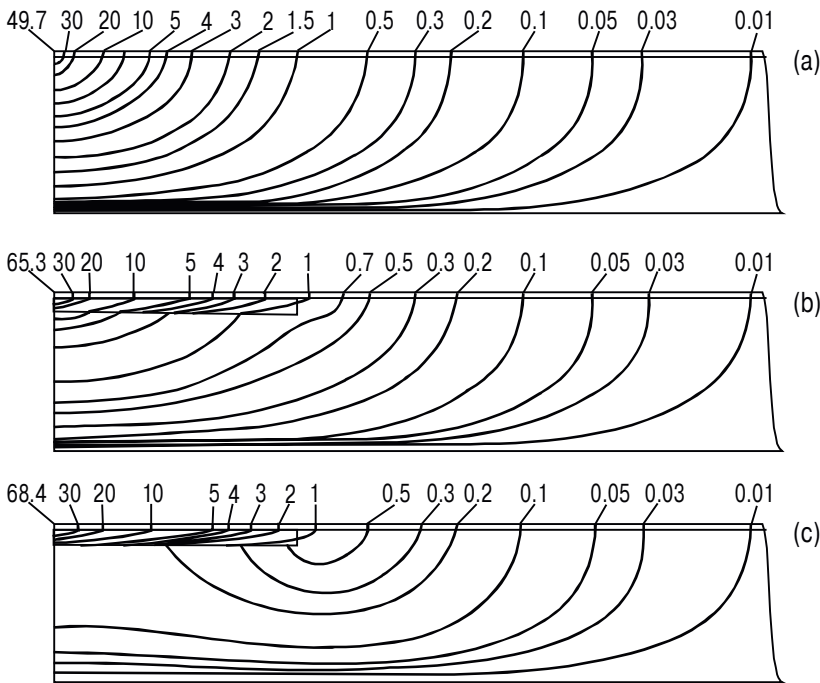


Fig.2.26. Isotherms for Si–Cu structures without (a) and with a defect layer: $\lambda_2 = 1 \text{ W/m}\cdot\text{K}$ (b), $10^{-2} \text{ W/m}\cdot\text{K}$ (c). (Isotherms are labeled by the temperature difference values; the conditions are steady.) $r_0 = 0.02 \text{ mm}$, $r_1 = r_3 = 4 \text{ mm}$, $r_2 = 0.6 \text{ mm}$; $z_1 = 0.5 \text{ mm}$, $z_2 = 0.05 \text{ mm}$, $z_3 = 0.01 \text{ mm}$; $\lambda_1 = 23.3 \text{ W/m}\cdot\text{K}$ (b) (silicon), $\lambda_3 = 390 \text{ W/m}\cdot\text{K}$ (b) (copper).

The presented patterns of temperature fields in the structures studied have clearly illustrated that presence of a “defect” results in increasing temperature difference in the structure, while presence of a metal layer leads to heat flow spreading and decrease of temperature difference. Broken curves in Figs.2.22–2.25 show the calculated dependencies of heat flow intensity on the structure parameters and irradiation mode.

One can see that for the structure studied and the chosen excitation mode ($t_p \approx 20$ ms) the results of calculations made for nonstationary conditions at $t \geq 20$ ms and stationary conditions are close. There is a reasonable qualitative agreement between the experimental and calculated curves. Taking into account the patterns of temperature fields for the structures studied, one can give justified explanations for the observed trends in regularities of the effect of structure parameters and irradiation mode on the measured thermal radiation. The fact that thermal radiation grows when the "defect" size increases and metal layer size decreases is due to increase of temperature difference and decrease of heat flow spreading (see Figs.2.22–2.25). It follows from this that the potentialities for "defect" detection with the laser-thermal technique decrease when the metal thickness grows and "defect" size goes down.

The gently sloping portion of the $P_T(r_2)$ curves (see Fig.2.24) is due to the fact that at $r_2 \ll r_0$ most of absorbed heat is spreading into the structure depth beyond the "defect" (in other words, flows around the "defect"). In this case the heat resistance R_h of the electrode section over the "defect" is of minor importance in formation of the structure temperature field.

At further increase of r_2 the total thermal radiation P_T increases abruptly. This is due to the action of the following two factors: (i) an increase of the heat resistance R_h and (ii) a decrease of heat Q flowing around the "defect". In this case the temperature difference jumps up abruptly (see Fig.2.26). The heat resistance R_h makes a decisive contribution to the temperature difference. At further growth of r_2 the $P_T(r_2)$ curve flattens out because Q no longer increases when $r_0 \ll r_2$.

Thus it has been shown in [85] that one can detect structural defects in metal–semiconductor contacts using the laser-thermal technique of diagnostics.

CONCLUSION

This book contains a review and analysis of a number of experimental works dealing with the effect of microwave and laser radiations on the electrophysical and structural properties of III-V (and some other) semiconductors and device structures based on them. Many of these works have been made by the authors of the book.

The analysis indicates at a substantial role in formation of properties of both near-surface semiconductor regions and SBs played by interactions between phases and defect production enhanced by the above radiations. The book may be considered as a direct extension of the previous one (A.E.Belyaev, J. Breza, E.F. Venger, M. Vesely, I.Yu. Il'in, R.V. Konakova, J. Liday, V.G. Lyapin, V.V. Milenin, I.V. Prokopenko and Yu.A. Tkhorik, "Radiation Resistance of GaAs-based Microwave Schottky-barrier Devices: Some physico-technological aspects", Інтерпрес АТД, Kiev, 1998). It supplements the general outline of the radiation-enhanced processes in semiconductor device structures.

The limited volume of this book did not enable the authors to give comprehensive presentation of all the aspects of this complex physico-technological problem. However, the numerous results of theoretical, experimental and physico-technological studies that have been already obtained make it possible to state that various beam treatments of semiconductors and devices (similar to those discussed here) can considerably extend application possibilities of radiation-enhanced processes and contribute to further advances in technology of semiconductor materials and devices.

REFERENCES

Introduction

1. Mirkin L.I. *Physical Foundations of Material Treatment with Laser Beams*. Moscow State Univ. Publ., Moscow (1975).*
2. *Problems in Radiation Technology of Semiconductors*. Ed. Smirnov L.S., Nauka, Novosibirsk (1980).*
3. Verkhovsky E.N. *Laser Technology in Manufacturing of Integrated Circuits*. Vysshaya Shkola, Moscow (1990).*
4. Syrovets P.A. *Industrial Application of Microwave Equipment (Novoye v Nauke, Tekhnike i Proizvodstve. Ser. Printsipial'no Novye Tekhnologii i Proizvodstva)*. UkrNIINTI Publ., Kiev (1990).*
5. Paton B.E., Sklyarevich V.E., Slusarczuk M.G. Gyrotron processing of materials. *MRS Bulletin*, 1993, **18**(11), 58-63.
6. Didenko A.P., Yushkov Yu.G. *High-power Pulses of Nanosecond Duration*. Energoatomizdat, Moscow (1984).*
7. Anisimov S.I., Imas Ya.A., Romanov G.S., Khodyko Yu.V. *Action of High-power Radiation on Metals*. Nauka, Moscow (1970).*
8. Varshava S.S., Baitsar R.I., Bortnik G.N. Modification of properties of semiconductor single crystals using laser radiation. In: *Proc. 2nd Intern. Conf. "Interaction of Radiation with Solids (IRS-97)"*, Minsk, Belarus, 1997, 131.*
9. Panov V.V., Sarkis'yan A.P. Some aspects of the problem of microwave facilities for functional damaging. *Zarubezhnaya Radioelektronika*, 1993, No 10-11-12, 3-10.*

* In Russian (throughout the list of references).

10. Perlman B.S. Microwave technology and device research in the army. *Microwave J.*, 1991, **34**(7), 81-83.
11. Kadukov A.E., Razumov A.V. The basics of technical and operation-technical application of electromagnetic weapons. *Peterburgsky Zhurn. Elektroniki*, 2000, No 2, 53-60.*
12. *Microwave Technologies in National Economy: Introduction, Problems, Prospects (Agricultural complex, industry, medicine)*, Pt. 2-3. Ed. Kalinin L.G. TES, Kiev-Odessa (2000).*
13. Pfeifer J., Badaljan E., Tekula-Buxbaum P., Kovács T., Geszti O., Tóth A.L., Lunk H.-J. Growth and morphology of $W_{18}O_{49}$ crystals produced by microwave decomposition of ammonium paratungstanate. *J. Cryst. Growth*, 1996, **169**, 727-733.
14. Vaidhyanathan B., Ganguli M., Rao K.J. A novel method of preparation of inorganic glasses by microwave irradiation. *J. Solid State Chemistry*, 1994, **113**(2), 448-452.
15. Vaidhyanathan B., Ganguli M., Rao J.J. Fast solid state synthesis of metal vanadites and chalcogenides using microwave irradiation. *Materials Research Bulletin*, 1995, **30**(9), 1173-1179.
16. Ning Yian Wang, Jiaqiang Hong Pijie. Influence of microwave radiation on properties and structure of Fe_2O_3/SO_2 solid superacid catalyst. *J. Materials Sci. and Technology*, 1996, **4**(4), 307-310.
17. Bykov Yu.V., Eremeev A.G., Pashkov V.I., Perevoschikov V.A., Skupov V.D. Gettering of impurities and defects in silicon at processing in microwave field. Deposited at VINITI, No 2322-B91, 1991.*
18. Abdurakhimov D.E., Vereschagin V.L., Kalinushkin V.P., Nikishin V.A., Ploppa M.G., Raizer M.D. Effect of pulsed microwave fields on the charge carrier lifetime in silicon. *Kratkie Soobscheniya po Fizike FIAN*, 1991, No 6, 27-29.*
19. Patent Ukraine # 13397 C1 HO1L 21/268. A technique for processing of semiconductor materials. Sklyarevich V.E., Shevelev M.V., Guroshhev V.I., Bunenko A.I. *Byulleten' Izobretений*, 1997, No 1, 15.*
20. Milenin V.V., Konakova R.V., Statov V.A., Sklyarevich V.E., Tkhorik Yu.A., Filatov M.Yu., Shevelev M.V. Physico-chemical processes at the Au/Pt/Cr/Pt/GaAs contact interface exposed to microwave annealing. *Pis'ma v ZhTF*, 1994, **20**(4), 32-35.*

21. Konakova R.V., Lyapin V.G., Milenin V.V., Sklyarevich V.E., Soloviev E.A., Shevelev M.V., Statov V.A., Bunenko A.I. Physico-chemical processes in the GaAs Schottky diodes stimulated by microwave treatment. *Funct. Materials*, 1995, **2**(4), 487-490.
22. Milenin V.V., Konakova R.V., Lyapin V.G., Statov V.A., Sklyarevich V.E., Tkhonik Yu.A., Shevelev M.V. Interactions between phases at the metal-GaAs, interfaces during microwave treatment. In: *Thin Films in Electronics (IV Intern. Sympos., Herson, Sept. 23–29, 1995)*, 1, 1995, 140-141.
23. Konakova R.V., Lyapin V.G., Milenin V.V., Soloviev E.A., Statov V.A., Tkhonik Yu.A., Shevelev M.V., Sklyarevich V.E., Filatov M.Yu. Physico-chemical processes in the GaAs Schottky diodes stimulated by microwave radiation. In: *Proc. 5th Intern. Sympos. on Recent Advances in Microwave Technology (ISRAMT-95)*, Kiev, 1995, **1**, 234-237.
24. Galst'yan E.A., Ravaev A.A. Thermal effect of pulsed microwave radiation on structurally nonuniform materials. *ZhTF*, 1992, **62**(1), 42-54.*
25. Voskresensky D.I., Ponomarev L.I., Rodin S.V. Interaction of electromagnetic fields with nonuniform media. *Zarubezhnaya Radioelektronika*, 1996, N 7, 6-14.*
26. Bokhan Yu.I. Charged impurity diffusion in a high-frequency field. *Pis'ma v ZhTF*, 1992, **18**(11), 6-8.*
27. Bekrenev A.N., Kamashev A.V. Determination of the fast mass-transport coefficient in metals at short-pulsed laser action. *Pis'ma v ZhTF*, 1994, **20**(6), 84-86.*
28. Astvatsatur'yan E.R., Akhabaev B.A., Skorobogatov P.K. Simulation of transient ionization effects in ICs using laser techniques. *Zarubezhnaya Elektronnaya Tekhnika*, 1988, No 6, 34-75.*
29. Pukhov V.V., Il'in Yu.D. Simulation of interference action of high-frequency and microwave signals on bipolar transistors. *Elektronnaya Tekhnika. Ser. 1. Elektronika SVCh*, 1986, No 10(394), 8-14.*
30. Rzhanov A.V., Gerasimenko N.N., Vasiliev S.V., Obodnikov V.I. Microwave heating as a technique for thermal processing of semiconductors. *Pis'ma v ZhTF*, 1981, **7**(20), 1221-1223.*

31. Covas M., Gay H.C. Recuit thermique rapide de semi-conducteur par energie. *J. Phys. III France*, 1993, **3**(5), 973-983.
32. Kachurin G.A., Pridachin N.B., Smirnov L.S. Annealing of radiation defects with pulsed laser irradiation. *FTP*, 1975, **9**(7), 1428-1429.*
33. Kachurin G.A., Nidaev E.V., Khodyachikh A.V., Kovaleva L.A. Annealing of implanted layers with a scanning laser beam. *FTP*, 1976, **10**(10), 1890-1893.*
34. Markevich M.I., Podol'tsev A.S., Piskunov F.A., Chen Chao, Yi Luo. Laser annealing of the GaAlAs/GaAs/GaAlAs/GaAl multilayer semiconductor structure. In: *Proc. 3rd Intern. Conf. "Interaction of Radiation with Solids (IRS-99)"*, Minsk, Belarus, 1999, Pt. 2, 68-69.*
35. Baitsar R.I., Bortnik G.N., Varshava S.S., Kurylo I.V. Influence of microwave irradiation on structure and properties of semiconductor crystals. In: *Proc. 3rd Intern. Conf. "Interaction of Radiation with Solids (IRS-99)"*, Minsk, Belarus, 1999, Pt. 2, 16-18.*
36. Pashkov V.I., Perevoschikov V.A., Skupov V.D. Effect of annealing in microwave radiation field on residual strain and impurity composition of near-surface silicon layers. *Pis'ma v ZhTF*, 1994, **20**(8), 14-17.*
37. Zavertannyi V.V., Zavertannaya L.S., Eremka V.D. The features of long-term process kinetics in nonuniform cadmium sulfide single crystals in microwave field. In: *8th Intern. Crimean Conf. "Microwave & Telecommunication Technology"*, Conf. Proc., Sevastopol, Weber Co. 1998, **1**, 162-164.*
38. Zavertannaya L.S., Zavertannyi V.V., Eremka V.D. Effect of microwave energy on nonequilibrium charged states in cadmium-sulfide detectors of radiation. In: *8th Intern. Crimean Conf. "Microwave & Telecommunication Technology"*, Conf. Proc., Sevastopol, Weber Co. 1998, **1**, 165-167.*
39. Abdurakhimov D.E., Vakhidov F.Sh., Vereschagin V.L., Kalinushkin V.P., Ploppa M.G., Raizer M.D. Change of semiconductor material properties due to action of microwave pulses of nano- and microsecond duration. *Mikroelektronika*, 1991, **20**(1), 21-25.*
40. Patent France # 8118656 C22F3/00, H01L 31/324. Procede de recuit superficiel par energie micro-onde pulsee de materiaux semiconducteurs. Cohen J., Kamarinos G., Chenevier P., Centre National de la Recherche Scientifique (CNRS), 1983.

41. Author's Certificate USSR # 989754. H05 B6/46. Method for heating of a dielectric or semiconductor material. Solin N.I., Samokhvalov A.A., Belomutov V.A., Afanasiev A.Ya., Gladkov G.I., Institute for Metal Physics of the Ural Scientific Center of the Academy of Sciences of USSR, 1980.*
42. Patent Japan # 4 517 026 H01L 211263. Method of backside heating a semiconductor substrate in an evacuated chamber by directed microwaves for vacuum treating and heating a semiconductor substrate. Minoru Inoue, Fujitsu Ltd., 1985.
43. Patent USA # 4 303 455 H01L 21/263. Low-temperature microwave annealing of semiconductor devices. Splinter M.R., Palys R.F., Bergawaia M.M., Rockwell Intern. Corp., 1980.
44. Patent Hungary # 194 444 H01L 21/263. Method of microwave annealing of semiconductor. Kovacs B., Mojzes I., Nemeth-Salay M., Veresegyhazy R., Gerasimenko N.N., Vasiliev S.V., 1985.
45. Patent Japan # 4 565 913 H05B 6/80. Method for the disintegration of silicon for semiconductor. Loshifumi Latsurugi, Meiseki Katayama, Komatsu Electronic Metals Co. Ltd., 1984.
46. Patent USA # 4 314 128 H068 6/80, 6/72. Silicon growth technique and apparatus using controlled microwave heating. Sanjeev R., Photowatt Intern. Inc., 1982.
47. Usanov D.A., Venig S.B., Orlov V.E. Signal generation by a tunnel diode induced with external microwave radiation. In: *Proc. 5th All-Russian Scientific and Technical Conf. "Actual Problems of Solid-state Electronics and Microelectronics"*, Ed. Konoplev B.G., Taganrog State Univ. of Radio Engineering, Taganrog, 1998, 113.*
48. Usanov D.A., Venig S.B., Orlov V.E. Negative differential resistance of a tunnel diode induced by external microwave signal. *Pis'ma v ZhTF*, 1999, **25**(2), 39-42.*
49. Usanov D.A., Skripal' A.V., Uglyumova N.V. Induction of S-type sections of $I-V$ curves for diodes with nondegenerate $p-n$ junctions under action of microwave radiation. In: *Proc. 5th All-Russian Scientific and Technical Conf. "Actual Problems of Solid-state Electronics and Microelectronics"*, Ed. Konoplev B.G., Taganrog State Univ. of Radio Engineering, Taganrog, 1998, 120.*

50. Usanov D.A., Skripal' A.V., Uglyumova N.V. Appearance of negative resistance in the p - n junction-based structures in microwave field. *FTP*, 1998, **32**(11), 1399-1402.*
51. Usanov D.A., Skripal' A.V., Uglyumova N.V. Appearance of S -type sections of I - V curves for diodes with p - n junction under action of microwave radiation. *Pis'ma v ZhTF*, 1999, **25**(1), 42-45.*
52. Usanov D.A., Skripal' A.V., Uglyumova N.V. Effect of lattice temperature on I - V curves for diodes with p - n junction under strong microwave field. In: *Proc. 6th All-Russian Scientific and Technical Conf. "Actual Problems of Solid-state Electronics and Microelectronics"*, Ed. Konoplev B.G., Taganrog State Univ. of Radio Engineering, Taganrog, 1999, 103.*
53. Blinov L.M., Vavilov V.S., Galkin G.N. Variation of optical properties and charge carrier concentration in Si and GaAs at intense photoexcitation with a ruby laser. *FTP*, 1967, **1**(9), 1351-1357.*
54. Bobrova E.A., Vavilov V.S., Galkin G.N. Photoconductivity and photomagnetic effect in germanium illuminated with laser pulses. *FTP*, 1969, **3**(8), 1232-1237.*
55. Fairfield J.M., Schwuttke G.H. Silicon diodes made by laser irradiation. *Solid-St. Electron.*, 1968, **11**(12), 1175-1176.
56. Harper F.E., Cohen M.I. Properties of Si diodes prepared by alloying Al into n -type Si with heat pulses from a Nd:YAG laser. *Solid-St. Electron.*, 1970, **13**(7), 1103-1109.
57. Khaibullin I.B., Shtyrkov E.I., Zaripov M.M., Gallyautdinov M.F., Bayazitov R.M. Annealing of ion-implanted layers under action of laser radiation. Deposited at VINITI, Moscow, No 2661-74.*
58. Khaibullin I.B., Titov V.V., Shtyrkov E.I., Zaripov M.M., Strashko V.P., Kuzmin K.P. Laser annealing of implanted layers. In: *Proc. Intern. Workshop on Ion Doping of Semiconductors, Budapest*, 1975, 212-246.*
59. Shtyrkov E.I., Khaibullin I.B., Zaripov M.M., Gallyautdinov M.F., Bayazitov R.M. On mechanism for laser annealing of implanted layers. In: *Proc. Intern. Workshop on Ion Doping of Semiconductors, Budapest*, 1975, 247-262.*
60. Shtyrkov E.I., Khaibullin I.B., Zaripov M.M., Gallyautdinov M.F., Bayazitov R.M. Local laser annealing of ion-implanted semiconductor layers. *FTP*, 1975, **9**(10), 2000-2002.*

61. Dvurechensky A.V., Kachurin G.A., Nidaev E.V., Smirnov L.S. *Pulsed Annealing of Semiconductor Materials*. Nauka, Moscow, 1982.*
62. Eckhardt G., Anderson C.L., Hess L.D., Krumm C.F. Laser-annealed ohmic contacts for GaAs microwave devices. In: *Laser-solid Interactions and Laser Processing*, 1978. AIP, New York, 1979, 641-646.
63. Laren G., Hess L.D., Olson L. Electrical characteristics of laser-annealed polysilicon resistors for device application. In: *Laser and Electron Beam Processing of Materials*, 1980. Academic Press, New York, 1980, 481-486.
64. Gibbons J.F., Letoila A., Nissim Y.I., Wu F.C. Application of CW beam processing to semiconductor device fabrication. In: *Laser and Electron Beam Processing of Materials*, 1980. Academic Press, New York, 1980, 593-607.
65. Zuev V.A., Litovchenko V.G., Glinchuk K.D., Litovchenko N.M., Sukach G.A., Linnik L.F. Processes of charge carrier recombination at Ge and Si surfaces at laser excitation. *FTP*, 1972, **6**(10), 1936-1944.*
66. Lysenko V.S., Nazarov A.N., Lokshin M.M., Kaschieva S.B. Effect of laser irradiation on electrophysical properties of interface in MIS structures implanted with B^+ ions. *FTP*, 1977, **11**(11), 2254-2257.*
67. Fedorenko L.L., Malyutenko V.K., Bolgov S.S. Activation of the InSb photoconductivity by laser illumination. *Ukr. Fiz. Zhurn.*, 1975, **20**(12), 2041-2044.**
68. Brodin M.S., Romanenko I.L., Shabliy I.Yu. Change of photoelectric properties of CdS single crystals after laser pulse action. *FTP*, 1975, **9**(7), 1418-1419.*
69. Brodin M.S., Davydova N.A., Shabliy I.Yu. Action of laser radiation on optical spectra of CdS single crystals. *FTP*, 1976, **1**(4), 625-630.*
70. Tovstyuk K.D., Plyatsko G.V., Orletsky V.B., Kiyak S.G., Bobitsky Ya.V. Formation of p - n and n - p junctions in semiconductors by laser radiation. *Ukr. Fiz. Zhurn.*, 1976, **21**(11), 1918-1920.**
71. Author's Certificate USSR # 555761. Method for fabrication of p - n junctions. Tovstyuk K.D., Plyatsko G.V., Orletsky V.B., Kiyak S.G. *Byulleten' Izobretenii*, 1981, No 15, 291.*

** In Ukrainian (throughout the list of references).

72. Kiyak S.G. Changing of physical properties and structure of semiconductors on exposure to pulsed laser radiation. *Izv. AN SSSR. Ser. Fiz.*, 1982, **46**(6), 1090-1096.*

Part 1

1. Pukhov V.V., Il'in Yu.D. Action of high-frequency and microwave fields on semiconductor devices and integrated circuits. *Elektronnaya Tekhnika. Ser. Elektronika SVCh*, 1986, No 9(393), 25-28.*
2. Antipin V.V., Godovitsyn V.A., Gromov D.V., Kozhevnikov A.S., Ravaev A.A. Effect of high-power pulsed microwave disturbances on semiconductor devices and integrated microcircuits. *Zarubezhnaya Radioelektronika*, 1995, N 1, C.37-53.*
3. Bludov S.B., Gadetskiy N.P., Kravtsov K.A., Lonin Yu.F., Magda I.I., Naisteter S.I., Prasol E.A., Prokopenko Yu.V., Pushkarev S.S., Tkach Yu.V., Kharchenko I.F., Chumakov V.N. Generation of high-power ultrashort microwave pulses and their action on the products of electronic industry. *Fizika Plazmy*, 1994, **20**(7-8), 712-717.*
4. Brigidin A.M., Titovich N.A., Kirillov V.M., Yusov Yu.P., Listopad N.I., Yasulya G.I. Effect of electromagnetic disturbances on serviceability of semiconductor devices and integrated circuits. *Elektronnaya Tekhnika. Ser. 8. Upravlenie kachestvom, standartizatsiya, metrologiya, ispytaniya*, 1992, N 1(148), 3-13.*
5. Rzhanov A.V., Gerasimenko N.N., Vasiliev S.V., Obodnikov V.I. Microwave heating as a technique for thermal processing of semiconductors. *Pis'ma v ZhTF*, 1981, **7**(20), 1221-1223.*
6. Vinnik E.V., Guroshev V.I., Prokhorovich A.V., Shevelev M.V. Use of high-power microwave radiation for rapid annealing of gallium arsenide. *Optoelektronika i Poluprovodnikovaya Tekhnika*, 1989, N 15, C.48-50.*
7. Pashkov V.I., Perevoschikov V.A., Skupov V.D. Effect of annealing in microwave radiation field on residual strain and impurity composition of near-surface silicon layers. *Pis'ma v ZhTF*, 1994, **20**(8), 14-17.*
8. Abdurakhimov D.E., Vereschagin V.L., Kalinushkin V.P., Nikishin V.A., Ploppa M.G., Raizer M.D. Effect of pulsed microwave fields on

the charge carrier lifetime in silicon. *Kratkie Soobscheniya po Fizike FIAN*, 1991, N 6, 27-29.*

9. Breza J., Venger E.F., Konakova R.V., Lyapin V.G., Milenin V.V., Statov V.A., Tkhonik Yu.A. Physico-chemical features of metal-III-V compound interface formation and capabilities for prediction of interactions between phases. *Poverkhnost'*, 1998, N 5, 110-127.*
10. Seidman A.A. Reactive deposition of titanium nitride layers in a vacuum and their use in contact metallization systems of semiconductor devices. *Obozry po Elektronnoi Tekhnike. Ser. 2 Poluprovodnikovye Pribory*, 1988, No (6).*
11. Herman M.A. *Semiconductor Superlattices*. Akademie-Verlag, Berlin, 1986.
12. Pavlov L.P. *Methods for Determination of the Principal Parameters of Semiconductor Materials*. Vysshaya Shkola, Moscow, 1975.*
13. Rhoderick E.H. *Metal-semiconductor Contacts*. Clarendon Press, Oxford, 1978.
14. *Practical Surface Analysis by Auger and X-ray Photoelectron Spectroscopy*. Eds. Briggs D., Seach M.P. John Wiley & Sons, Chichester-New York-Brisbane-Toronto-Singapore, 1983.
15. Ermolovich I.B., Venger E.F., Konakova R.V., Milenin V.V., Svechnikov S.V., Sheveljev M.V. Photoluminescent investigations of SHF-irradiation effect on defect states in GaAs:Sn(Te) and InP crystals. *Proc. SPIE*, 1997, **3359**, 265-272.
16. Gavrilenko V.I., Grekhov A.M., Korbutyak D.I., Litovchenko V.G. *Optical Properties of Semiconductors (A Handbook)*. Naukova Dumka, Kiev, 1987.*
17. Geguzin L.E. *Diffusion Zone*. Nauka, Moscow, 1978.*
18. Sheinkman M.K., Ermolovich I.B., Belen'ky G.L. Mechanisms for orange, red and infrared photoluminescence in CdS single crystals and parameters of the corresponding luminescent centers. *FTT*, 1968, **10**(9), 2628-2638.*
19. Belyaev A.A., Belyaev A.E., Ermolovich I.B., Komirenko S.M., Konakova R.V., Lyapin V.G., Milenin V.V., Soloviev E.A., Shevelev M.V. Effect of microwave processing on electrophysical characteristics of semiconductors and surface-barrier structures of industrial importance. *ZhTF*, 1998, **68**(12), 49-53.*

20. Belyaev A.E., Belyaev A.A., Venger E.F., Ermolovich I.B., Komirenko S.M., Konakova R.V., Lyapin V.G., Magda I.I., Milenin V.V., Prokopenko I.V., Svechnikov S.V., Soloviev E.A., Tkhonik Yu.A., Shevelev M.V. Effect of microwave radiation on structural, physico-chemical and electrophysical properties of a number of semiconductor materials and device structures. In: *6th Intern. Crimean Conf. "Microwave & Telecommunication Technology", Conf. Proc.*, Sevastopol, Weber Co., 1996, 71-89.*
21. Strikha V.I., Buzanova E.V. *Physical Foundations of the Metal–semiconductor Contact Reliability in Integrated Electronics*. Radio i Svyaz', Moscow, 1987.*
22. Venger E.F., Konakova R.V., Korotchenkov G.S., Milenin V.V., Russu E.V., Prokopenko I.V. *Interactions between Phases and Degradation Mechanisms in Metal-InP and Metal-GaAs Structures*. Information-editing Dept. of the Institute of Semiconductor Physics of the National Academy of Sciences of Ukraine, Kiev, 1999.*
23. Brillson L.S., Brucker C.F., Katnani A.D., Stoffel N.G., Daniels R., Margaritondo G. Fermi-level pinning and chemical structure of InP–metal interfaces. *J. Vac. Sci. Technol.*, 1982, **21**(2), 564.
24. Breza J., Milenin V.V., Konakova R.V., Lyapin V.V., Statov V.A., Tkhonik Yu.A., Shevelev M.V., Filatov M.Yu. Interactions between phases in Au–Cr–GaAs contacts enhanced by thermal and microwave annealing. *Poverkhnost'*, 1997, N 10, 83-85.*
25. Belyaev A.A., Belyaev A.E., Ermolovich I.B., Konakova R.V., Lyapin V.G., Milenin V.V., Soloviev E.A., Statov V.A., Svechnikov S.V., Venger E.F. Effect of microwave radiation on the physico-chemical properties of some semiconductor materials (GaAs, GaP, InP) and heterostructures, as well as on the parameters of surface-barrier diode structures. *CAS'99 Proc. (1999 Int. Semicond. Conf., Oct. 5–9, 1999, Sinaia, Romania)*, 1999, **1**, 385-388.
26. Oshina M., Kawamura T., Macayana S., Migahara T. Combined surface analyses by synchrotron radiation photoemission spectroscopy and surface extended x-ray adsorption fine structure of oxidation features of metal-deposited GaAs. *J. Vac. Sci. Technol. A*, 1988, **6**(3), 1451-1455.
27. Konakova R.V., Lyapin V.G., Milenin V.V., Sklyarevich V.E., Soloviev E.A., Shevelev M.V., Statov V.A., Bunenko A.I. Physico-

- chemical processes in the GaAs Schottky diodes stimulated by microwave treatment. *Funct. Materials*, 1995, **2**(4), 487-490.
- 28. *Thin Films. Interdiffusion and Reactions*. Eds. Poate J.M., Tu K.N., Mayer W. Wiley, 1978.
 - 29. Sinha A.R., Poate J.M. Effect of alloying behavior on the electrical characteristics of *n*-GaAs Schottky diodes metallized with W, Au, and Pt. *Appl. Phys. Lett.*, 1973, **23**(12), 666-668.
 - 30. Yu K.M., Walukiewicz W., Jaklevic J.M., Haller E.E. Effects of interface reactions on electrical characteristics of metal-GaAs contacts. *Appl. Phys. Lett.*, 1987, **51**(3), 189-191.
 - 31. Vinetsky V.L., Chaika G.E. Theory of recombination-induced atomic jumps in non-metal crystals. *FTT*, 1986, **28**(11), 3389-3395.*
 - 32. Sinischuk I.K., Chaika G.E., Shishyanu F.S. Radiation-stimulated atomic diffusion in a metal-semiconductor contact. *FTP*, 1985, **19**(4), 674-677.*
 - 33. Bass F.G., Gurevich Yu.G. *Hot Electrons and High Electromagnetic Fields in Semiconductor and Gas Discharge Plasmas*. Nauka, Moscow, 1965.*
 - 34. Chaika G.E., Konakova R.V., Lyapin V.G., Milenin V.V. Effect of microwave radiation on the metal-semiconductor contact formation. In: *8th Intern. Crimean Conf. "Microwave & Telecommunication Technology"*, *Conf. Proc.*, Sevastopol, Weber Co. 1998, **2**, 727-728.*
 - 35. Milenin V.V., Konakova R.V., Statov V.A., Sklyarevich V.E., Tkhorik Yu.A., Filatov M.Yu., Shevelev M.V. Physico-chemical processes at the Au/Pt/Cr/Pt/GaAs contact interface exposed to microwave annealing. *Pis'ma v ZhTF*, 1994, **20**(4), 32-35.*
 - 36. Milenin V.V., Konakova R.V., Lyapin V.G., Statov V.A., Sklyarevich V.E., Tkhorik Yu.A., Shevelev M.V. Interactions between phases at the metal-GaAs, interfaces during microwave treatment. In: *Thin Films in Electronics (IV Intern. Sympos., Herson, Sept. 23-29, 1995)*, **1**, 1995, 140-141.
 - 37. Borkovskaya O.Yu., Dmitruk N.L., Konakova R.V., Lyapin V.G., Milenin V.V., Prokopenko I.V., Statov V.A., Tkhorik Yu.A., Breza J., Liday J. Metal (Cr, Mo, W)-GaAs contacts. In: *Frontiers in Nanoscale Science of Micron/Submicron Devices, Series E: Applied Sci-*

- ences*, **328**. Eds. Jauho A.-P., Buzaneva E.V. Kluwer Academic Publishers, Dordrecht/Boston/London, 1996, 385-388.
38. Konakova R.V., Lyapin V.G., Milenin V.V., Soloviev E.A., Statov V.A., Tkhorik Yu.A., Shevelev M.V., Sklyarevich V.E., Filatov M.Yu. Physico-chemical processes in the GaAs Schottky diodes stimulated by microwave radiation. In: *Proc. 5th Intern. Sympos. on Recent Advances in Microwave Technology (ISRAMT-95)*, Kiev, 1995, **1**, 234-237.
 39. Belyaev A.A., Belyaev A.E., Ermolovich I.B., Komirenko S.M., Konakova R.V., Lyapin V.G., Milenin V.V., Tkhorik Yu.A., Shevelev M.Yu. Effect of microwave irradiation on physico-chemical properties of a number of semiconductors and Schottky-barrier diode structures. In: *Proc. 4th All-Russian Scientific and Technical Conf. "Actual Problems of Solid-state Electronics and Microelectronics"*, Ed. Konoplev B.G., Taganrog State Univ. of Radio Engineering, Taganrog, 1997, 86-88.*
 40. Ismailov K.A., Statov V.A., Konakova R.V., Kamalov A.B. Non-thermal mechanisms for microwave radiation effect on characteristics of a metal–semiconductor contact. In: *Abstr. Intern. Conf. "Modern Problems of Semiconductor Physics"*, Nukus, 8–11 Sept. 1997, 69-70.*
 41. Venger E.F., Ermolovich I.B., Konakova R.V., Milenin V.V., Svechnikov S.V. Effect of high-power electromagnetic radiation on defect structure of III–V semiconductor materials. In: *7th Intern. Crimean Conf. "Microwave & Telecommunication Technology"*, Conf. Proc., Sevastopol, Weber Co. 1997, **1**, 278-281.*
 42. Milenin V.V. Modification of the properties of GaAs and metal–GaAs structures by action of γ -radiation and microwave radiations. In: *Proc. 2nd Intern. Conf. "Interaction of Radiation with Solids (IRS-97)"*, Minsk, Belarus, 1997, 118.*
 43. Venger E.F., Ermolovich I.B., Milenin V.V., Konakova R.V., Chaika G.E. Effect of external radiation, microwave and mechanical excitations on defect production in nonmetallic crystals. *Voprosy Atomnoi Nauki i Tekhniki. Ser. Fizika Radiatsionnykh Povrezhdeniy i Radiatsionnoe Materialovedenie*, 1999, No 3(75), 60-73.*
 44. Statov V.A. *Investigation of Physics of Interactions between Phases at the Refractory Metal–Gallium Arsenide Interface*. Author's Abstract of the Candidate of Phys.-Math. Sci. Thesis. Kiev, Institute of Semiconductor Physics of the National Academy of Sciences of Ukraine, 1996.*

45. Ermolovich I.B., Milenin V.V., Konakova R.V., Chaika G.E. Effect of external radiation and mechanical excitations on defect production in nonmetallic crystals. *Voprosy Atomnoi Nauki i Tekhniki. Ser. Fizika Radiatsionnykh Povrezhdeniy i Radiatsionnoe Materialovedenie*, 1998, No 1(67), 2(68), 37-39.*
46. Belyaev A.E., Breza J., Venger E.F., Vesely M., Il'in I.Yu., Konakova R.V., Liday J., Lyapin V.G., Milenin V.V., Prokopenko I.V., Tkhorik Yu.A. *Radiation Resistance of GaAs-based Microwave Schottky-barrier Devices (Some physico-technological aspects)*. Interpress LTD, Kiev, 1998.
47. Skupov V.D., Tetel'baum D.I. On the effect of elastic stresses on transformation of defect aggregates in semiconductors. *FTP*, 1987, **21**(8), 1495-1497.*
48. Usanov D.A., Korotin B.N., Orlov V.E., Skripal' A.V. Degeneration removal in *p*- and *n*-regions of a tunnel diode by an external microwave signal. *Pis'ma v ZhTF*, 1990, **16**(8), 50-51.*
49. Usanov D.A., Orlov V.E., Korotin B.N., Skripal' A.V. Operation of a generator with tunnel diode exposed to an external microwave signal. Negative resistance devices and integrated converters on their basis. In: *Abstr. All-Union Scientific-Technical Conf., 15-17 Oct. 1991, Baku*, 1991, 65.*
50. Usanov D.A., Orlov V.E., Korotin B.N., Skripal' A.V. Effect of external microwave signal on operation of the microwave generator with tunnel diode. *Izv. Vuzov. Radiofizika*, 1991, **34**(1), 98-100.*
51. Usanov D.A., Skripal' A.V., Korotin B.N., Orlov V.E. Effect of heating microwave field on the form of *I-V* curve of tunnel diode. *Pis'ma v ZhTF*, 1993, **19**(7), 81-85.*
52. Usanov D.A., Skripal' A.V., Korotin B.N., Orlov V.E. The influence of warming microwave field on the working of devices with tunneling-thin *p-n* transitions. In: *Proc. 10th Intern. Microwave Conf. MIKON-94, May 30-June 2, 1994, Ksiaz Castle (Poland)*, 1994, **1**, 151-155.
53. Usanov D.A., Skripal' A.V., Korotin B.N., Orlov V.E., Tyazhlov V.S., Vasilieva A.V. Investigation of physical processes in semiconductor devices for microwave range under optical radiation and static magnetic field. In: *Simulation and Design of Devices and Systems for Mi*

- cro- and Nanoelectronics*. Ed. Chaplygin Yu.A. MGIET (TU) Publ., Moscow, 1994, 36-45.*
54. Usanov D.A., Skripal' A.V., Orlov V.E., Korotin B.N. Regulation of the form of $I-V$ curve of tunnel diodes connected in series by heating microwave field. *Izv. Vuzov. Elektronika*, 1996, N 1-2, 129-133.*
 55. Usanov D.A., Skripal' A.V. *Physics of Semiconductors. Transport Phenomena in Structures with Tunneling-thin Semiconductor Layers*. Saratov Univ. Publ., Saratov, 1996.*
 56. Usanov D.A., Skripal' A.V. Microwave radiation control of semiconductor structures with tunneling-thin $p-n$ transitions. In: *Proc of 21st Intern. Conf. on Microelectronics MIEL'97, 14–17 September, 1997, Nis (Yugoslavia)*, 1997, **1**, 249-251.
 57. Usanov D.A., Venig S.B., Orlov V.E. Signal generation by a tunnel diode stimulated by external microwave radiation. In: *Proc. 5th All-Russian Scientific and Technical Conf. "Actual Problems of Solid-state Electronics and Microelectronics"*, Ed. Konoplev B.G., Taganrog State Univ. of Radio Engineering, Taganrog, 1998, 113.*
 58. Skripal' A.V. *Investigation of the Features of Interaction between Electromagnetic Fields and Semiconductor Devices in Microwave Circuits*. Author's Abstract of the Doctor of Phys.-Math. Sci. Thesis. Saratov, 1998.*
 59. Usanov D.A., Skripal' A.V., Uglyumova N.V., Venig S.B., Orlov V.E. Appearance of the negative differential resistance mode and switching in a tunnel diode under external microwave signal action. *FTP*, 2000, **34**(5), 567-571.*
 60. Vitusevich S.A., Dózsa L., Konakova R.V., Pódör B., Badaljan E., Belyaev A.E. Effect of microwave treatment on the current formation processes in a two-barrier AlGaAs/GaAs heterostructure. In: *Proc. VI Intern. Conf. on Physics and Technology of Thin Films, Ivano-Frankivsk, Ukraine, 1997*, Pt. 1, 118.*
 61. Badaljan E., Dózsa L., Pódör B., Vo Van Tuyen, Belyaev A.E., Konakova R.V., Vitusevich S.A., Kravchenko L.N., Mojzes I. Effect of microwave heat treatment on the current-voltage characteristics of GaAlAs/GaAs resonant tunneling diodes. In: *Proc. XXVIII Intern. School on Physics of Semiconducting Compounds, Jaszowiec'99*, 1999, 174-176.

62. Belyaev A.E., Konakova R.V., Soloviev E.A., Sheka D.I., Pödör B., Badaljan E. Effect of high-power microwave radiation on characteristics of combined resonant-tunneling structures. In: *5th Intern. Workshop on Expert Evaluation and Control of Compound Semiconductor Materials and Technologies, Crete, Greece, 2000*, 74.
63. Belyaev A.E., Boltovets N.S., Konakova R.V., Soloviev E.A., Sheka D.I., Pödör B., Badaljan E., Vitusevich S.A. Effect of thermal annealing and high-power microwave radiation on characteristics of combined resonant tunneling structures. In: *ASDAM 2000 Conf. Proc. (The Third Intern. Euroconference on Advanced Semiconductor Devices and Microsystems), Smolenice Castle, Slovakia, Oct. 16–18, 2000*, 457-460.
64. Jafarov T.D. *Radiation-induced Diffusion in Semiconductors*. Energoatomizdat, Moscow, 1991.*
65. Schubert E.F. Delta-doping of III–V compound Semiconductors. *J. Vac. Sci. Technol. A*, 1990, **8**(3), 2980-2996.
66. Tkhorik Yu.A., Khazan L.S. *Plastic Deformation and Misfit Dislocations in Heteroepitaxial Systems*. Naukova Dumka, Kiev, 1983.*
67. Venger E.F., Grendel M., Daniška V., Konakova R.V., Prokopenko I.V., Tkhorik Yu.A., Khazan L.S. *Structural Relaxation in Semiconductor Crystals and Device Structures*. Phoenix, Kiev, 1994.*
68. Kryshtab T.G., Semenova G.N., Lytvyn P.M., Konakova R.V., Prokopenko I.V., Mazin M.A. Nonmonotony of the structural relaxation processes at microwave processing of gallium arsenide. *Optoelektronika i Poluprovodnikovaya Tekhnika*, 1996, No 31, 140-145.*
69. Lytvyn P.M. *Transformation of the Defect Structure of Single Crystals and Epitaxial Structures Based on GaAs under Effect of External Excitations Revealed with x-ray Diffraction Techniques*. Author's Abstract of the Candidate of Phys.-Math. Sci. Thesis. Kiev, Institute of Semiconductor Physics of the National Academy of Sciences of Ukraine, 1997.**
70. Pödör B., Badaljan E.G., Venger E.F., Semenova G.N., Semtsiv M.P., Kryshtab T.G., Lytvyn P.M. Effect of microwave radiation on the properties of silicon-doped gallium arsenide. In: *Abstr. Intern. Conf. "Modern Problems of Semiconductor Physics", Nukus, 8–11 Sept. 1997, 6-7*.*

71. Kryshtab T.G., Lytvyn P.M., Mazin M.A., Prokopenko I.V. Relaxation processes in single crystals and epitaxial structures at microwave treatments. In: *Proc. VI Intern. Conf. on Physics and Technology of Thin Films, Ivano-Frankivsk, Ukraine, 1997*, Pt. 1, 28-29.**
72. Pódör B., Badaljan E.G., Venger E.F., Semenova G.N., Kryshtab T.G., Semtsiv M.P., Lytvyn P.M., Prokopenko I.V. Modification of impurity-defect complexes in gallium arsenide at microwave irradiation. In: *Proc. 2nd Intern. Conf. "Interaction of Radiation with Solids (IRS-97)", Minsk, Belarus, 1997*, 70.*
73. Kryshtab T.G., Lytvyn P.M., Mazin M.A., Prokopenko I.V. The structural relaxation in single crystals stimulated by microwave radiation. *Metallofizika i Noveishie Tekhnologii*, 1997, **19**(5), 21-26.
74. Kryshtab T.G., Lytvyn O.S., Lytvyn P.M., Mazin M.A., Prokopenko I.V. Structural transformation in bulk GaAs and structures under microwave treatment. In: *Proc. of European Materials Research Society Spring Meeting, France, Strasbourg, 1998*, 9.
75. Kamalov A.B., Konakova R.V., Milenin V.V., Rengevych A.E., Sоловьев Е.А. Effect of microwave radiation on the characteristics of GaAs MESFETs. *Optoelektronika i Poluprovodnikovaya Tekhnika*, 2000, No 35, 145-149.*
76. Kamalov A.B., Konakova R.V., Milenin V.V., Rengevych A.E., Sоловьев Е.А. Effect of microwave radiation on parameters of GaAs MESFETs. In: *10th Intern. Crimean Conf. "Microwave & Telecommunication Technology", Conf. Proc.*, Sevastopol, Weber Co. 2000, 133-134.*
77. Venger E.F., Il'in I.Yu., Konakova R.V., Korotchenkov G.S., Milenin V.V., Prokopenko I.V., Rengevych A.E., Rusu E.V., Soloviev E.A., Chaika G.E. Radiation effects in GaAs- and InP-based MESFETs. In: *8th Intern. Crimean Conf. "Microwave & Telecommunication Technology", Conf. Proc.*, Sevastopol, Weber Co. 1998, **1**, 109-112.*
78. Konakova R.V., Milenin V.V., Soloviev E.A., Statov V.A., Stovpovoi M.A., Rengevych A.E., Tarielashvili G.T. Effect of radiation on the $I-V$ curves of gallium-arsenide MESFETs. *Izv. Vuzov. Radioelektronika*, 1999, **42**(4), 73-76.*
79. Konakova R.V., Milenin V.V., Soloviev E.A., Statov V.A., Stovpovoi M.A., Rengevych A.E., Prokopenko I.V., Tarielashvili G.T. Effect of

- ^{60}Co γ -radiation on electrophysical properties of gallium-arsenide MESFETs. *Izv. Vuzov. Radioelektronika*, 2000, **43**(6), 45-52.*
80. Bosyi V.I., Ivaschuk A.V., Il'in I.Yu., Semashko E.M., Sunduchkov K.S. Low-noise transistors for millimeter and submillimeter wavelength ranges. Materials and Technology. In: *6th Intern. Crimean Conf. "Microwave & Telecommunication Technology"*, Conf. Proc., Sevastopol, Weber Co. 1996, 3-9.*
 81. Il'in I.Yu., Konakova R.V., Milenin V.V., Soloviev E.A., Stovpovoi M.A., Rengevych A.E., Prikhodenko V.I. Radiation effects in ohmic and barrier contacts of gallium-arsenide MESFETs. In: *Proc. XIV Intern. Conf. on Physics of Radiation Phenomena and Radiation Materials Science, Alushta, 12-17 June 2000*, 335-336.*
 82. Ismailov K.A., Il'in I.Yu., Konakova R.V., Milenin V.V., Malinin V.G., Prokopenko I.V., Statov V.A., Tkhorik Yu.A. Effect of structural nonuniformity of gallium arsenide substrate on radiation tolerance of Schottky barriers. *Peterburgsky Zhurn. Elektroniki*, 1994, Suppl. 2. "Radiation-reliability characteristics of electronic products under extreme operation conditions", 80-86.*
 83. Breza J., Vesely M., Il'in I.Yu., Ismailov K.A., Konakova R.V., Liday J., Milenin V.V., Pavlenko A.A., Prokopenko I.V., Statov V.A., Tkhorik Yu.A., Khazan L.S. Radiation methods in processing of semiconductor materials and devices. In: *Proc. 5th Intern. Sympos. on Recent Advances in Microwave Technology (ISRAMT-95)*, Kiev, 1995, **3**, 844-927.
 84. Il'in I.Yu., Ismailov K.A., Koval'chuk G.A., Prokopenko I.V., Slutsky M.I., Tarielashvili G.T., Duriček L. Radiation stability of gallium-arsenide MESFETs. In: *Proc. IV Intern. Conf. on Physics and Technology of Thin Films, Ivano-Frankivsk, Ukraine*, 1993, Pt. 1, 102.*
 85. Bobyl' A.V., Konakova R.V., Kononov V.K., Malinin V.G., Malyshev M.M., Prokopenko I.V., Slutsky M.I., Tkhorik Yu.A. Interaction of gallium arsenide with ionizing radiation and problems of radiation tolerance of gallium-arsenide devices. *Elektronnaya Tekhnika. Ser. 8. Upravlenie kachestvom, standartizatsiya, metrologiya, ispytaniya*, 1992, No 4(151)-5(152), 31-40.*
 86. Konakova R.V., Milenin V.V., Soloviev E.A., Statov V.A., Stovpovoi M.A., Rengevych A.E. Radiation defect production in gallium-arsenide MESFETs. In: *3rd Intern. Conf. "Interaction of Radiation with Solids (IRS-99)"*, Minsk, Belarus, 1999, Pt. 1, 116-118.*

87. Venger E.F., Il'in I.Yu., Konakova R.V., Korotchenkov G.S., Milenin V.V., Prokopenko I.V., Rengevych A.E., Russu E.V., Sоловьев Е.А. Radiation effects in GaAs and InP MESFETs. In: *Proc. 5th All-Russian Scientific and Technical Conf. "Actual Problems of Solid-state Electronics and Microelectronics"*, Ed. Konoplev B.G., Taganrog State Univ. of Radio Engineering, Taganrog, 1998, 72.*
88. Boyko S.I., Osinsky V.I., Sinischuk I.K., Tverdyakov V.V. Investigation of the effect of radiation defects on dynamic parameters of Schottky transistors using the electron-probe-induced current technique. In: *Proc. Third All-Union Conf. "Physical Foundations of Reliability and Degradation of Semiconductor Devices"*, Kishinev Polytechnic Institute Publ., Kishinev, 1991, Pt. 1, 75-76.*
89. Rengevych A.E. Radiation effects in HEMTs. *Pis'ma v ZhTF*, 1999, **25**(8), 55-58.*
90. Badaljan E.G., Gerasimenko N.N., Kovac B., Mojzes I., Nemeth-Salay M., Vasiliev S.V., Veresegyhazy R. Microwave heat treatment of metallized compound semiconductor wafers. In: *Proc. of Spring Meeting Sympos. of MRS, Pittsburg, Apr. 15–21, 1990*, 1990, 16-20
91. Magda I.I., Bludov S.B., Gadetskiy N.P., Kravtsov K.A., Pushkarev S.S., Tkach Yu.V., Chumakov V.N., Malinin V.G., Starikov V.V., Usychenko V.G., Yakimov A.V., Lobkov M.N. Investigation of physical mechanisms for electronic product degradation in high-power electromagnetic fields. In: *Proc. III Intern. Crimean Conf. "Microwave Facilities and Reception via Satellites"*, Sevastopol, Weber Co. 1993, **5**, 523-526.*
92. Gadetskiy N.P., Kravtsov K.A., Magda I.I., Prokopenko Yu.V., Chumakov V.N., Novikov V.E., Tkach Yu.V. Investigation of the action of ultrashort pulsed electromagnetic radiations on microwave-range electronic facilities. In: *6th Intern. Crimean Conf. "Microwave & Telecommunication Technology"*, Conf. Proc., Sevastopol, Weber Co. 1996, 441-446.*
93. Gadetskiy N.P., Kravtsov K.A., Magda I.I. PC malfunction under action of ultrashort electromagnetic pulses. In: *9th Intern. Crimean Conf. "Microwave & Telecommunication Technology"*, Conf. Proc., Sevastopol, Weber Co. 1999, 326-328.*

94. Gadetskiy N.P., Magda I.I., Kravtsov K.A., Prokopenko Yu.P. Studies of electromagnetic radiation of ultrashort duration pulse interference on UHF electronics devices. In: *AMEREM'96 Conference. Book of Abstracts. Albuquerque, USA, 1996*, 79.
95. Vasiliev K.B., Klyuchnik A.V., Solodov A.V. Statistics of digital IC failures due to pulsed radiation. In: *9th Intern. Crimean Conf. "Microwave & Telecommunication Technology", Conf. Proc.*, Sevastopol, Weber Co. 1999, 329-330.*
96. Gorelkina E.M., Marshalko L.N., Ropiy A.I. The features of *p-i-n* diode damage under microwave power action. *Elektronnaya Tekhnika. Ser. 2. Poluprovodnikovye Pribory*, 1989, No 4(201), 93-97.*
97. Gusyatiner M.S., Gorbachev A.I. *Microwave Semiconductor Diodes*. Radio i Svyaz', Moscow, 1983.*
98. Starostenko V.V., Grigoriev E.V., Taran E.P. Effect of electromagnetic fields on IC stability. In: *6th Intern. Crimean Conf. "Microwave & Telecommunication Technology", Conf. Proc.*, Sevastopol, Weber Co. 1996, 433-436.*
99. Starostenko V.V., Taran E.P., Grigoriev E.V., Borisov A.A. Action of electromagnetic fields on ICs. *Izmeritel'naya Tekhnika*, 1998, No 4, 65-67.*
100. Taran E.P., Starostenko V.V., Grigoriev E.V., Borisov A.A. Dynamics of degradation processes in ICs. In: *6th Intern. Crimean Conf. "Microwave & Telecommunication Technology", Conf. Proc.*, Sevastopol, Weber Co. 1996, 437-440.*
101. Grigoriev E.V. Study of IC degradation and failure reasons as function of their orientation under action of pulsed electromagnetic fields. In: *Proc. IV Intern. Crimean Conf. "Microwave Facilities and Reception via Satellites"*, Sevastopol, Weber Co. 1994, 2, 345-346.*
102. Starostenko V.V., Malishevsky S.V., Taran E.P., Shadran A.A. Effect of higher-kind waves on the electromagnetic field distribution near a uniformity. In: *9th Intern. Crimean Conf. "Microwave & Telecommunication Technology", Conf. Proc.*, Sevastopol, Weber Co. 1999, 331-332.*
103. Taran E.P., Starostenko V.V., Grigoriev E.V., Laschennikov D.E. Current distribution and heat localization in IC plating under action of electromagnetic fields. In: *10th Intern. Crimean Conf. "Microwave &*

Telecommunication Technology", Conf. Proc., Sevastopol, Weber Co. 2000, 478-479.*

104. Magda I.I., Gadetskiy N.P., Skachek G.V., Bolotov V.N., Denisov S.V., Novikov V.E., Tkach Yu.V. Chaos parameters of excitation modes in highly-sensitive microwave receiving devices in the conditions of ultrashort electromagnetic interferences. In: *8th Intern. Crimean Conf. "Microwave & Telecommunication Technology"*, Conf. Proc., Sevastopol, Weber Co. 1998, **2**, 759-762.*
105. Bolotov V.N., Denisov S.V., Novikov V.E., Tkach Yu.A. Information concept of chaos excitation. In: *7th Intern. Crimean Conf. "Microwave & Telecommunication Technology"*, Conf. Proc., Sevastopol, Weber Co. 1997, **1**, 260-261.*
106. Denisov S.V. What is the probability for chaos to rise in the microelectronic devices?. In: *8th Intern. Crimean Conf. "Microwave & Telecommunication Technology"*, Conf. Proc., Sevastopol, Weber Co. 1998, **2**, 763-764.*

Part 2

1. Mada Y., Inoue N. *p-n* junction formation using laser induced donors in silicon. *Appl. Phys. Lett.*, 1986, **48**(18), 1205-1207.
2. Medvid' A., Knite M., Kaupuzs J., Frishfelds V. Reversible phase change optical recording on SiO_2 -(Co + Si)- SiO_2 -Si multilayer structure. *Proc. SPIE*, 1996, **2968**, 135-139.
3. Medvid' A., Knite M., Kaupuzs J., Frishfelds V. Mechanism of recording and erasing of optical information by laser radiation on SiO_2 (Co+Si)- SiO_2 -Si multilayer structure. *Appl. Surf. Sci.*, 1997, **115**, 393-398.
4. Baranets S.V., Dikiy S.P., Fedorenko L.L., Kaganovich E.B., Svechnikov S.V., Antonov V.A. Thermal stable laser produced low-ohmic contact to nanometer *p*-GaAs layers of barrier structures for fast optoelectronic devices. *Proc. SPIE*, 1996, **2968**, 144-148.
5. Yakimkin V.N., Ushakov V.V., Gippius A.A., Vavilov V.S., Sedelnikov A.E., Dravin V.A., Chernyaev V.V., Ponomarev N.Yu. Laser annealing of implanted GaAs. Role of implantation defects. *FTP*, 1988, **22**(9), 1563-1568.*

6. Blums J., Medvid' A. The generation of donor centers using double frequency of YAG:Nd laser. *Phys. stat. sol. (a)*, 1995, **147**, K91-K95.
7. Fedorenko L.L., Malyutenko V.K., Bolgov S.S. Activation of the InSb photoconductivity by laser illumination. *Ukr. Fiz. Zhurn.*, 1975, **20**(12), 2041-2044.**
8. Meyer C.R., Krueger M.R., Bartoli F.J. Optical heating in semiconductors: Laser damage in Ge, Si, InSb, and GaAs. *J. Appl. Phys.*, 1980, **51**(10), 5513-5522.
9. Emel'yanov V.I. Laser-induced generation of metastable diffusion-deformation structures on solid surfaces. *Izv. AN SSSR, Ser. Fiz.*, 1992, **56**(4), 76-90.*
10. Bogatyrev V.A., Kachurin G.A. Low-resistance n -layer formation on p -InSb by pulsed laser irradiation. *FTP*, 1977, **11**(1), 100-103.*
11. Kashkarov P.K., Petrov V.I., Timoshenko V.Yu. The features of laser-induced phase transitions in III-V semiconductors. *Izv. AN SSSR, Ser. Fiz.*, 1991, **55**(8), 1655-1659.*
12. Dobrynina E.S., Petrov V.I., Djijoev M.S., Zenkov Yu.V., Kashkarov P.K., Platonenko V.T., Popov V.K. Defect production in gallium phosphide induced by laser irradiation. *Izv. AN SSSR, Ser. Fiz.*, 1986, **50**(4), 816-819.*
13. Gusakov G.M., Kondratova T.N., Kapsky K.S., Laryushin A.I. Effect of pulsed laser irradiation on the mobility and conductivity profiles in epitaxial GaAs layers. *FTP*, 1989, **23**(10), 1864-1868.*
14. Dmitriev A.G., Dorin V.A., Karful R., Pogarsky M.A., Shul'ga M.I. Production of deep-level centers in GaAs under laser irradiation. *FTP*, 1992, **26**(2), 397-398.*
15. Grigoriev N.N., Kudykina T.A., Tomchuk P.M. Thermal-diffusion spreading of inclusions and accumulation effect in laser material damage. In: *Kvantovaya Elektronika*, Naukova Dumka, Kiev, 1989, No 37, 84-91.*
16. Vasiliev A.G., Kononov V.I., Korshunov A.B., Orlicovsky A.A., Tokachov V.N., Chaplin N.I. In: *Laser Processing and Diagnostics*. Ed. Banerle D., Springer-Verlag, Berlin-New-York-Tokyo, 1984, 67.
17. Shumskii M.G., Bublik V.T., Gorelik S.S., Gurevich M.A. The temperature dependence of mean square dynamic displacements of atoms in sublattices of some semiconducting compounds of $A^{III}B^V$ type. *Kristallografiya*, 1971, **16**(4), 779-783.*

18. Madelung O. *Physics of III-V Compounds*. John Wiley and Sons, Inc., New York–London–Sydney, 1964.
19. Kaupuzs J., Medvid' A. New conception in transistor technology using nonhomogeneous temperature field. *Proc. SPIE*, 1994, **2335**, 134-147.
20. Voronkov V.P., Gurchenok G.A. Impurity diffusion in semiconductors at pulsed laser annealing. *FTP*, 1990, **24**(10), 1831-1834.*
21. Medvid' A., Fedorenko L.L., Snitka V. The mechanism of generation of donor centers in *p*-InSb by laser radiation. *Appl. Surface Sci.*, 1999, **142**, 280-285.
22. Kaupuzs J., Medvid' A. Distribution of impurity atoms over a crystal in a nonhomogeneous temperature field. *Ukr. Fiz. Zhurn.*, 1995, **40**(9), 1015-1020.
23. Svechnikov S.V., Fedorenko L.L., Kaganovich E.B., Plakhotny V.P., Baranets S.V., Antonov V.A. Laser-thermal diagnostics of multilayer opto- and microelectronic structures. *Proc. SPIE*, 1993, **2113**, 180-185.
24. Welker H. Zur Theorie der galvanomagnetischen Effekte bei gemischten Leitung. *Z. Naturforsch.*, 1951, **6a**(4), 184-191.
25. Malyutenko V.K., Teslenko G.I. Determination of diffusion length and surface recombination velocity from semiconductor photoconductivity in a transverse magnetic field. *Optoelektronika i Poluprovodnikovaya Tekhnika*, 1987, No 11, 14-16.*
26. Andreeva V.D., Jumamkhamubetov N.G., Dmitriev A.G. Thermal annealing of GaAs crystals modified by laser radiation. *FTP*, 1991, **25**(9), 1624-1628.*
27. Efimova A.I., Prudnikov R.V. Defect generation at the GaAs surface under pulsed laser action. In: *Proc. IX All-Union Sympos. “Electronic Processes at Semiconductor Surfaces and in Thin Semiconductor Layers”*, SO AN SSSR, 1983, Pt.1, 163-164.*
28. Levitas T., Pozhela J. (Ed.), Stalyeraitis K. *Semiconductor Transducers*, **2**, Mokslas, Vilnius, 1980, 75.
29. Alferov Zh.I., Koval'chuk Yu.V., Pogorelsky Yu.V., Smol'sky O.V., Sokolov I.A. A new phase transition in Si and GaAs at action of picosecond laser pulses. *Pis'ma v ZHTF*, 1983, **9**(22), 1373-1376.*
30. Vasiliev A.N., Karpov S.Yu., Koval'chuk Yu.V., Myachin V.E., Pogorelsky Yu.V., Silova M.Yu., Sokolov I.A., Fokin G.A. Formation of

- metastable states in a liquid phase during melting of III-V semiconductor compounds by nanosecond laser pulses. *ZhETF*, 1989, **96**(4 (10)), 1459-1472.*
31. Author's Certificate USSR # 1028204 H 01L 21/66. Method for determination of bipolar diffusion coefficient for nonequilibrium charge carriers. Almazov L.A., Malyutenko V.K., Fedorenko L.L. *Byulleten' Izobretenii*, 1983, No 48.*
 32. Almazov L.A., Malyutenko V.K., Fedorenko L.L. Effect of degeneration on the properties of nonequilibrium semiconductor plasma produced by surface excitation. *Ukr. Fiz. Zhurn.*, 1981, **26**(5), 734-739.*
 33. Almazov L.A., Liptuga A.I., Malyutenko V.K., Fedorenko L.L. Properties of nonequilibrium high-density plasma in InSb. *FTP*, 1980, **14**(10), 1940-1946.*
 34. Malyutenko V.K., Fedorenko L.L. New techniques for determination of nonequilibrium charge carrier parameters in narrow-gap semiconductors. *Optoelektronika i Poluprovodnikovaya Tekhnika*, 1988, No 13, 1-13.*
 35. Almazov L.A., Malyutenko V.K., Fedorenko L.L. Charge carrier diffusion and recombination at high excitation levels. *FTP*, 1980, **14**(10), 2063-2064.*
 36. Vavilov V.S., Galkin G.N., Shatkovsky E.V. Plasma resonance of nonequilibrium charge carriers in indium arsenide. *Kratkie Soobshcheniya po Fizike FIAN*, 1970, No 7, 56-61.*
 37. Vakhnenko I.F., Strizhevsky V.L. Plasma reflection due to nonequilibrium charge carriers in semiconductors. *FTP*, 1969, **3**(12), 1844-1856.*
 38. Kostyuk N.M., Peshko I.I., Ponomarenko Yu.V., Fedorenko L.L. Photoconductivity in InSb under picosecond excitation. *Ukr. Fiz. Zhurn.*, 1984, **29**(6), 888-892.*
 39. Fauchet P.M. Optical probing of Auger-governed decay of laser-induced plasma in InSb. *phys. stat. sol. (a)*, 1980, **58**(2), K211-K214.
 40. Fauchet P.M. The Auger rate in highly excited indium antimonide. *phys. stat. sol. (b)*, 1982, **110**(1), K11-K15.
 41. Schwarts B.D., Nurmiikko A.V. Picosecond infrared spectroscopy in narrow-gap semiconductors. *Bunsek kagaku* # 15479, 1980, **14**, 303-307.

42. Nurmikko A.V., Schwarts B.D. Some properties of a high-density electron-hole plasma in $Hg_{1-x}Cd_xTe$. *J. Vac. Sci. Technol.*, 1982, **21**(1), 229-230.
43. Peshko I.I. Dynamic holographic patterns in Si and CdTe crystals. Preprint No 6, Institute of Physics of the Academy of Sciences of the UkrSSR, 1983.*
44. Shank C.V., Auston D.H. Ultrafast phenomena in semiconductor devices. *Science*, 1982, **215**(4534), 797-801.
45. Abakumov V.N., Yassievich I.N. Photoelectric phenomena at electron heating by light with allowance made for surface recombination. *FTP*, 1969, **3**(5), 736-743.*
46. Auston D.H., Shank C.V. Picosecond ellipsometry of transient electron-hole plasmas in germanium. *Phys. Rev. Lett.*, 1974, **32**(20), 1120-1123.
47. Van Cong H. Diffusion coefficients in degenerate semiconductors. *phys. stat. sol. (b)*, 1980, **101**(1), K27-K29.
48. Hollis J.E.L., Choo S.C., Heasell E.L. Recombination centers in InSb. *J. Appl. Phys.*, 1967, **38**(4), 1626-1636.
49. Fujisada H. Effects of diffusion current on galvanomagnetic properties in thin intrinsic InSb at room temperature. *J. Appl. Phys.*, 1974, **45**(8), 3530-3540.
50. Bruhns H., Kruse H. Lifetime of charge carriers in intrinsic indium antimonide. *phys. stat. sol. (b)*, 1980, **97**(1), 125-133.
51. Beattie A.R., Smith G. Recombination in semiconductors by a light hole Auger transition. *phys. stat. sol. (b)*, 1967, **19**(2), 577-586.
52. Tamashkyavicius A.V., Shatkovsky E.V. Photoconduction and photoelectromagnetic effect in highly excited InSb. In: *Abstr. All-Union Conf. "Physics of III-V Compounds"*, Leningrad, Oct. 1978. Leningrad Polytechnic Inst. Publ., Leningrad, 1978, 77-78.*
53. Almazov L.A., Malyutenko V.K., Fedorenko L.L. Recombination and diffusion of nonequilibrium plasma in InSb at high excitation levels. *FTP*, 1983, **17**(7), 1211-1216.*
54. Peshko I.I., Soskin M.S., Khizhnyak A.I. Ultrashort pulse laser with adjustable parameters. *Izv. AN SSSR, Ser. Fiz.*, 1982, **46**(10), 1949-1955.*
55. Rupprecht H., Weber R., Weiss H. Über die galvanomagnetischen Eigenschaften von InSb Einkristallen mit Te-Dotierung. *Z. Naturforsch. A*, 1960, **15**(9), 783-794.

56. Haug A. Carrier density dependence of Auger recombination. *Solid-St. Electron.*, 1978, **21**(11/12), 1281-1284.
57. Gel'mont B.L. Auger recombination in narrow-gap semiconductors. *FTP*, 1980, **14**(10), 1913-1918.*
58. Malyutenko V.K., Guga K.Yu., Malozovskii Yu.M. Magnetoconcentration effect at Auger recombination of current carriers. *phys. stat. sol. (a)*, 1981, **65**(1), 131-140.
59. Zitter R.N., Strauss A.J., Attard A.E. Recombination processes in *p*-type indium antimonide. *Phys. Rev.*, 1959, **115**(2), 266-273.
60. Regel A.R., Glazov V.M. *The Regularities in Electronic Melt Formation*. Nauka, Moscow, 1982.*
61. Poltavtsev Yu.G. *Structure of Semiconductor Melts*. Metallurgiya, Moscow, 1984.*
62. Kalinina E.V., Koval'chuk Yu.V., Prischepa G.V., Smol'sky O.V. Influence of the ultrashort laser pulses on the electrophysical properties of silicon carbide. *Pis'ma v ZhTF*, 1985, **11**(11), 669-671. *
63. Pikhtin A.N., Popov V.A., Yas'kov D.A. Ohmic contacts to semiconductors obtained using laser. *FTP*, 1969, **3**(11), 1646-1648. *
64. Fedorenko L., Kiselev V., Svechnikov S., Saltykov P., Yusupov M. Low-ohmic contact to α -SiC produced by laser technology method. In: *Proc. 22nd Intern. Conf. on Microelectronics (MIEL-2000)*, Nis, Serbia, 14-17 May 2000, **2**, 473-476.
65. *Physical Quantities: A Handbook*. Eds. Grigoriev I.S., Meilikhov E.S. Energoatomizdat, Moscow, 1991.*
66. *Properties of Silicon Carbide*. Ed. Harris G.L. Washington DC, 1995.
67. Kassamakova L., Kakanakov R., Kassamakov I., Nordell N., Savage S., Hjorvarsson B., Svedberg E.B., Abom L., Madsen L.D. Temperature Stable Pd Ohmic Contacts to *p*-type 4H-SiC Formed at Low Temperatures. *IEEE Trans. Electron. Devices*, 1999, **ED-46**(3), 598-604.
68. Raskin A.A., Shalimov S.V. Ohmic contacts to gallium arsenide. *Zarubezhnaya Elektronnaya Tekhnika*, 1990, No 12, 32-47.*
69. Kaganovich E.B., Svechnikov S.V. Fabrication of ohmic contacts to III-V semiconductor compounds. (A review). *Optoelektronika i Poluprovodnikovaya Tekhnika*, 1992, No 22, 1-16.*

70. Goldberg Yu.A. Metal-III-V semiconductor ohmic contact: Formation techniques and properties. *FTP*, 1994, **28**(10), 1681-1698.*
71. Baca A.G., Ren F., Zolper J.C., Briggs R.D., Pearton S.J. A survey of ohmic contacts to III-V compound semiconductors. *Thin Sol. Films*, 1997, **308-309**, 599-606.
72. Piotrowska A., Guivarc'h A., Pelous G. Ohmic contacts to III-V compound semiconductors: A review of fabrication techniques. *Solid-St. Electron.*, 1983, **26**(3), 179-197.
73. Dutta R., Robbins M., Lambrecht V.G. Electrical and structural properties of W-In based ohmic contact to GaAs. *Solid-St. Electron.*, 1990, **33**(12), 1601-1605.
74. Rajeswaran G., Kahlen K.B., Lawrence D.J. Studies of Zn diffusion in GaAs by rapid thermal processing. *J. Appl. Phys.*, 1990, **69**(3), 1359-1365.
75. Shen T.C., Fan Z.F., Gao G.B., Morkoç H., Rockett A. Molecular-beam-epitaxy-deposited nonalloyed Al contacts to *n*-type and *p*-type InGaAs. *Appl. Phys. Lett.*, 1991, **59**(18), 2254-2256.
76. Vavilov V.P. *Techniques for Thermal Inspection of Composite Structures and Electronic Devices*. Radio i Svyaz', Moscow, 1984.*
77. Alper R.I., Traub A.C. Laser inspection of soldered connections. *Proc. SPIE*, 1986, **611**, 92-99.
78. Ryvkin S.M., Salmanov V.M., Yaroshetsky I.D. Thermal radiation from silicon under laser beam action. *FTT*, 1968, **10**(4), 1022-1024.*
79. Nikoshiba N., Nakamura H., Toubouski K. Nondestructive observation of defects in semiconductors with photoacoustic and photothermal radiation microscopes. In: *Ultrasonic Symposium, 1984*, 651-655.
80. Mandelis A., Care F., Chan K.K., Miranda L.C.M. Photopyroelectric detection of phase transitions in solids. *Appl. Phys.*, 1985, **A38**(2), 117-122.
81. Uglov A.A., Ermolaev A.N., Zavidey V.I. Optical measurement of metal surface temperature at pulsed laser irradiation. *Kvantovaya Elektronika*, 1990, **17**(4(214)), 519-522.*
82. Improved laser soldering plant. *Elektronika*, 1986, No 14, 34-38.*
83. Kaganovich E.B., Moin M.D., Plakhotny V.P., Svechnikov S.V., Fedorenko L.L. Laser-pyrometric diagnostics of a metal-semiconductor system. In: *Abstr. VI All-Union Conf. "Analytical Techniques for In-*

vestigation of Materials and Microelectronic Facilities", Kishinev, 1991, 89.*

84. Svechnikov S.V., Antonov V.A., Kaganovich E.B., Plakhotny V.P., Fedorenko L.L. Laser thermal diagnostics of model metal– semiconductor structure. *Electron Technology*, 1993, **26**(2/3), 3-13.
85. Antonov V.A., Kaganovich E.B., Plakhotny V.P., Svechnikov S.V., Fedorenko L.L. Laser-excited thermal radiation from a model metal–semiconductor contact structure. *Optoelektronika i Poluprovodnikovaya Tekhnika*, 1993, No 26, 53-60.*
86. Rykalin N.N., Zuev I.V., Uglov A.A. *The Foundations of Electron-beam Processing of Materials*. Mashinostroenie, Moscow, 1978.*
87. Segerdlind L.J. *Applied Finite Element Analysis*. John Wiley and Sons, Inc., New York/London/Sidney/Toronto, 1976.
88. Amusin V.Z., Fadeev A.B. *The Finite Element Method in Solving the Mining Geomechanics Problems*. Nedra, Moscow, 1975.*
89. Plakhotny V.P., Smovzh A.K. The features of optoelectronic potentiometric facilities designing with the finite element method. *Optoelektronika i Poluprovodnikovaya Tekhnika*, 1987, No 12, 54-63.*

FTP – Fizika i Tekhnika Poluprovodnikov

FTT – Fizika Tverdogo Tela

ZhETF – Zhurnal Eksperimental'noi i Teoreticheskoi Fiziki

ZhTF – Zhurnal Tekhnicheskoi Fiziki

Наукове видання

Беляєв Олександр Євгенович, доктор фіз.-мат. наук, проф.;
Венгер Євген Федорович, член-кор. НАН України,
доктор фіз.-мат. наук, професор;
Єрмолович Ірина Борисівна, доктор фіз.-мат. наук;
Конакова Раїса Василівна, доктор техн. наук, професор;
Литвин Петро Мар'янович, кандидат фіз.-мат. наук;
Мілєнін Віктор Володимирович, кандидат фіз.-мат. наук;
Прокопенко Ігор Васильович, доктор фіз.-мат. наук;
Свєчніков Георгій Сергійович, кандидат фіз.-мат. наук;
Соловйов Євген Олександрович, кандидат техн. наук;
Федоренко Леонід Леонідович, кандидат фіз.-мат. наук

ВПЛИВ НВЧ І ЛАЗЕРНОГО ВИПРОМІНЮВАНЬ НА ПАРАМЕТРИ НАПІВПРОВІДНИКОВИХ СТРУКТУР

Київ, "Інтас", 2002

Загальна редакція Р.В. Конакової

Комп'ютерна верстка О.С. Литвин

Здано на виробництво 17.06.02. Підписано до друку 17.06.02.
Формат 60×84 1.16. Папір друкарський № 1. Друк офсетний.
Гарнітура Балтіка. Умовн. друк. арк. 12. Умовн. фарб.-відб. 12.
Облік.-вид. арк. 12.
Наклад 1 000 прим. Зам. № .

Віддруковано з готових діапозитивів
на "Інтас",
вул. Білоруська, 26, Київ 04005
Свідоцтво № 3841442